

# MECHANICAL TESTING OF ADVANCED COATING SYSTEM

## VOLUME 1

By

T. A. Cruse  
A. Nagy  
C. F. Popelar

### FINAL REPORT

SwRI Project No. 06-1778-001  
Cooperative Agreement No. NCC 3-89

Prepared for  
National Aeronautics and Space Administration  
Lewis Research Center  
Cleveland, Ohio

June 1990

(NASA-CR-186725) MECHANICAL TESTING OF  
ADVANCED COATING SYSTEM, VOLUME 1 Final  
Report (Southwest Research Inst.) 113 p  
CSCL 110

N91-17636

undlc

05/27 0291036



**SOUTHWEST RESEARCH INSTITUTE**

SAN ANTONIO  
WASHINGTON, DC

HOUSTON

DETROIT  
DALLAS/FT. WORTH

# MECHANICAL TESTING OF ADVANCED COATING SYSTEM

## VOLUME 1

By

T. A. Cruse  
A. Nagy  
C. F. Popelar

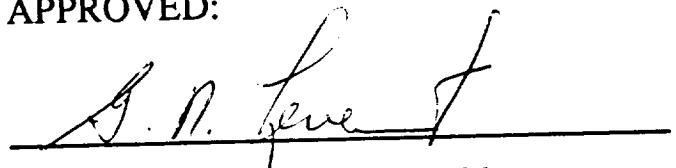
### FINAL REPORT

SwRI Project No. 06-1778-001  
Cooperative Agreement No. NCC 3-89

Prepared for  
National Aeronautics and Space Administration  
Lewis Research Center  
Cleveland, Ohio

June 1990

APPROVED:



Ulric S. Lindholm, Vice President  
Engineering and Materials Sciences

## TABLE OF CONTENTS

		<u>Page</u>
	List of Tables	iii
	List of Figures	iv
1	Acknowledgments	1
2	EBPVD Coating Constitutive Tests	2
	2.1 Specimen Design	2
	2.2 Test Setup	2
	2.2.1 Compression Setup	3
	2.2.2 Tension Setup	3
	2.2.3 Test Matrix	4
	2.2.4 Correlation of the Strain Measurements	4
	2.3 Data Reduction	4
	2.3.1 Composite Specimen Model	7
	2.3.2 Data Reduction Procedure	8
	2.3.3 Compression Data	8
	2.3.4 Tension Data	8
	2.4 Data Interpretation	8
	2.4.1 Compression Data	10
	2.4.2 Tension Data	12
	2.4.3 Creep Data	13
3	References	14
4	EBPVD Tables and Figures	50
5	Appendix A: Elastic Bimaterial Model	54
6	Appendix B: Failed Specimen Photographs	66
7	Appendix C: Computer Plots of Compression Tests	87
8	Appendix D: Computer Plots of Tension Tests	103
9	Appendix E: Computer Plots of Creep Tests	107
10	Appendix F: MS-DOS ASCII Data Files (Floppy Disks)	107

## LIST OF TABLES

<u>Table</u>		<u>Page</u>
I	Compression Test Matrix	15
II	Tensile Test Matrix	16
III	Ceramic Modulus in Compression versus Temperature for Unexposed and Exposed TBC	17
IV	Ceramic Modulus in Tension versus Temperature for Unexposed TBC	18
V	Creep Rate Data Compression Tests	19

## LIST OF FIGURES

<u>Figure</u>		<u>Page</u>
1	Compression Specimen	20
2	Tensile Specimen	21
3	Biaxial Transducer	22
4	Compression Test Setup	23
5	Tension Test Setup	24
6	Schematic Compression Test Response	25
7	Schematic Tension Test Response	25
8	Compression Test Specimen	26
9	Schematic of Test Model	26
10	Linear Elastic Model Flow Chart	27
11	Substrate Modulus vs Temperature as Determined at NASA and SwRI	28
12	Deduced Ceramic Response in Compression for Unexposed Specimen 18A at 75°F	29
13	Deduced Ceramic Response in Compression for Unexposed Specimen 19 at 1400°F	30
14	Deduced Ceramic Response in Compression for Unexposed Specimen 21D at 1400°F	31
15	Deduced Ceramic Response in Compression for Unexposed Specimen 25 at 1800°F	32
16	Deduced Ceramic Response in Compression for Unexposed Specimen 26 at 1800°F	33
17	Deduced Ceramic Response in Compression for Exposed Specimen 30 at 1000°F	34
18	Deduced Ceramic Response in Compression for Exposed Specimen 24 at 1800°F	35
19	Deduced Ceramic Response in Compression for Exposed Specimen 28 at 2200°F	36
20	Deduced Ceramic Modulus as a Function of the Test Temperature	37

## LIST OF FIGURES (CONCLUDED)

<u>Figure</u>		<u>Page</u>
21	Deduced Ceramic Response in Tension for Unexposed Specimen 652801 at 72°F	38
22	Deduced Ceramic Response in Tension for Unexposed Specimen 652805 at 72°F	39
23	Deduced Ceramic Response in Tension for Unexposed Specimen 653502 at 1400°F	40
24	Deduced Ceramic Response in Tension for Unexposed Specimen 653602 at 1400°F	41
25	Deduced Ceramic Response in Tension for Unexposed Specimen 653704 at 1600°F	42
26	Deduced Ceramic Response in Tension for Unexposed Specimen 653503 at 1800°F	43
27	Deduced Ceramic Response in Tension for Unexposed Specimen 652802 at 1800°F	44
28	Deduced Ceramic Response in Tension for Unexposed Specimen 653603 at 2000°F	45
29	Deduced Ceramic Response in Tension for Unexposed Specimen 652803 at 2200°F	46
30	Deduced Ceramic Response in Tension for Unexposed Specimen 653504 at 2200°F	47
31	Deduced Ceramic Response in Tension for Unexposed Specimen 653504 at 2200°F	48
32	Deduced Ceramic Modulus as a Function of the Test Temperature	49

## **1 Acknowledgments**

The authors appreciate the technical support of Dr. Robert A. Miller at NASA Lewis Research Center, and also that of Pratt & Whitney Aircraft in supplying the test specimens. Mr. David Nissley, Ms. Sue Manning, and Mr. Keith Sheffler at Pratt & Whitney are acknowledged for their technical support and interaction on the test matrix.

## 2 EBPVD Coating Constitutive Tests

### 2.1 Specimen Design

The EB-PVD coating material has a highly columnar microstructure, and as a result it was expected to have very low tensile strength. To be able to fabricate the required compression and tensile specimens, a substrate was required to provide structural integrity for the specimens. Substrate and coating dimensions were adjusted, based on data previously generated under NASA Contract NAS3-23944 for plasma sprayed thermal barrier coating, to provide sufficient sensitivity to resolve the projected loads carried by the EB-PVD coating.

The use of two distinctively different strain transducer systems, for tension and compression loadings, mandated two vastly different specimen geometries. Compression specimens were of a short tubular configuration, as shown in Figure 1<sup>1</sup>, with 0.705 or 0.660-inch inside diameters, 0.022 or 0.045-inch substrate wall thicknesses, and 0.085 or 0.075-inch coating thicknesses, respectively. Specimen length for all compression specimens was 0.874 inch.

The tensile specimen geometry used in the program is shown in Figure 2. The long, tubular configuration was required to accommodate internal mounting of the biaxial, capacitive transducer shown mounted in a cutaway biaxial specimen in Figure 3. Offset of the gage section from the center of the specimen was necessary to provide appropriate space for the sensing element (body) of the transducer, as it should not be exposed to elevated temperatures. Substrate wall thickness for all tensile specimens was in the 0.0050 to 0.0067-inch range with an EB-PVD coating thickness range of 0.050 to 0.105 inch. Although thinner substrates would be desirable, machining and coating practices did not permit further reduction.

### 2.2 Test Setup

#### 2.2.1 Compression Setup

Testing of the tubular compression specimens was performed using the setup shown in Figure 4. The compression load train consisted of two loading anvil assemblies mounted on the stationary load cell and the hydraulic actuator shaft of a 22 KIP capacity MTS, servo hydraulic test machine. The loading anvil assemblies were composed of 1-inch diameter SiC and AD995 rods mounted in tandem with the SiC rods positioned in the hot zone, at the specimen-anvil interface. The AD995 rods were supported in water-cooled, flanged collets. Parallelism between the SiC anvil faces was adjusted to better than 0.0005 inch.

Heating of the test specimens was accomplished using an Instron Model 3118-008 high temperature short furnace with a 1.13-inch diameter by 3 1/2-inch long cylindrical working hot zone. The specimen was sandwiched between the two SiC anvils, and the assembly was centered in the hot section. Temperature deviation from the nominal within the specimen gage section was measured to be less than  $\pm 5^\circ\text{F}$ .

Strain measurements were made using an Instron Model 3118-151 capacitive strain transducer with a working range of 0.080 inch. The transducer employs two, small diameter, alumina reachrods to transfer the generated displacement to the sensing elements. The reachrods penetrate the high temperature furnace through small, strategically located ports, creating minimal thermal disturbance.

---

<sup>1</sup> Figures and tables are given in Section 4.



Contact by the reachrods to the load train was made on the loading anvils immediately next to the specimen/load anvil interfaces, thereby minimizing measurement of extraneous strains. In addition to the use of the extensometer, the room temperature tests were instrumented with strain gages to obtain additional data on coating behavior.

Loading of the specimens took place under appropriate crosshead displacement control, which produced an average strain rate of  $2 \times 10^{-4} \text{ sec}^{-1}$ .

### 2.2.2 Tension Setup

Testing of the tubular tensile specimens was performed using the test setup shown in Figure 5. The setup utilized the 22 KIP MTS servo hydraulic test machine used in the compression tests. The specimens were coupled to the test machine through plug type, pinned, superalloy extension rods, which in turn were attached to pinned couplings at both ends of the specimen, as shown. Use of the pinned couplings facilitated final alignment of the specimens.

Heating of the tensile specimens was again accomplished with the Instron high temperature short furnace used in the compression test setup. The specimen gage section was centered in the hot zone of the furnace, and the shanks of the specimens extended to the outside of the furnace, where they were coupled to the extension rods. Additional insulation was provided around the extension rods to reduce heat loss through the rods and thereby enhance generation of a more uniform temperature profile within the gage section of the specimen. The maximum observed deviation from the nominal test temperature within the gage section was  $\pm 11^\circ\text{F}$ . Water cooling of the upper extension rod at its connection to the pinned coupling was required to prevent heat conduction to the load cell of the test machine.

Strain measurements were made using a high temperature, biaxial, capacitive strain transducer developed by SwRI. The transducer consists of two sets of capacitive sensing elements housed in the body of the transducer. These elements are capable of measuring axial and torsional strains independently. In these tests the transducer was used in the axial mode only. The transducer is mounted inside the tubular test specimen with two sets of three mounting arms equipped with knife edge type contact points, as shown in Figure 3. The arms are internally water cooled, permitting their use at high temperatures. The arms exert sufficient contact force to support the transducer inside the specimen in a stable, vertically suspended position. Initial positioning of the supporting knife edge contacts establishes the starting gage length for strain measurements. The small water cooling lines and the miniature electrical cables of the transducer are routed through appropriately sized holes in the lower shank of the specimen located above the pinned, extension rods. The biaxial transducer was used on all tensile test specimens for strain measurements. On two of the tensile specimens, supplemental strain measurements were made using the reachrod type Instron extensometer utilized in the compression test setup. In addition, some of the room temperature tests were instrumented with strain gages to obtain additional information regarding the behavior of the EB-PVD coating. This attempt appeared to be unsuccessful because of premature debonding and possible localized reinforcing effect of the bonding agent used in the installation of the strain gages.

### 2.2.3 Test Matrix

The test program was comprised of 15 compression and 18 tensile tests. All the tests were conducted at an average strain rate of  $2 \times 10^{-4} \text{ sec}^{-1}$ . The test temperature range was between 75 and 2200°F. Identification numbers of the specimens tested, the type of specimen construction, such as substrate, coated, etc., test modes and test temperatures, and relevant dimensional data for the compression and tension specimens are summarized in Tables I and II, respectively.

As evidenced by the test matrices, baseline (substrate) data, in both compression and tension modes, were generated for nearly all test temperatures, as permitted by specimen availability. Testing of the coated specimens was divided between standard, monotonic compression and tension tests and optional tests. Optional tests covered modulus probing, stress relaxation behavior, creep, and multiple unloading and reloading paths, as shown in Tables I and II.

#### **2.2.4 Correlation of the Strain Measurements**

To verify the accuracy of strain measurements using the high temperature Instron extensometer, two of the compression specimens, No. 20 (thin wall substrate), and No. 18 (thin wall coated), were instrumented with foil type strain gages in a half bridge configuration. Strain data obtained with the two measurement methods on the substrate specimen were in good agreement. The coated specimen exhibited a slightly diverging trend until the substrate reached plastic values. Subsequent readings tracked in good agreement.

During performance of the tensile tests, attempts were made to measure the relative strain behavior of the substrate and the EB-PVD coating. Two tensile specimens, 652801 and 652805, were instrumented with foil type strain gages. On specimen 653801, the strain gages were mounted with a light coat of M-Bond 200 adhesive. The strain gages prematurely debonded during the test, and no useful data were obtained.

On specimen 652805, the intended sites for the strain gages were prepared by filling the voids between the columnar structure of the coating with AE-10 bonding agent until an even area was established for gage mounting. The strain gages were again mounted with M-Bond 200. Relatively early debonding was again observed during the loading process.

Strain values generated by the strain gages were approximately a factor of two lower than those obtained by the extensometers. This difference in amplitudes may imply a localized reinforcing effect by the additional bonding agent applied.

A custom built "spider" like clip gage was also mounted on the coated surface of the specimen. This extensometer was selected over the high temperature Instron extensometer used on the compression specimens because of its ability to measure larger strains. Readings between the biaxial extensometer, mounted on the substrate, and the "spider" gage were in good agreement below the 0.005 in/in strain amplitude. At approximately 0.005 in/in strain amplitude, the clip gage trace shows a sudden change in continuity, implying a possible partial debonding of the coating.

The high temperature Instron extensometer was used on specimens 652803 and 653704 to monitor strain behavior of the EB-PVD coating. As in the case of the strain gage measurements on specimen 652805, the strain values obtained on the coatings were approximately a factor of two lower than those measured on the substrate.

### **2.3 Data Reduction**

#### **2.3.1 Composite Specimen Model**

In order to deduce the mechanical response of the ceramic from the test data of the ceramic/substrate bimaterial system response, an analytical procedure was developed. Typically, the response of the substrate may be considered as elastic - perfectly plastic. In compression and in tension, the bimaterial response is generally bilinear. In the compression tests, the onset of the bilinear response is assumed to occur when the substrate becomes plastic, as shown schematically in Figure 6. However,

in the tension tests, the bilinear response is attributed to cracking and debonding of the ceramic, after which the load is assumed to be carried by the substrate. A schematic of the tension test behavior is shown in Figure 7.

The deduced ceramic response when the substrate is perfectly plastic or the ceramic debonds is trivial. Static equilibrium is sufficient to determine the loads in both components. When both materials are linearly elastic, however, the system is statically indeterminate. Thus, it is necessary to apply compatibility conditions, in addition to static equilibrium, to solve for the individual loads in the ceramic and substrate. As this solution is non-trivial, the purpose of this subsection is to describe the development of the formula necessary to deduce the loads and hence the response of the ceramic. A detailed description of this development is given in Appendix A.

The assumptions are that (1) both materials are linearly elastic, (2) the axial strains in the ceramic and substrate are equal, (3) no debonding occurs, (4) the specimen does not buckle, and (5) the measured loads and strains are not influenced by end effects. Note that in the following analyses and discussions, all loads are taken as tensile and all pressures are considered to be positive. The mathematical symbols used in the derivations are defined in Appendix A.

The test specimen, shown in Figure 8, is subjected to an axial load,  $P_T$ , and the corresponding axial strain,  $\epsilon_{xx}$ , is measured. To deduce the individual stress state in each material, the ceramic and substrate were considered to be closed-ended, thick-walled cylinders [1,2]<sup>2</sup> whose state of stress is described by

$$\sigma_{xx}^c = \frac{P_c}{\pi(c^2 - b^2)} + \frac{pb^2}{(c^2 - b^2)} \quad (1a)$$

$$\sigma_{rr}^c = \frac{pb^2}{c^2 - b^2} - \frac{pc^2b^2}{r^2(c^2 - b^2)} \quad (1b)$$

$$\sigma_{\theta\theta}^c = \frac{pb^2}{c^2 - b^2} + \frac{pc^2b^2}{r^2(c^2 - b^2)} \quad (1c)$$

and

$$\sigma_{xx}^s = \frac{P_s}{\pi(b^2 - a^2)} + \frac{pb^2}{(b^2 - a^2)} \quad (2a)$$

$$\sigma_{rr}^s = \frac{-pb^2}{b^2 - a^2} + \frac{pb^2a^2}{r^2(b^2 - a^2)} \quad (2b)$$

$$\sigma_{\theta\theta}^s = \frac{-pb^2}{b^2 - a^2} - \frac{pb^2a^2}{r^2(b^2 - a^2)} \quad (2c)$$

for the ceramic and substrate, respectively.

---

<sup>2</sup>References are given in Section 3.

The elastic modulus and Poisson's ratio of the ceramic, denoted by  $E_C$  and  $\nu_C$ , are generally different from those of the substrate, denoted by  $E_S$  and  $\nu_S$ . The result of these differences in the mechanical properties is an "interfacial" pressure,  $p$ , which comes about with the application of an axial load, shown schematically in Figure 9. During a compression (tension) test, the substrate tries to expand (contract) radially more than the ceramic. Thus, there is a pressure (suction) at the ceramic/substrate interface. This interfacial pressure is related to the material properties (see Appendix A) through

$$p = \frac{\nu_C E_S A_S P_C - \nu_S E_C A_C P_S}{\pi \{E_S A_S [(1 - 2\nu_C)b^2 + (1 + \nu_C)c^2] + E_C A_C [(1 - 2\nu_S)b^2 + (1 + \nu_S)a^2]\}} \quad (3)$$

The pressure results in a triaxial state of stress for the ceramic and substrate, as is seen from Equations (1) and (2).

Because the system is statically indeterminate when both materials are linearly elastic, it is necessary to apply compatibility conditions, in addition to the equilibrium condition, to solve for the individual loads in the ceramic and substrate. While the details of this work are given in Appendix A, it can be shown that the load in the ceramic is related to the total applied load through

$$P_C = K(E_C)P_T \quad (4)$$

where, for convenience,  $K(E_C)$  is defined as

$$K(E_C) = \frac{b^2 [E_C A_C (1 - 2\nu_S) + E_S A_S (1 - 2\nu_C)] \nu_S E_C A_C + D E_C A_C}{D E_S A_S + b^2 [E_C A_C (1 - 2\nu_S) + E_S A_S (1 - 2\nu_C)] (\nu_S E_C A_C + \nu_C E_S A_S) + D E_C A_C} \quad (5)$$

where

$$D = E_S A_S [(1 - 2\nu_C)b^2 + (1 + \nu_C)c^2] + E_C A_C [(1 - 2\nu_S)b^2 + (1 + \nu_S)a^2] \quad (6)$$

It is possible (see Appendix A) to relate the ceramic modulus used in Equation (4) to the measured axial strain and applied load by

$$\epsilon_{ax}^C = \frac{P_T}{E_C A_C} \left\{ K(E_C) + b^2 \left[ \frac{\nu_C E_S A_S K(E_C) - \nu_S E_C A_C (1 - K(E_C))}{D} \right] (1 - 2\nu_C) \right\} \quad (7)$$

Although Equation (7) can be reduced to directly solve for the ceramic modulus, it was more convenient to solve for the modulus by iterating on the ceramic modulus until the right-hand side of Equation (7) agreed with the corresponding axial strain.

Thus, for a given axial strain and applied load, Equation (7) can be used to determine the ceramic modulus, knowing the substrate modulus, Poisson's ratios for both the ceramic and the substrate, and the specimen geometry. The ceramic modulus can then be used to calculate the axial load in the ceramic by Equation (4). Equation (1) is used to calculate the triaxial stress state in the ceramic.

The technique described above is only valid when both materials remain linearly elastic. During the compression tests, the substrate becomes plastic (taken to be perfect-plasticity). Conversely in the

tension tests, the substrate remains elastic, but the ceramic undergoes severe damage in the form of cracking and/or debonding. In either situation, the linear elastic approach is not valid and an additional technique is required to analyze the test data.

For the compression tests, the substrate is assumed to become perfectly plastic for strains greater than a critical strain,  $\epsilon_{crit}$ , after which the substrate is assumed to carry no further load than the load,  $P_{flow}$ , corresponding to flow in the substrate. The system is then statically determinate. From static equilibrium, the axial load in the ceramic is simply the difference between the total applied load and the load in the substrate,  $P_{flow}$ . Thus,

$$P_C = P_T - P_{flow} \quad (8)$$

Further, the interfacial pressure is assumed to be nonexistent. As a result, the state of stress becomes uniaxial, as seen from Equations (1) and (2).

As was noted previously, cracking in and/or debonding of the ceramic occurs in the tension testing. Because damage is not accounted for in the analysis, the linear elastic analysis is valid only to the onset of severe damage to the ceramic. Presently, no technique is used to analyze the bimaterial response beyond this point.

### 2.3.2 Data Reduction Procedure

The previous discussions described the development of the analytical technique used to deduce the ceramic response from the ceramic/substrate bimaterial response. The following discussion describes how to exercise the analytical technique to systematically reduce the experimental data (i.e., applied load and corresponding axial strain data). A flow chart of this analytical procedure is shown in Figure 10.

In order to reduce the bimaterial response, specimen geometry and substrate material property data are required. The substrate moduli in tension and compression were determined as a function of temperature from tests conducted at SwRI. The data are shown in Figure 11. An "eyeball" fit to these data is used to interpolate to intermediate temperatures. The substrate moduli are compared to apparent moduli data derived from dynamic moduli data [3]. Poisson's ratios for the ceramic and substrate were taken as 0.25 and 0.4, respectively. It is noted that Poisson's ratio was found to have only a second-order effect on the deduced response.

The applied load and corresponding axial strain are also required inputs. If the axial strain is less than the critical strain denoting the onset of plastic behavior in the substrate, an initial estimate of the ceramic modulus is made. From this estimate, the right-hand side of Equation (7) is used to compute an axial strain. If the computed axial strain does not reasonably agree with the measured strain, the ceramic modulus is adjusted, and this iterative process is repeated until the strains agree. Once the ceramic modulus is determined, the triaxial stress state is computed using Equation (1).

Should the axial strain exceed the critical strain denoting the onset of plasticity in the substrate, the axial load in the ceramic is simply calculated by taking the difference between the applied load and the load corresponding to plastic flow of the substrate. The uniaxial stress state is computed by ignoring the interfacial pressure, as previously discussed.

Hooke's law

$$e_{xx}^c = \frac{1}{E_c} [\sigma_{xx}^c - \nu_c (\sigma_{rr}^c + \sigma_{\theta\theta}^c)] \quad (9)$$

is used to relate the stress state of the ceramic coating to the axial strain. As it is convenient to plot Hooke's law so that the slope of the plot is identically equal to the elastic modulus,  $\sigma_{xx}^c - \nu_c (\sigma_{rr}^c + \sigma_{\theta\theta}^c)$  is plotted against the axial strain in the ceramic.

### 2.3.3 Compression Data

The results of the compression testing of the exposed and unexposed ceramic/substrate bimaterial specimens are shown in Figures 12-19. These data include the assumed and measured substrate response, the measured bimaterial response, and the deduced ceramic response. The substrate and bimaterial responses are for uniaxial compression along the tube axis. It should be noted that the small dip in the deduced ceramic response comes about from the difference between assumed and actual substrate responses near the onset of yielding in the substrate.

The compressive ceramic modulus of the exposed and unexposed bimaterial specimens is given as a function of temperature in Table III. Figure 20 shows these data as a function of test temperature.

### 2.3.4 Tension Data

The results of the tension testing for the unexposed ceramic/substrate bimaterial specimens are shown in Figures 21-31. These data include the measured bimaterial response and the deduced ceramic response. The bimaterial response is for uniaxial tension along the tube axis. As was previously noted, the ceramic begins to crack and/or debond prior to yielding of the substrate. Thus, both materials are assumed to be linear elastic throughout these calculations. The computations were carried only to the point where the ceramic was thought to undergo severe damage.

The ceramic modulus in tension of the unexposed bimaterial specimens is given as a function of temperature in Table IV. Figure 32 shows these data as a function of test temperature.

## 2.4 Data Interpretation

### 2.4.1 Compression Data

The substrate modulus test data are plotted in Figure 11, along with Pratt & Whitney-supplied dynamic modulus data. Static data for the tension and compression tests were in good agreement with each other at the various test temperatures, and slightly higher than the dynamic data. The test values for the compression modulus at 1000°F are quite low, indicating a possible misalignment of the single crystal axis relative to the test direction.

The ceramic modulus is inferred from the test records plotted in Figures 12-19 by taking a single point fit to the bimaterial test curve at a point in the perceived linear regime. The analysis method of Section 1.3 was then applied to derive the ceramic response below the yield strain of the substrate. The resulting linear value of modulus is shown against each of the ceramic curves. As will be discussed for each case, this approach was not always successful due to nonlinear behavior of the composite specimen at low strains. Figure 20 plots the resulting ceramic modulus results versus temperature. Shifting lines for some of the data occur as a result of applying engineering judgment to some of the test results. These judgments will be presented below, for each test case.

The apparent ceramic modulus at room temperature seems exceptionally high compared to the trend line through the rest of the data. The RT test record has an anomaly, seen in Figure 12, when compared with the other test records. The bimaterial stress-strain curve appears to be trilinear, rather than the expected bilinear form. The yieldpoint of the substrate is set in this figure to the second break point in the bimaterial response curve. The result using the first break point was visibly less satisfactory in terms of the deduced ceramic response, resulting in an increase in the modulus of the ceramic after the break. The modulus fit used the two segments below the knee, as indicated. The resulting stress-strain curve for the ceramic indicates a continued linear response, rather than a softening response. The second linear region seems implausible. Most likely, the substrate modulus is far off, and the ceramic response should be linear over all three of the linear portions of the test record. Use of only the last segment of the ceramic stress-strain curve indicates a modulus much more consistent with the extrapolated value from Figure 20, as shown by the shifting arrow on the data point.

This RT data interpretation is more consistent with the ceramic response at 1400°F in Figure 13, where the tangent to the ceramic curve does not show a pronounced bilinear break from elastic to inelastic response. If a straight line is fit to the deduced ceramic response below the cusp, this slope is still valid above the cusp, for a limited amount of further straining. The 1400°F data in Figure 14 contains a much longer cusp effect, and it seems that the initial low slope is not valid. Superimposing the two 1400°F curves gives a better feel for the gradual loss in linear elastic response starting at about 1% strain.

The test data at 1800°F (Figure 15) are linear above the cusp, although the response is offset in the stress direction, due to the data interpretation system. This is best seen by parallel shifting a straight-edge below to above the cusp. The linear behavior appears to extend to about 2% strain. The 1800°F data in Figure 16 indicate that the ceramic did not take up load until after about 0.8% strain. If the two curves are superimposed but shifted in the strain direction, one can again see a reasonable sense of an initial linear portion of the curve, to about 2% strain, before the ceramic shows nonlinear softening. The data in Figure 20 for 1800°F have been corrected by taking the fitting point for the data reduction model to be above the indicated cusp level.

The **exposed** specimen at 1000°F in Figure 17 is fitted by a high initial elastic slope (see Figure 20). However, if we use the trend from the earlier figures, we might take the modulus to be the fit from about 0.5% strain out to about 0.1% strain. This value of slope is more consistent with the trend line drawn in Figure 20, again shown by a shift in the original interpreted test point.

The initial modulus of the **exposed** 1800°F data (Figure 18) appears low, compared with the trend line. However, again consistent with the other 1800°F test data, if we take the elastic response from about 0.9% strain for fitting a linear response up to about 2% strain, the modulus agrees with the unexposed data. The exposed specimen response at 1800°F (Figure 18) may be very easily superimposed on the unexposed data (Figure 16). The negligible difference between these two is a strong contraindication of any effect of exposure, at least at the test temperature of 1800°F.

The 2000°F test data were limited to a very small strain range. The test record was linear. If the bimaterial response model is applied, the data point shown in Figure 20 predicts a very low modulus for the ceramic. However, if we assume, consistent with other **high** temperature test results, that the ceramic is not active over this range, the test record modulus is reasonably close to the substrate modulus at 2000°F data. Thus, we recommend using the trend line for this test condition.

The 2200°F data (Figure 19) also indicate a considerable strain in the bimaterial specimen before any effect of the ceramic can be seen. After about 0.8% strain, the response is nearly elastic with a slight effect of softening, due to creep in the bimaterial system (both constituents creeping). If the data after 0.8% strain are used to fit a modulus result, the data point appears quite consistent with the extrapolation of the trend line in Figure 20.

The ceramic response in compression is judged to be linearly elastic up to strain levels of about 1-3% strain with an onset of strain softening at that point, up to 1800°F. Beyond that temperature, the linear strain limit drops again to about 2%, a possible indication of rate effects due to creep. The actual, detailed results show considerable scatter at low strain levels, and engineering judgment is required to get consistent modulus results.

The onset of strain softening is seen to increase with strain level, from about 1% strain at RT to about 3% strain at 1800°F, prior to the onset of significant rate effects. A possible explanation for this could be the reduced notch sensitivity of the material at the higher temperatures (seen in plasma sprayed TBC), leading to less fracture sensitivity of the microdefects, in compression.

No effect of residual stress can be seen in the compression data. The strain at which the break in the substrate response is used for the bilinear curve is shown as an arrow head on the strain scale. Except for the RT test, the break point is on the order of 0.7-0.75% strain. If we use the likely explanation of the high breakpoint for the RT test, this breakpoint is consistent with the others.

No conclusion should be drawn regarding the existence of a residual stress for the actual component condition. The compressive specimen is relatively short, and the substrate is quite thin (flexible) compared with the component. We believe that the residual stress effect for these conditions is likely to be too small to detect, given the level of crudeness necessary in this data reduction system.

## 2.4.2 Tension Data

The tension testing was qualitatively more difficult to interpret than the compression testing data. The simple reason, of course, is the lack of any significant tensile strength in the ceramic. However, unlike the expectation prior to test, the ceramic does have *some* apparent tensile strength. The following discussion will attempt to provide some interpretation of the tension test results.

In general, the tensile behavior of the ceramic was seen to be elastic, up to a fracture strain. At that point the ceramic ceased to have axial load carrying capability, but did act to reinforce the substrate. In fact, the substrate single crystal material was found to exhibit absolutely simple, pure slip at RT without any indication of slip localization. The strain capacity of the substrate was enormous under these conditions. While of little design importance, the phenomenon of reinforcement was very striking. The reinforcement may affect the response of the substrate above the point of fracture of the ceramic.

The tensile testing procedure was changed from the original proposal to better evaluate some of the unique phenomena of the ceramic's tensile behavior. Based on the compression test results, we concluded that exposure had negligible, if any, effect on the ceramic response. We also deduced that above 1400°F, the ceramic indicated an increasing creep rate. This behavior would also be expected in tension, but is not judged to be of great importance, given the very limited tensile strength of the ceramic.



The deduced ceramic response is only meaningful out to the point of maximum predicted load. At that point, the ceramic does fracture (physical evidence during testing), and the load carrying capacity of the ceramic decreases, probably quickly as the strain is further increased and more cracking occurs. The test design did succeed in minimizing the effect of the substrate on the tensile bar stiffness, and the bulk of the initial stiffness response is due to the tensile stiffness of the ceramic.

The RT testing resulted both in pronounced, ideal slip in the bimaterial specimen data (Figure 21), and in sudden fracture of the substrate (Figure 22). The deduced RT tensile modulus was judged to be higher than the trend line (shown for the compression specimen data fit in Figure 32). The ceramic fracture strain in Figure 21 is about 0.2% strain. In the Figure 22 result, the substrate may have fractured prior to achieving fracture of the ceramic. After fracture of the ceramic, the tensile bar load is all being carried in the metal substrate. Due to ceramic load shedding during fracture, the substrate quickly acquires enough load to yield.

The first test result at 1400°F (Figure 23) shows linear substrate response following failure of the ceramic at about 0.2% strain. The second test record (Figure 24) indicates about the same general level of strain tolerance (0.2% strain), but considerably less stiffness. Vertical shifting of the test results for superposition indicates significant variability in substrate elastic response. The variability in the test results in tension, shown for these two specimens and the others, may be due both to thickness variations in these very thin metal substrates and to the possible effect of the thinness on elastic response of the single crystal.

The 1600°F data (Figure 25) clearly indicate linear substrate response with the fracture strain of the ceramic at about 0.1% strain. However, the substrate modulus indicated in the extended elastic response curve shows a value well below that expected for 1600°F. The low substrate modulus is consistent with overpredicting the ceramic response.

The 1800°F data in Figure 26 indicate the point of ceramic fracture to be about 0.08% strain. The second test result (Figure 27) probably has no ceramic strength in spite of what the data reduction system shows. The modulus of the substrate is again probably too low, resulting in an inference that the ceramic is carrying load. However, the linear response all the way to about 0.8% strain indicates that this is the response of the substrate, not the ceramic.

The fracture strains of the ceramic at 2000°F and 2200°F are probably positive, but so small that they are hard to record reliably (note that Figure 28 is plotted at a very high sensitivity). The data interpretation problem is compounded by the increased creep effect in the substrate at these temperatures. The best estimate in the fracture strain comes from the 2200°F record, where the maximum tensile ceramic strain seems to be about 0.025% strain. The creep in the substrate results in an apparent ceramic hardening above the fracture strain as deduced by the data reduction model, but this result is not judged to be real.

The reducing trend in the tensile fracture strain of the ceramic is probably an effect of the residual stresses. As manufactured, the tensile specimens will lock in a tensile stress in the substrate and a compressive stress in the ceramic. Due to the very thin substrate used, the load sharing between the two is significant. If we take the stress-free temperature to be above 2200°F (assuming zero tensile strength of the ceramic), the predicted residual strain in the ceramic is about 1.4%.

The tensile testing program included planned load reversals at various strain levels to evaluate whether the ceramic fractures would close, causing a re-stiffening of the bimaterial specimen. The full cyclic test records for these tests are shown in Appendix C. The conclusion from reviewing these test records is affirmative, in that as the strain is reduced to the range of the apparent ceramic fracture strain, the specimens exhibited higher stiffness, consistent with the stiffness prior to ceramic fracture. The data also indicate, as expected, that creep in the substrate negates this closure effect unless one were to drive the specimen into compression (this was not possible in the current loading arrangement). We therefore conclude that the mechanism of ceramic failure is consistent with reducing the stiffness to zero above a critical strain level, but requires a bilinear model to account for closure effects as strain is reduced below the critical value. Creep growth of the substrate must be included to obtain the correct interaction with ceramic crack closure.

The tensile modulus data have considerable scatter, owing to the extreme sensitivity of the data acquisition system for the bimaterial specimen. However, the data indications are consistent with the data obtained in compression. The failure mode in tension appears to be brittle fracture above a small strain, and the fracture strain may be strongly dependent on the stress-free temperature effect and creep of the substrate.

### 2.4.3 Creep Data

Three compressive, sustained load, creep tests were performed on Specimen 21, at three temperatures: 1400°F, 1600°F, and 1800°F. All three tests were performed at load levels below the proportional limit of the compression tests performed at the respective temperature levels. Using the fitted ceramic elastic modulus data from Figure 20 and the applied load value, the elastic stresses in the ceramic were 11037 psi, 8880 psi, and 7611 psi, respectively.

A viscoplastic model for the composite system is recommended to obtain the correct flow stress in each material. The reason is that the creep strain in each material is the same as the composite creep strain. The stress in each material is then that stress which will produce the resulting strain rate and satisfy equilibrium with the applied load. It can be expected that this stress will not be the same as the elastic stress, given above. Therefore, before final use of the strain rate versus stress for the ceramic, it is recommended that Pratt & Whitney apply the viscoplastic model for PWA 1480 at the strain rates given in Table V, predict the PWA 1480 stress level, and determine a corrected ceramic stress that satisfies equilibrium with the applied load.

The creep tests show a clear primary creep transition and approach a steady creep rate for each temperature. The creep rate data in Table V were obtained by a simple, estimated linear fit to the final portion of the strain versus time plot for these tests, for which the data are given in Appendix D. A preliminary comparison of the EB-PVD creep rate at 1800°F with that for plasma sprayed coating (PWA264) indicates that the current TBC is more creep resistant than the plasma sprayed coating.

### 3 References

1. Timoshenko, S. P., and Goodier, J. N., Theory of Elasticity, 3rd ed., McGraw-Hill Book Co., New York, 1970, pp. 69-71.
2. Boresi, A. P., and Sidebottom, O. M., Advanced Mechanics of Materials, 4th ed., John Wiley and Sons, New York, 1985, pp. 492-500.
3. Private Communication (FAX re Elastic Modulii for PWA 1480 SC), Mr. David Nissley, Pratt & Whitney, 31 January 1990.

---

## 4 EBPVD Tables and Figures

**TABLE I**  
**COMPRESSION TEST MATRIX**

Specimen Number	Specimen Type	Test Mode	Temp (°F)	Specimen Inside Diameter (Inch)	Ceramic Thickness (Inch)	Substrate Wall Thickness (Inch)
17	Substrate	Compr	1400	0.7046	--	0.022
18	Coated	Compr	RT	0.7060	0.085	0.022
19	Coated	Compr	1400	0.7061	0.085	0.022
20	Substrate	Compr	RT	0.7040	--	0.022
21	Coated	Str Relax	1400	0.7056	0.085	0.022
		Creep	1400			
		Creep	1600			
		Creep	1800			
		Compr	1400			
24	Exp-Coated	Compr	1800	0.6598	0.069	0.045
25	Coated	Compr	1800	0.6598	0.082	0.045
26	Coated	Compr	1800	0.6598	0.082	0.045
27	Coated	Modulus	400	0.6599	0.074	0.045
		Modulus	800			
		Modulus	1000			
		Modulus	1200			
		Modulus	1600			
		Modulus	2000			
28	Exp-Coated	Compr	2200	0.6597	0.076	0.045
30	Exp-Coated	Compr	1000	0.7060	0.077	0.022
31	Substrate	Compr	2200	0.6596	--	0.045
32	Substrate	Compr	1800	0.6599	--	0.045
33	Substrate	Compr	1000	0.6590	--	0.045
34	Substrate	Compr	1000	0.7005	--	0.022

**TABLE II**  
**TENSILE TEST MATRIX**

Specimen Number	Specimen Type	Test Mode	Temp (°F)	Specimen Inside Diameter (Inch)	Interface Diameter (Inch)	Outside Diameter (Inch)
653601	Substrate	Standard	RT	0.7506	N/A	0.7632
653605	Substrate	Standard	1400	0.7518	N/A	0.7652
653701	Substrate	Standard	1800	0.7515	N/A	0.7649
653702	Substrate	Standard	2200	0.7524	N/A	0.7652
652801	Coated	Standard	RT	0.7510	0.7636	0.8690
652805	Coated	Standard	RT	0.7505	0.7637	0.9620
652902	Coated	Standard	1400	0.7507	0.7641	0.9510
653503	Coated	Standard	1800	0.7502	0.7630	0.9535
653504	Coated	Standard	2200	0.7517	0.7647	0.9495
653602	Coated	Standard	1400	0.7499	0.7633	0.9530
653603	Coated	Standard	2000	0.7527	0.7655	0.9520
653704	Coated	Standard	1600	0.7517	0.7641	0.9422
652802	Coated	Optional	1800	0.7525	0.7659	0.9752
652803	Coated	Optional	2200	0.7510	0.7636	0.9525
653502	Coated	Optional	1400	0.7530	0.7630	0.8635

**TABLE III**  
**CERAMIC MODULUS IN COMPRESSION VERSUS TEMPERATURE**  
**FOR UNEXPOSED AND EXPOSED TBC**

Specimen ID	Temperature (°F)	Ceramic Modulus (x10 <sup>6</sup> psi)
Unexposed		
18A	75	6.96
27A1	400	3.50
27B1	800	2.82
27C2	1000	2.44
27D2	1200	2.52
19	1400	2.31
21D	1400	2.50
21E	1400	5.40 <sup>(1)</sup>
27E2	1600	2.12
25	1800	2.48
26	1800	0.373
27F2	2000	0.544
Exposed		
30	1000	3.79
24	1800	0.957
28	2000	0. <sup>(2)</sup>

- (1) Specimen was a second test of 21D.  
(2) Ceramic modulus is very small.

**TABLE IV**  
**CERAMIC MODULUS IN TENSION VERSUS**  
**TEMPERATURE FOR UNEXPOSED TBC**

Specimen ID	Temperature (°F)	Ceramic Modulus (x10 <sup>6</sup> psi)
Unexposed		
652801	72	6.15
652805	72	6.12
653502	1400	4.92
653602	1400	0.770
652902	1400	0.874
653704	1600	4.10
653503	1800	4.28
652802	1800	0.607
652803	2200	2.08
653504	2200	2.03



**TABLE V**  
**CREEP RATE DATA**  
**COMPRESSION TESTS**

<b>Temperature (°F)</b>	<b>Load (Pounds)</b>	<b>Strain Rate (in/in/sec)</b>
1400	6110	2.4E-8
1600	5020	5.6E-8
1800	4250	8.3E-8

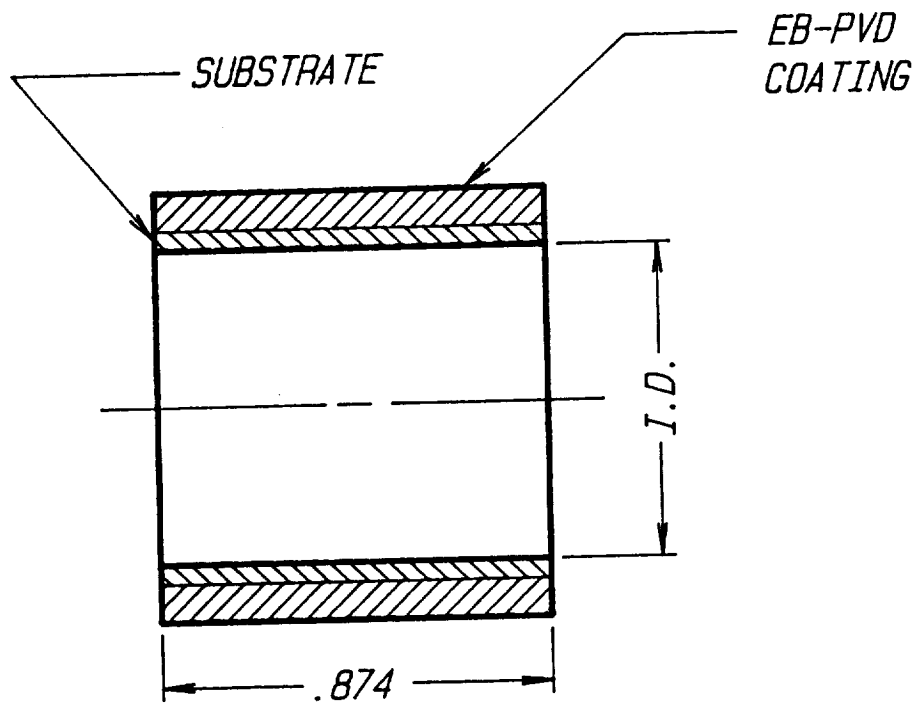


FIGURE 1. COMPRESSION SPECIMEN

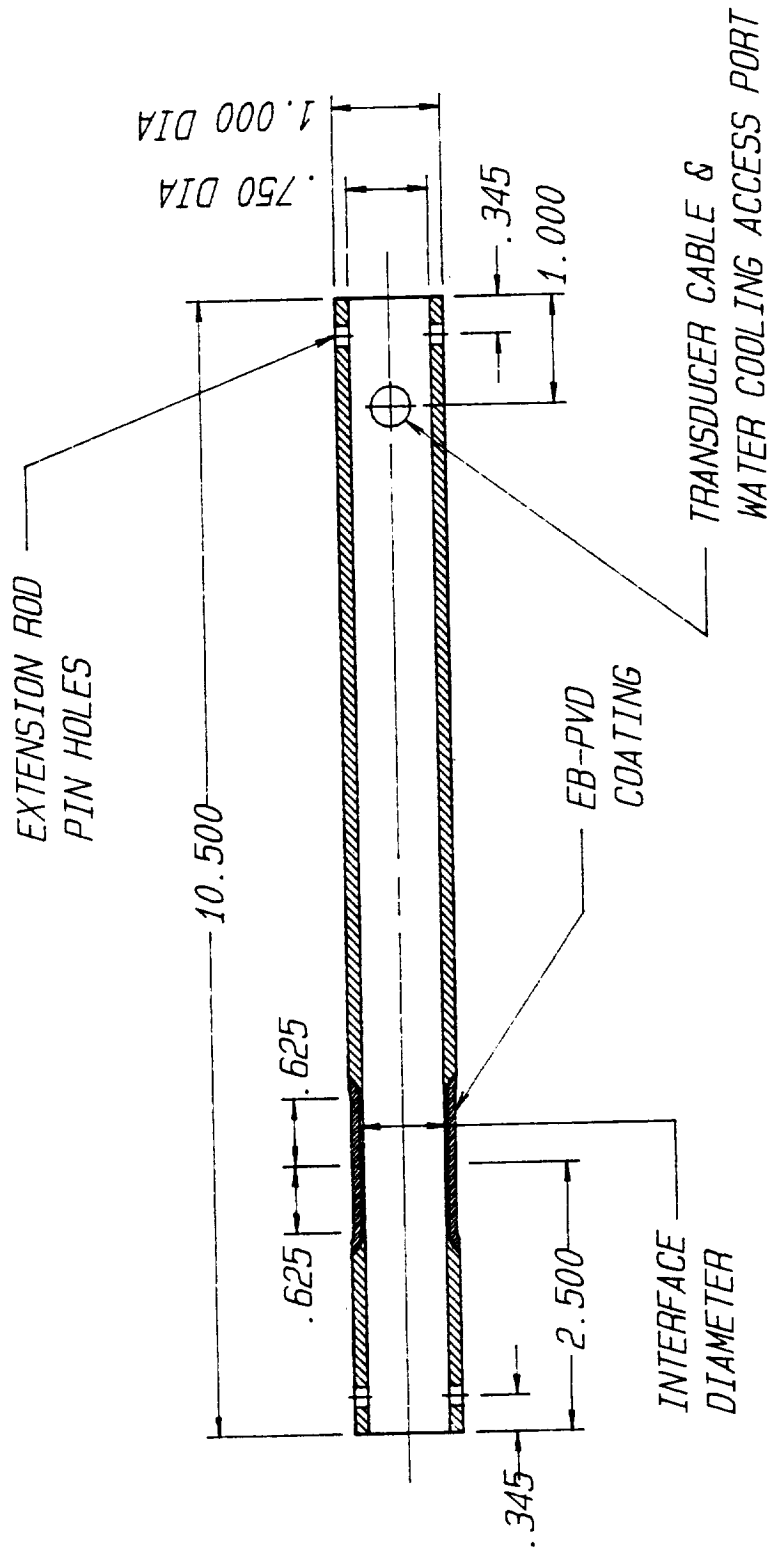


FIGURE 2. TENSILE SPECIMEN

ORIGINAL PAGE  
BLACK AND WHITE PHOTOGRAPH

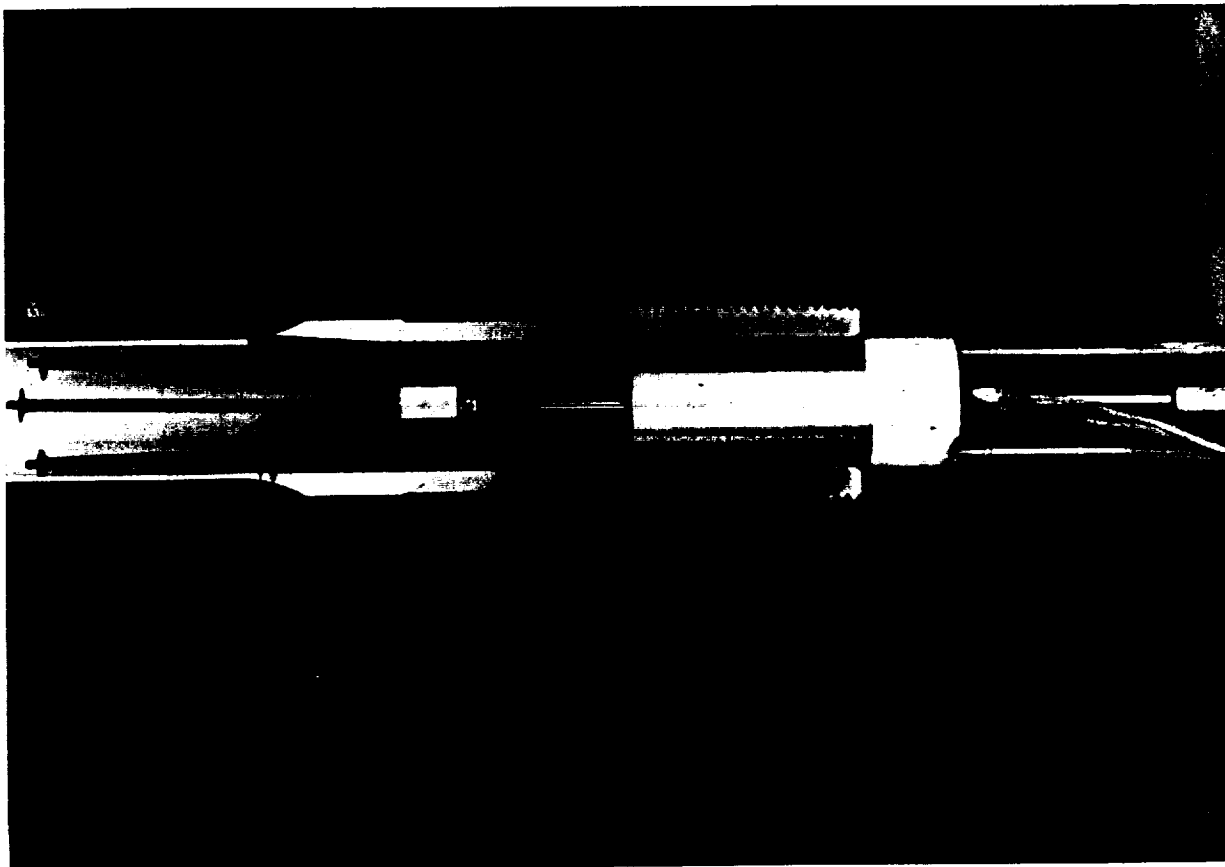


FIGURE 3. BIAXIAL TRANSDUCER

ORIGINAL PAGE IS  
OF POOR QUALITY

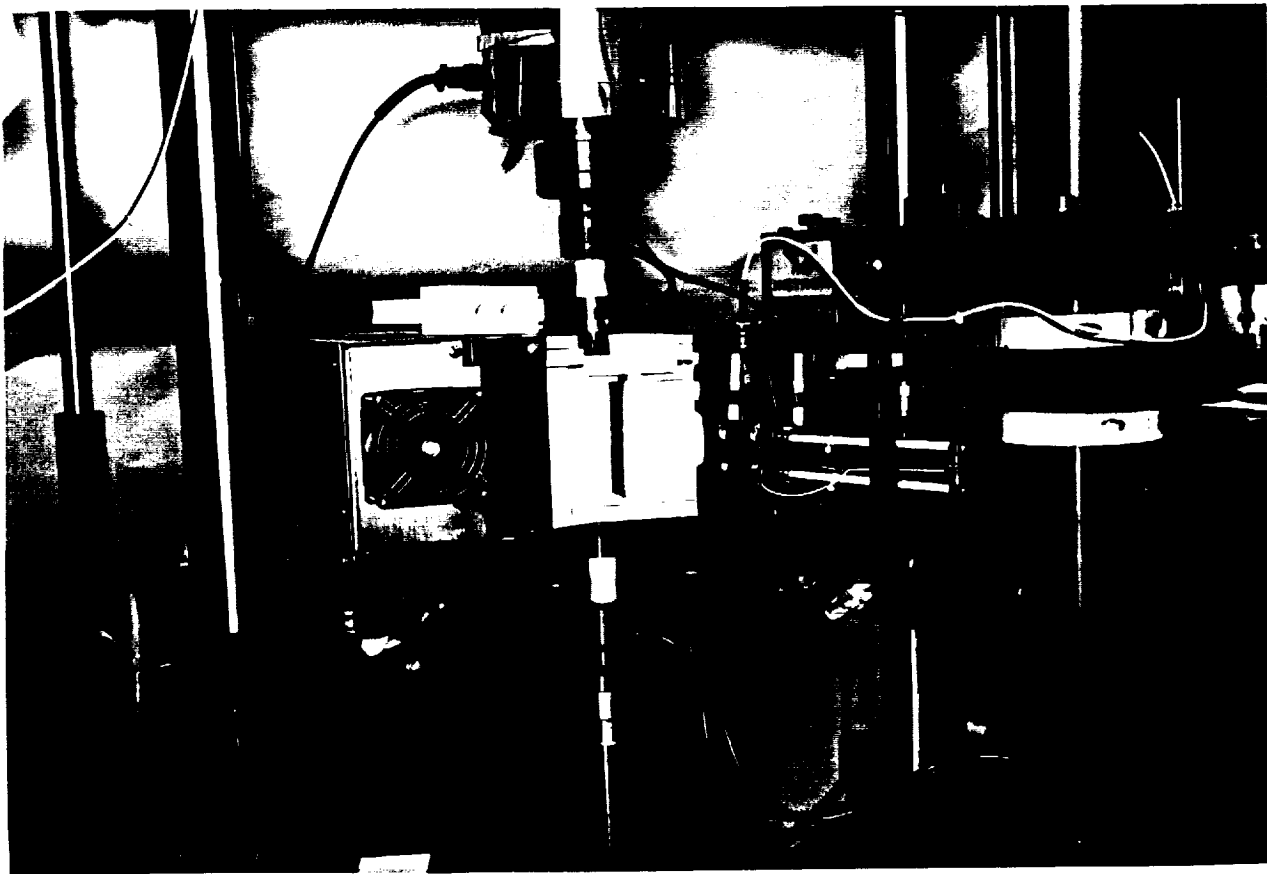
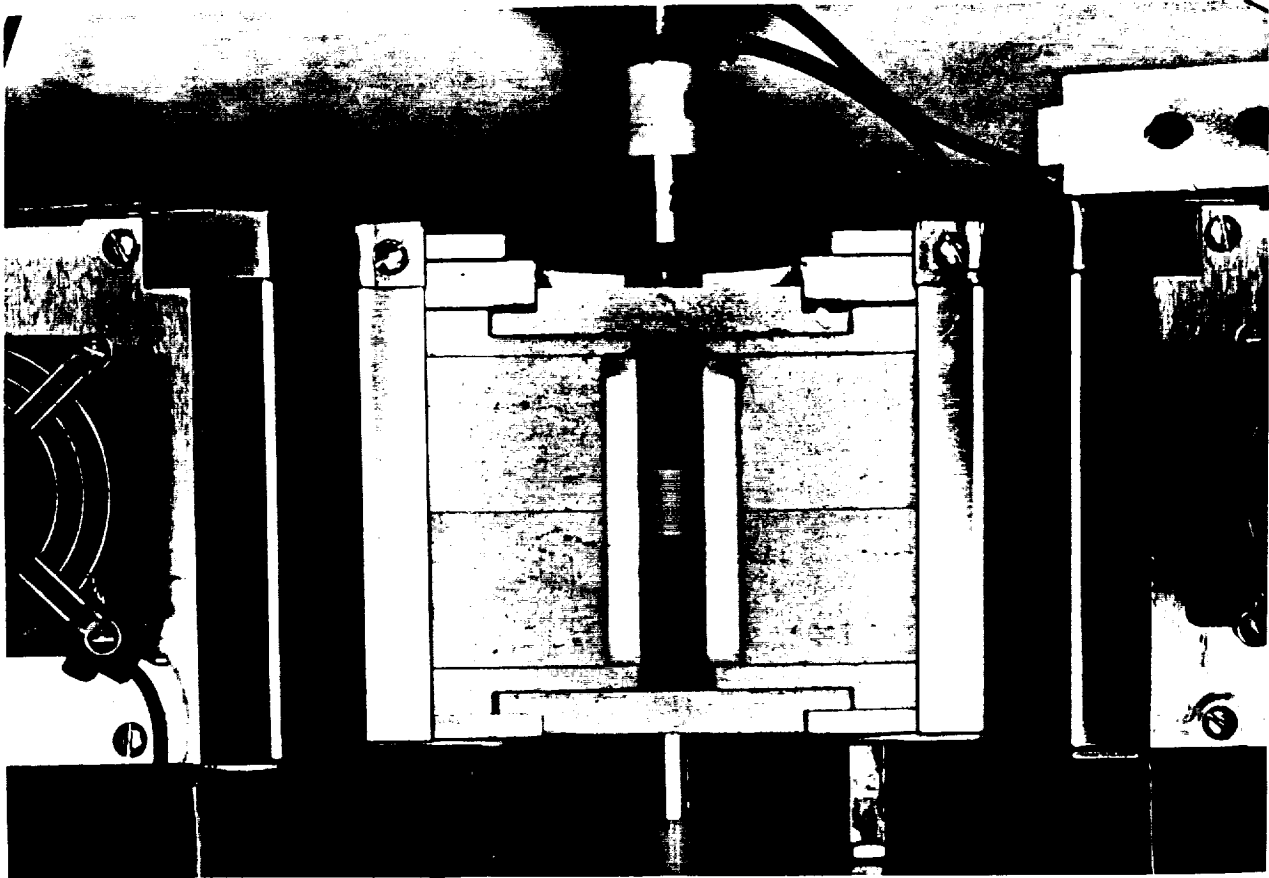
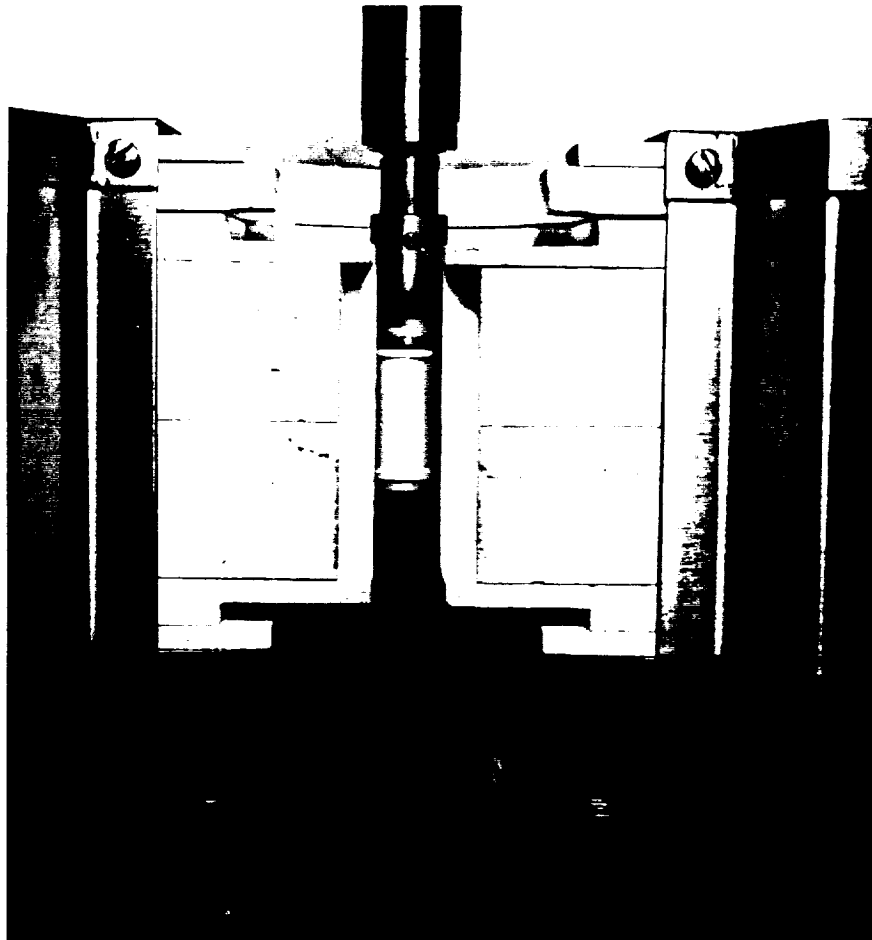
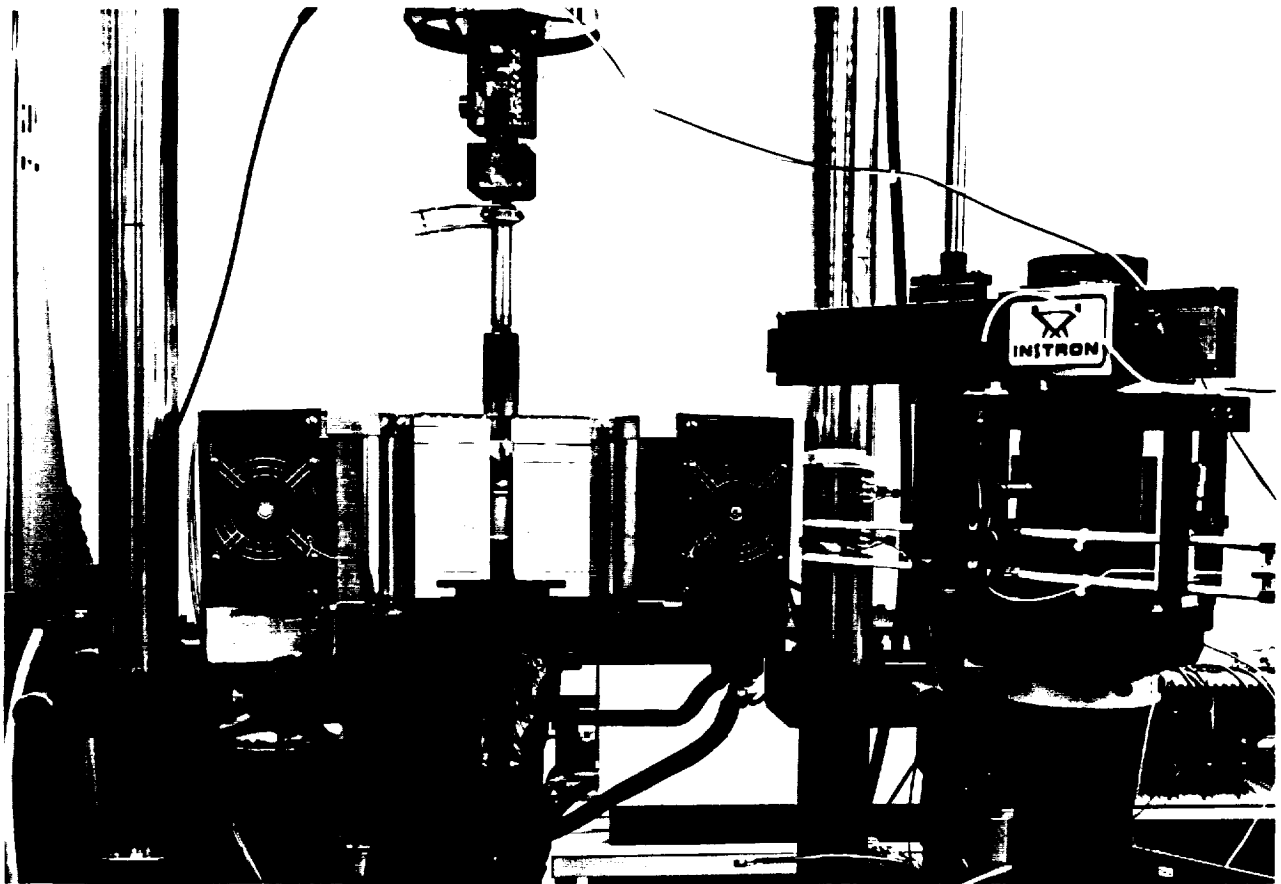


FIGURE 4. COMPRESSION TEST SETUP



ORIGINAL PAGE IS  
OF POOR QUALITY

FIGURE 5. TENSION TEST SETUP

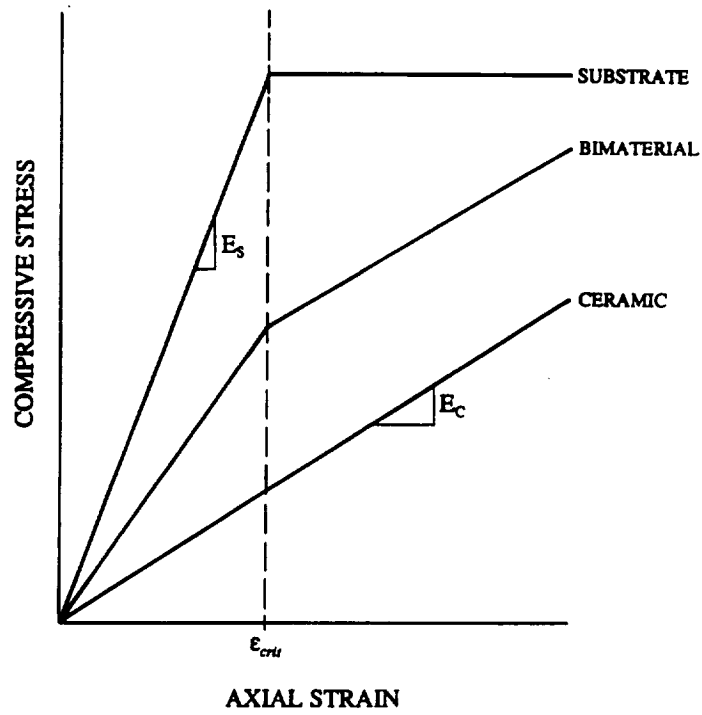


FIGURE 6. SCHEMATIC COMPRESSION TEST RESPONSE

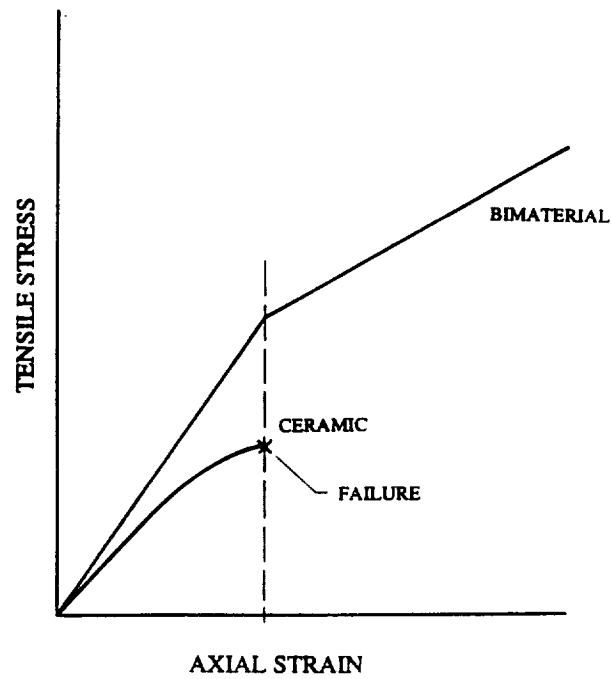


FIGURE 7. SCHEMATIC TENSION TEST RESPONSE

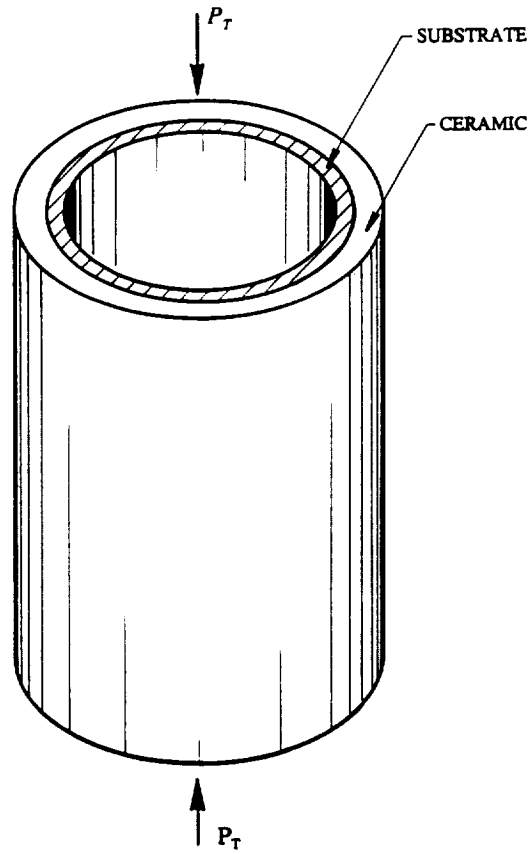


FIGURE 8. COMPRESSION TEST SPECIMEN

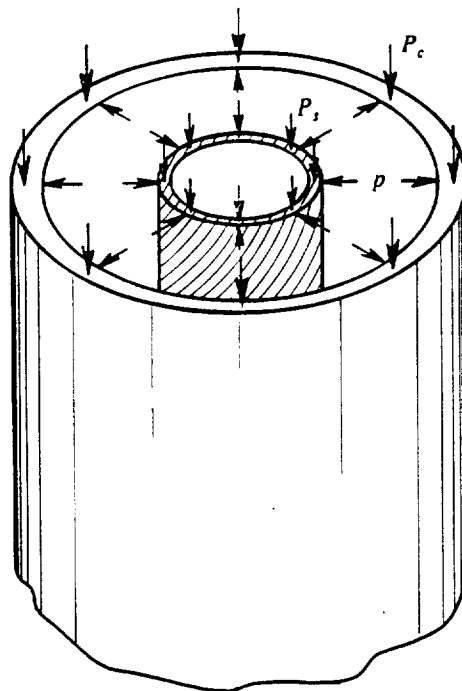


FIGURE 9. SCHEMATIC OF TEST MODEL



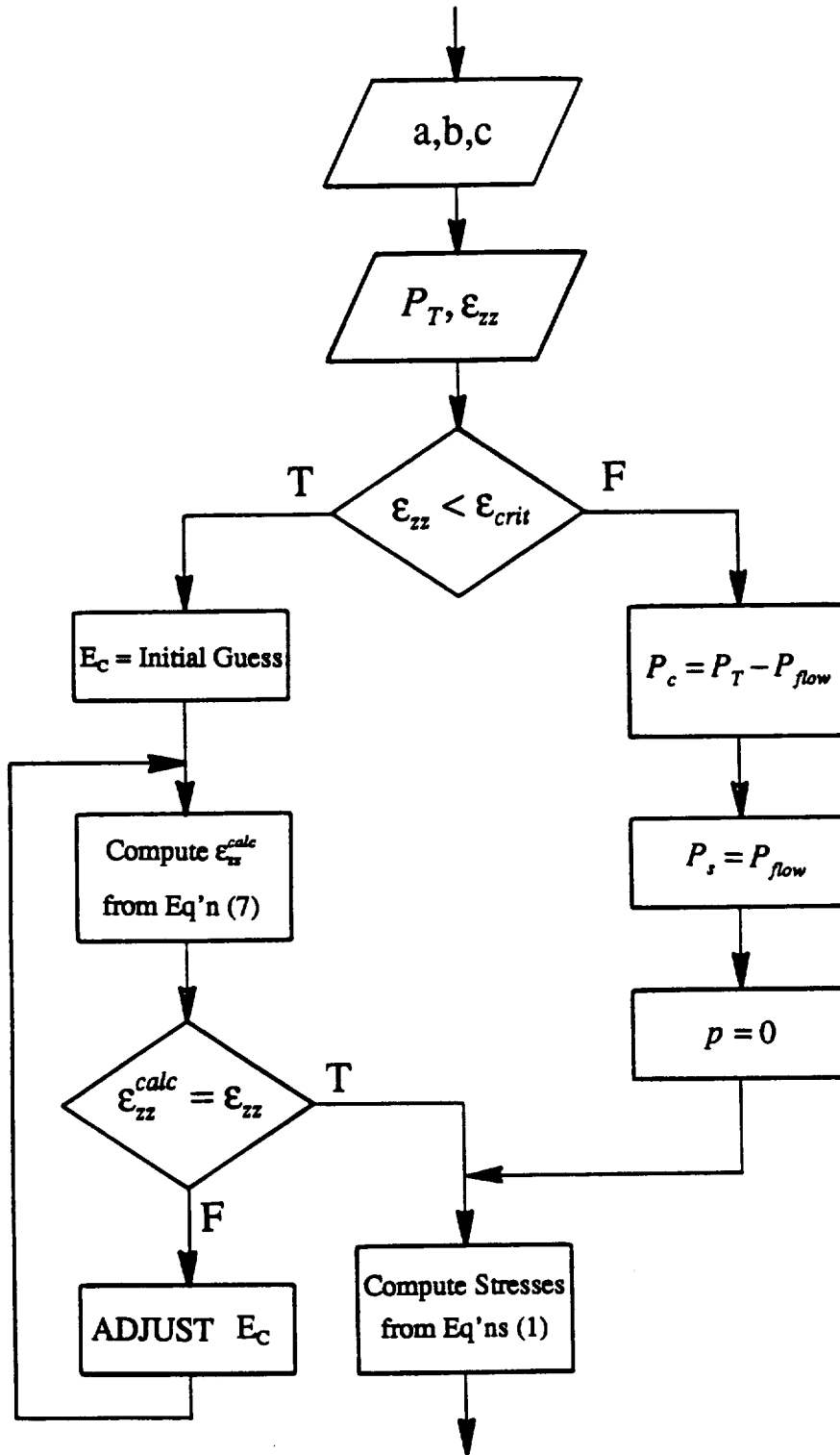


FIGURE 10. LINEAR ELASTIC MODEL FLOW CHART

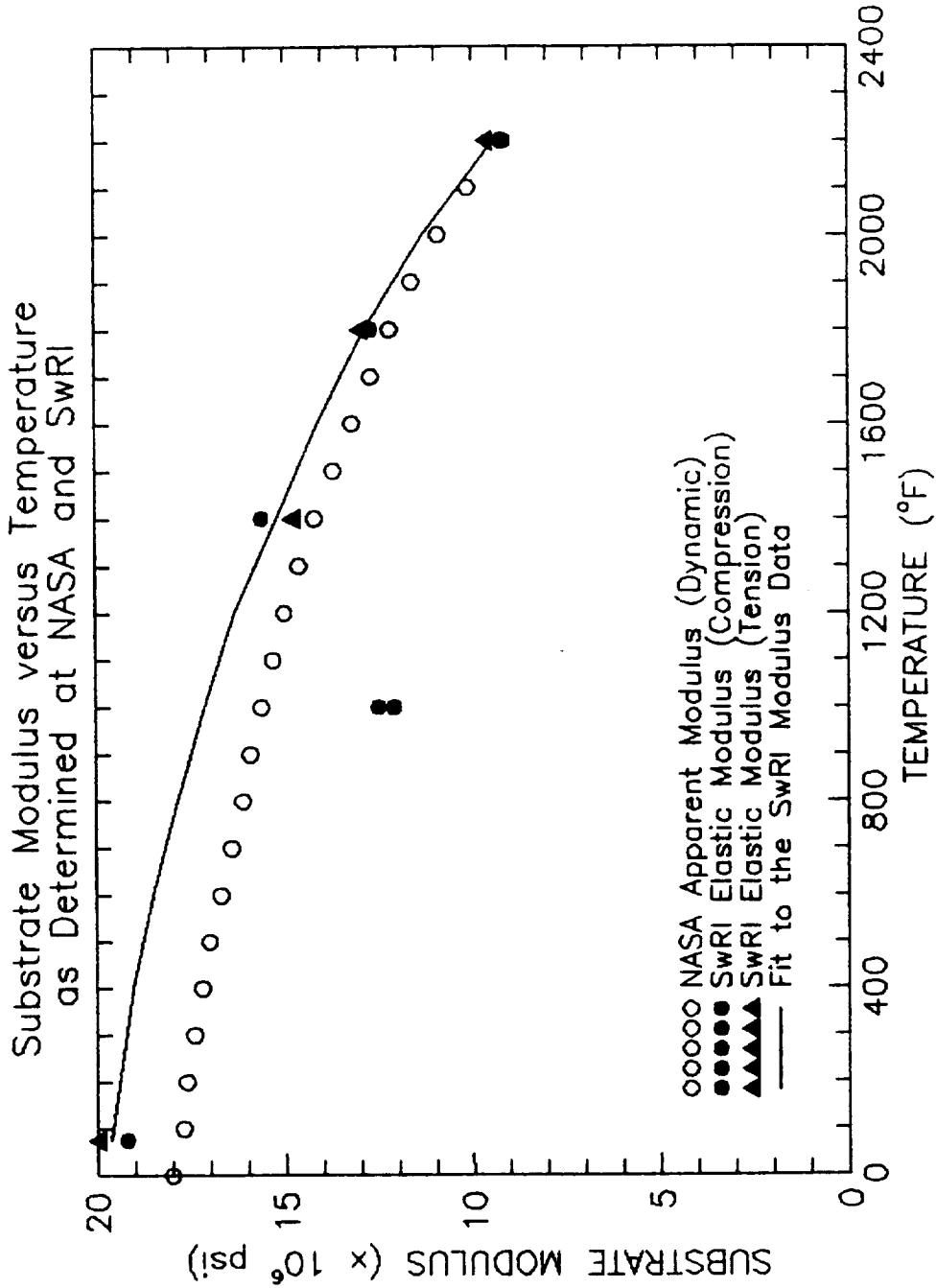


FIGURE 11. SUBSTRATE MODULUS VS TEMPERATURE  
AS DETERMINED AT NASA AND SwRI

Deduced Ceramic Response in Compression  
for Unexposed Specimen 18A at 75 °F

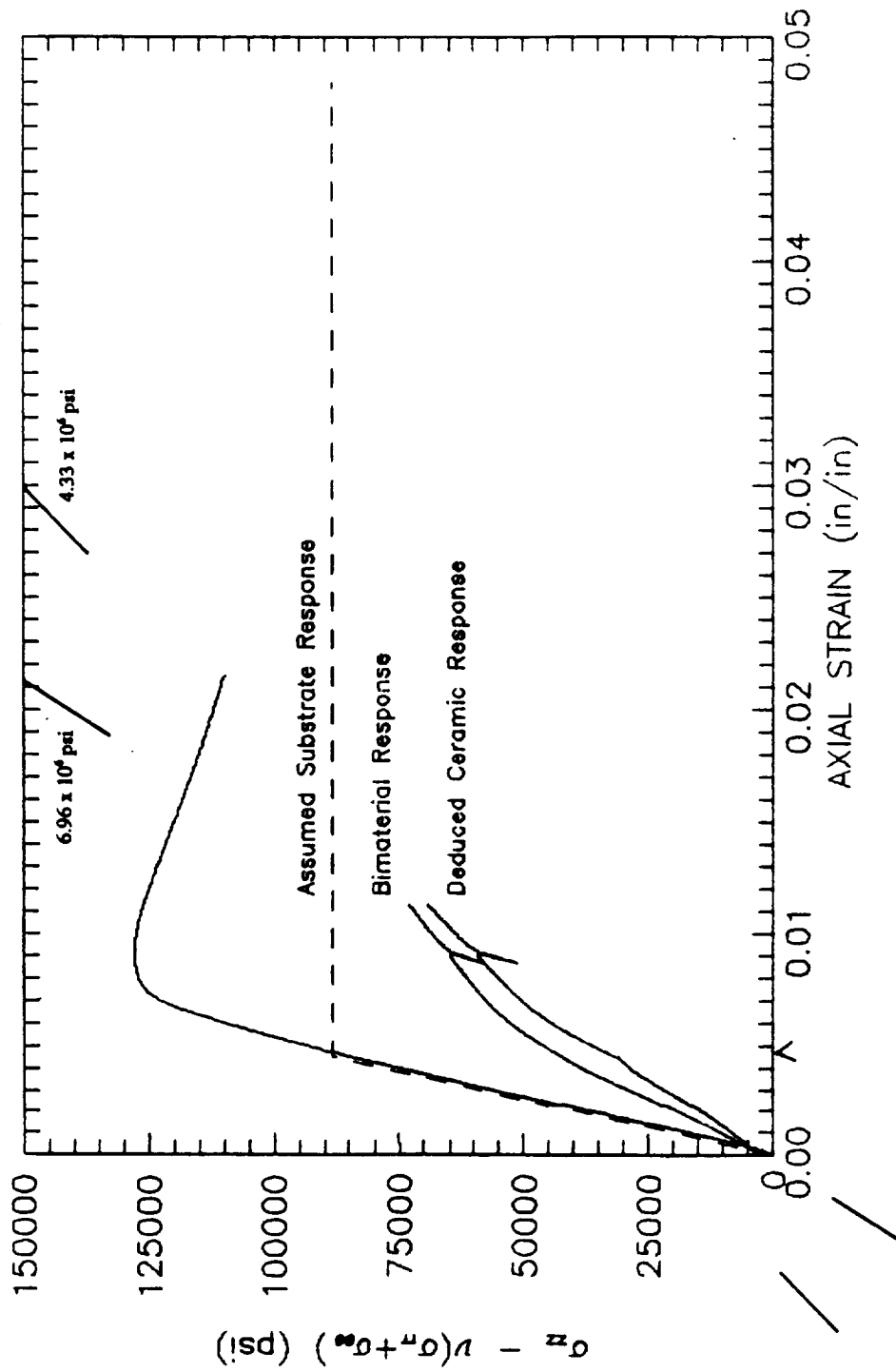


FIGURE 12. DEDUCED CERAMIC RESPONSE IN COMPRESSION  
FOR UNEXPOSED SPECIMEN 18A AT 75°F

Deduced Ceramic Response in Compression  
for Unexposed Specimen 19 at 1400°F

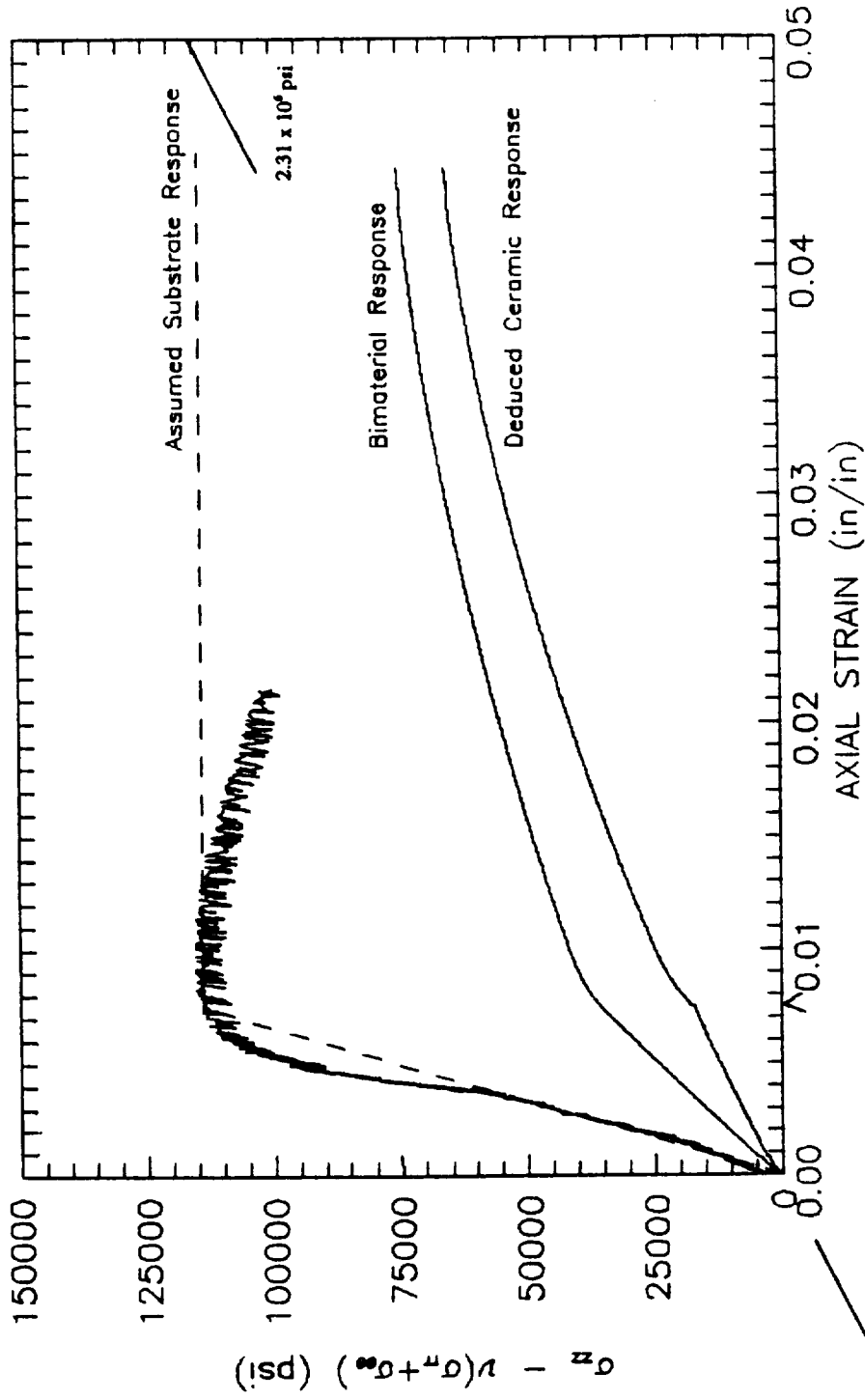


FIGURE 13. DEDUCED CERAMIC RESPONSE IN COMPRESSION  
FOR UNEXPOSED SPECIMEN 19 AT 1400°F

Deduced Ceramic Response in Compression  
for Unexposed Specimen 21D at 1400 °F

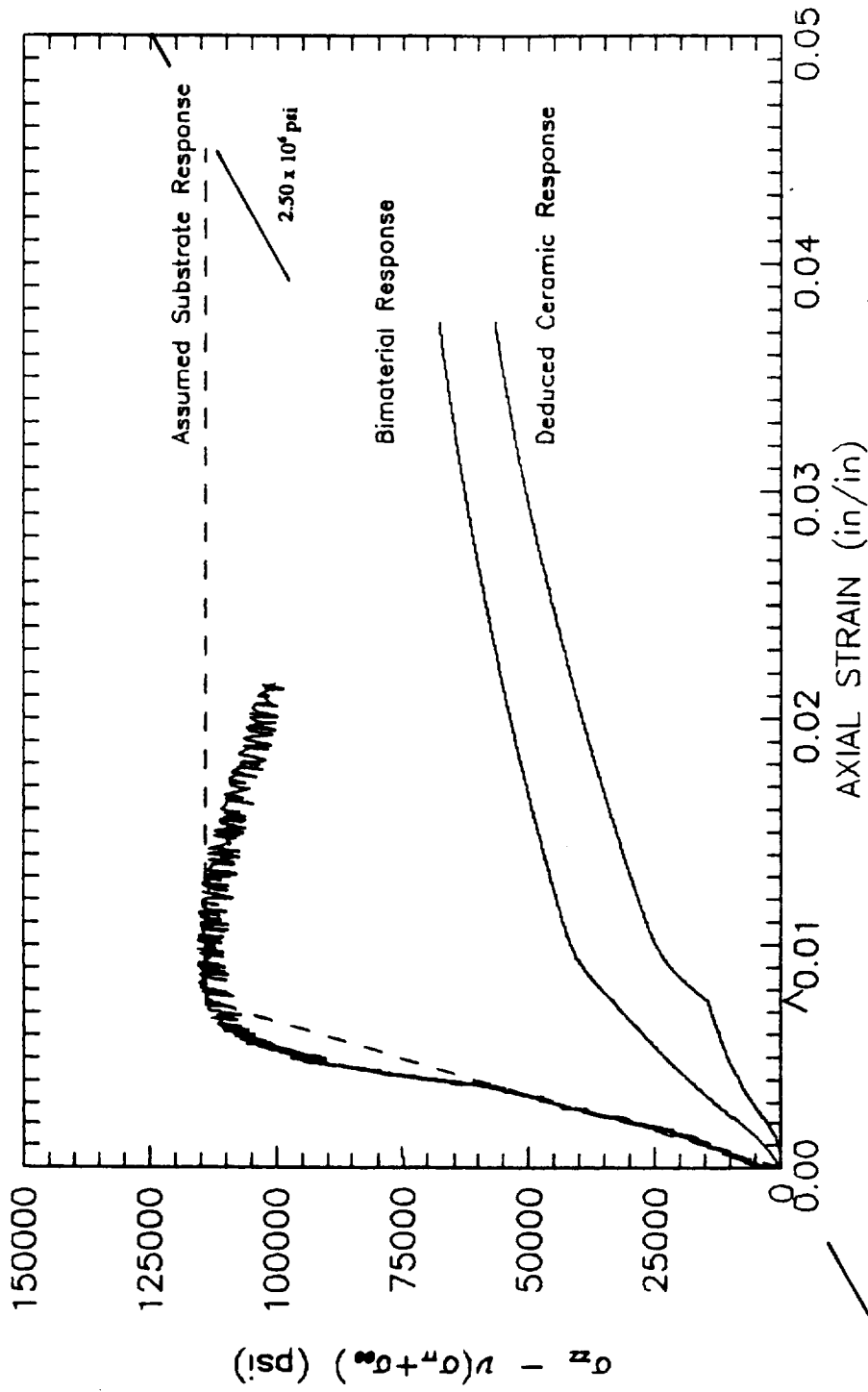


FIGURE 14. DEDUCED CERAMIC RESPONSE IN COMPRESSION  
FOR UNEXPOSED SPECIMEN 21D AT 1400°F

Deduced Ceramic Response in Compression  
for Unexposed Specimen 25 at 1800 °F

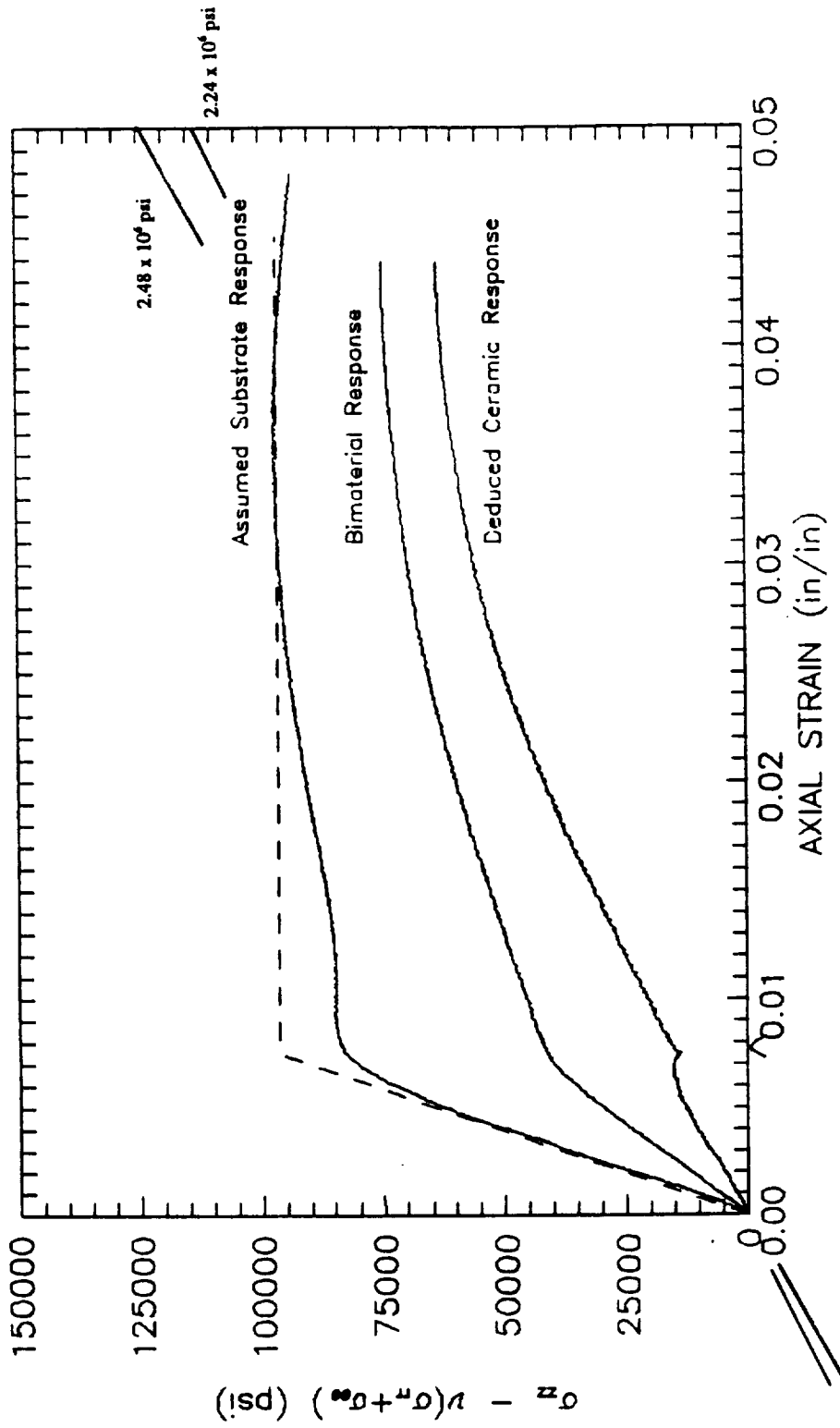


FIGURE 15. DEDUCED CERAMIC RESPONSE IN COMPRESSION  
FOR UNEXPOSED SPECIMEN 25 AT 1800°F

Deduced Ceramic Response in Compression  
for Unexposed Specimen 26 at 1800°F

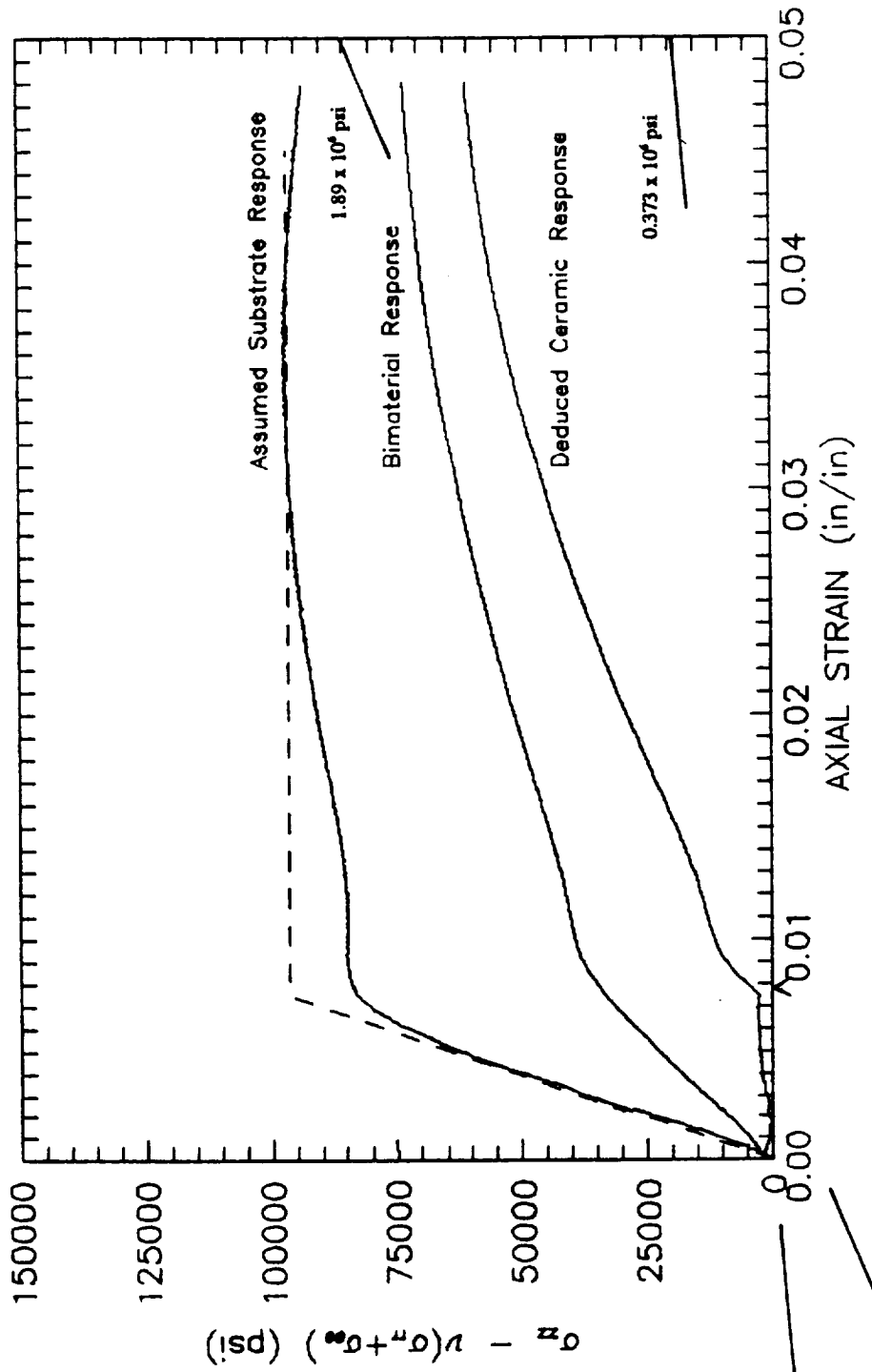


FIGURE 16. DEDUCED CERAMIC RESPONSE IN COMPRESSION  
FOR UNEXPOSED SPECIMEN 26 AT 1800°F

Deduced Ceramic Response in Compression  
for Exposed Specimen 30 at 1000 °F

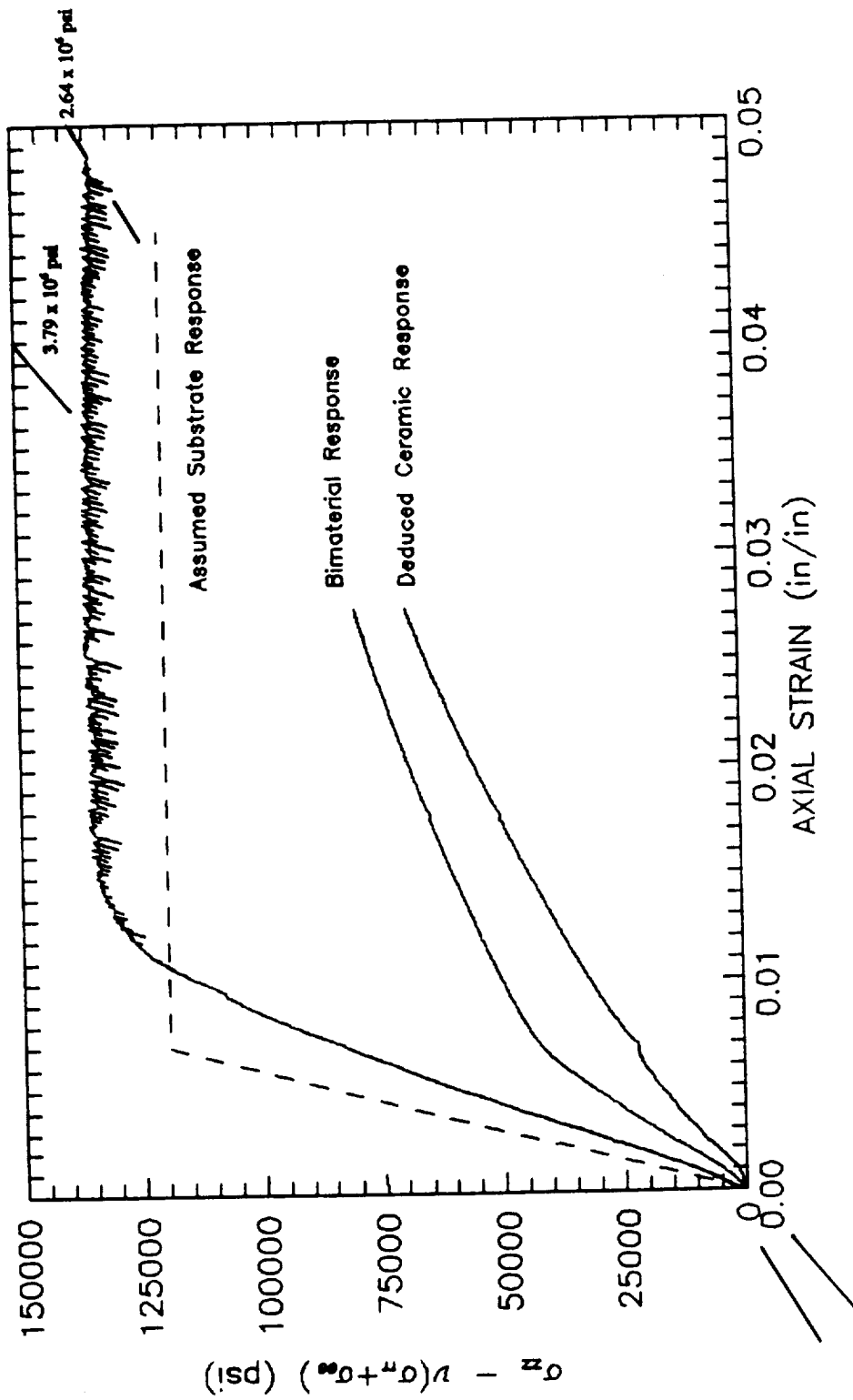


FIGURE 17. DEDUCED CERAMIC RESPONSE IN COMPRESSION  
FOR EXPOSED SPECIMEN 30 AT 1000°F



Deduced Ceramic Response in Compression  
for Exposed Specimen 24 at 1800 °F

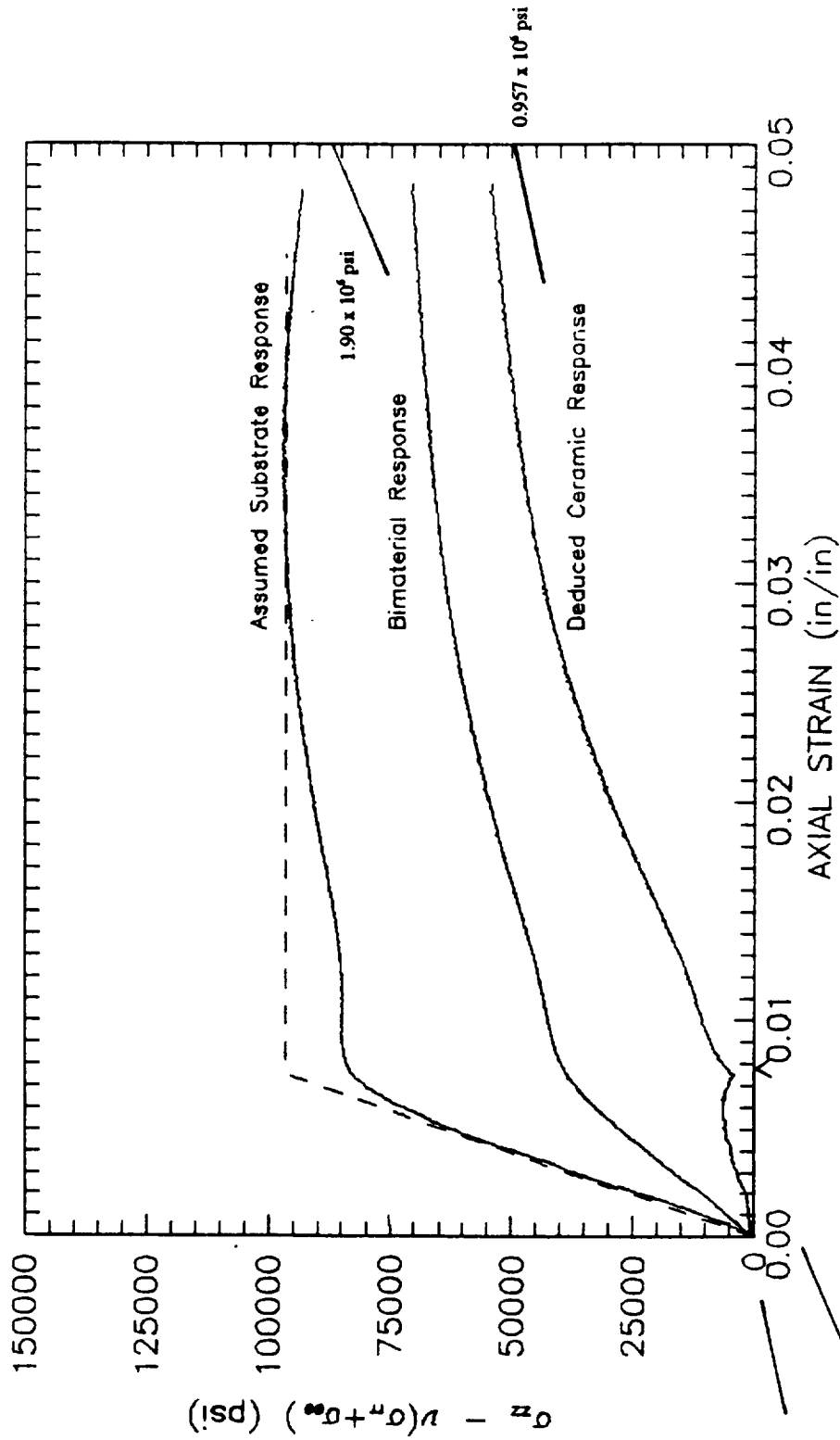


FIGURE 18. DEDUCED CERAMIC RESPONSE IN COMPRESSION  
FOR EXPOSED SPECIMEN 24 AT 1800°F

Deduced Ceramic Response in Compression  
for Exposed Specimen 28 at 2200 °F

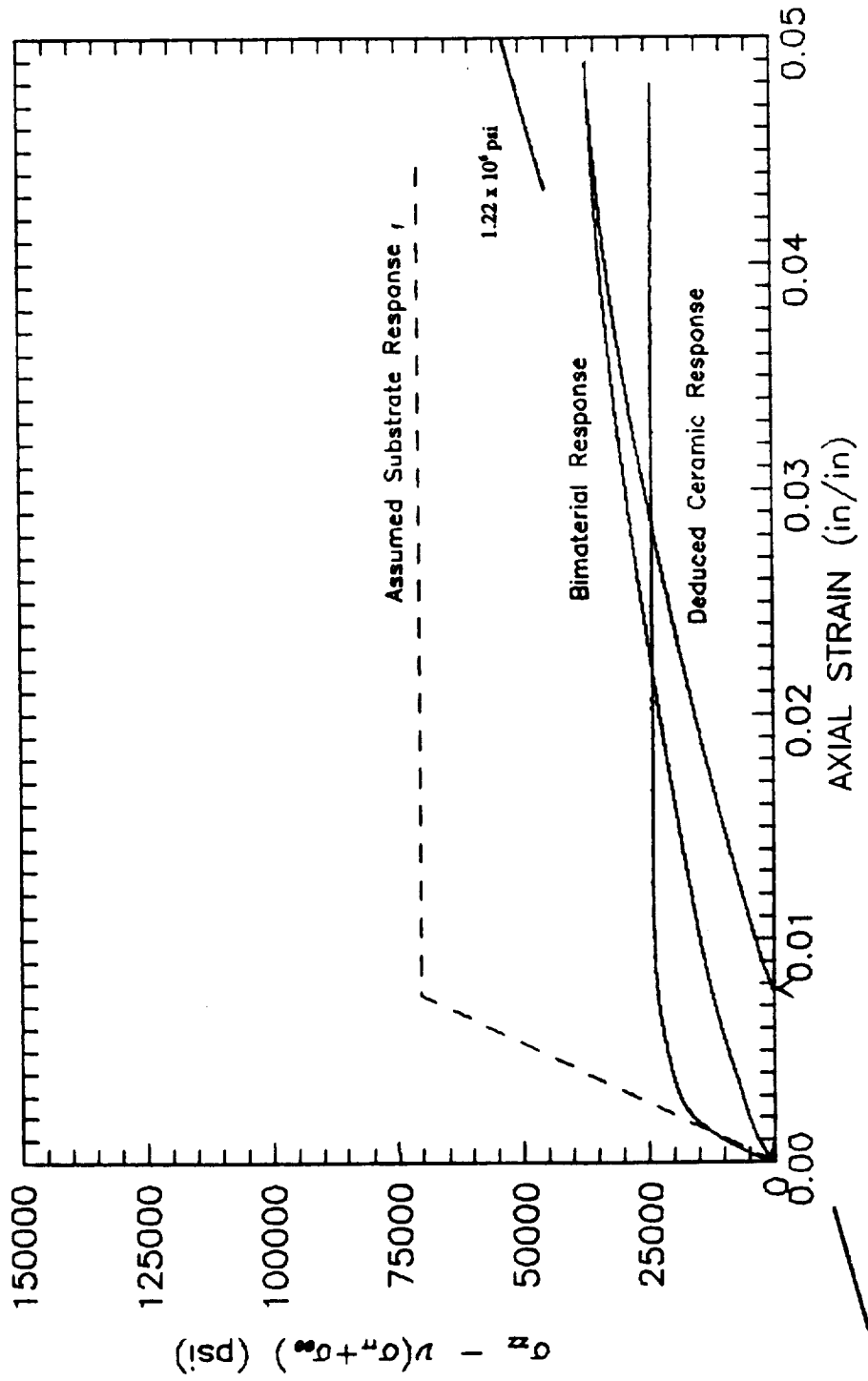


FIGURE 19. DEDUCED CERAMIC RESPONSE IN COMPRESSION  
FOR EXPOSED SPECIMEN 28 AT 2200°F

Compressive Ceramic Modulus as a Function  
of the Test Temperature

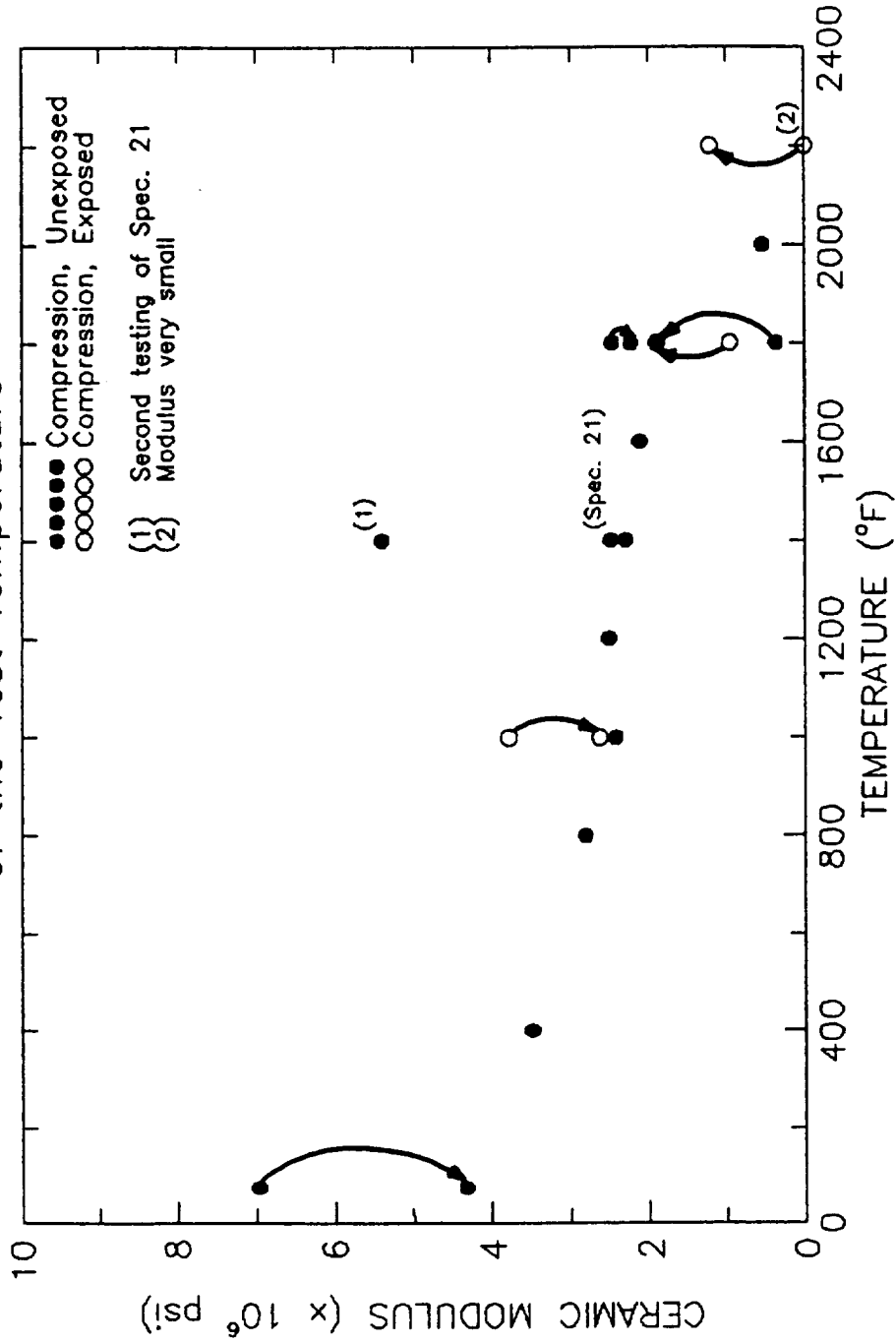


FIGURE 20. DEDUCED CERAMIC MODULUS AS A FUNCTION OF THE TEST TEMPERATURE

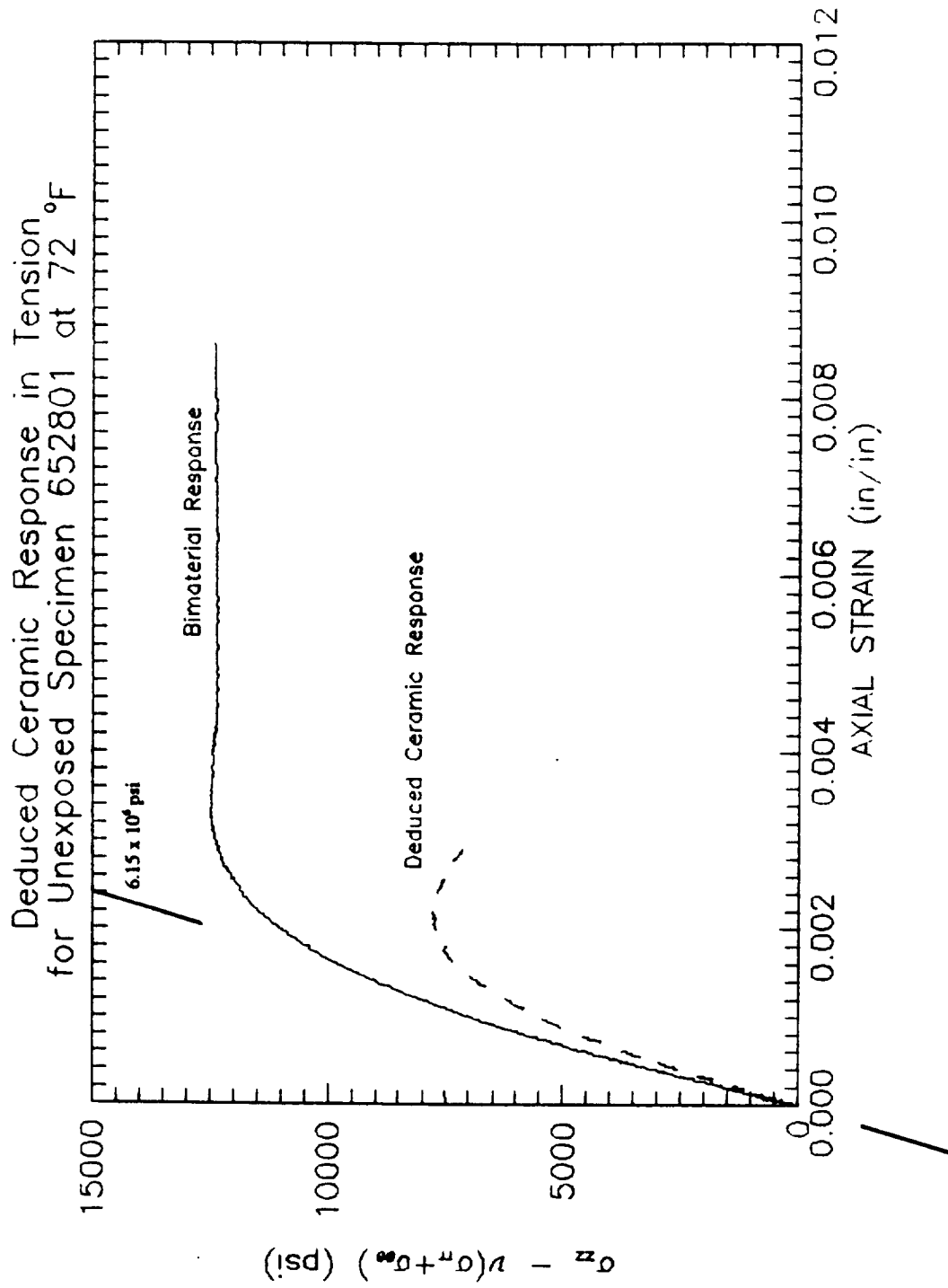


FIGURE 21. DEDUCED CERAMIC RESPONSE IN TENSION  
FOR UNEXPOSED SPECIMEN 652801 AT 72°F

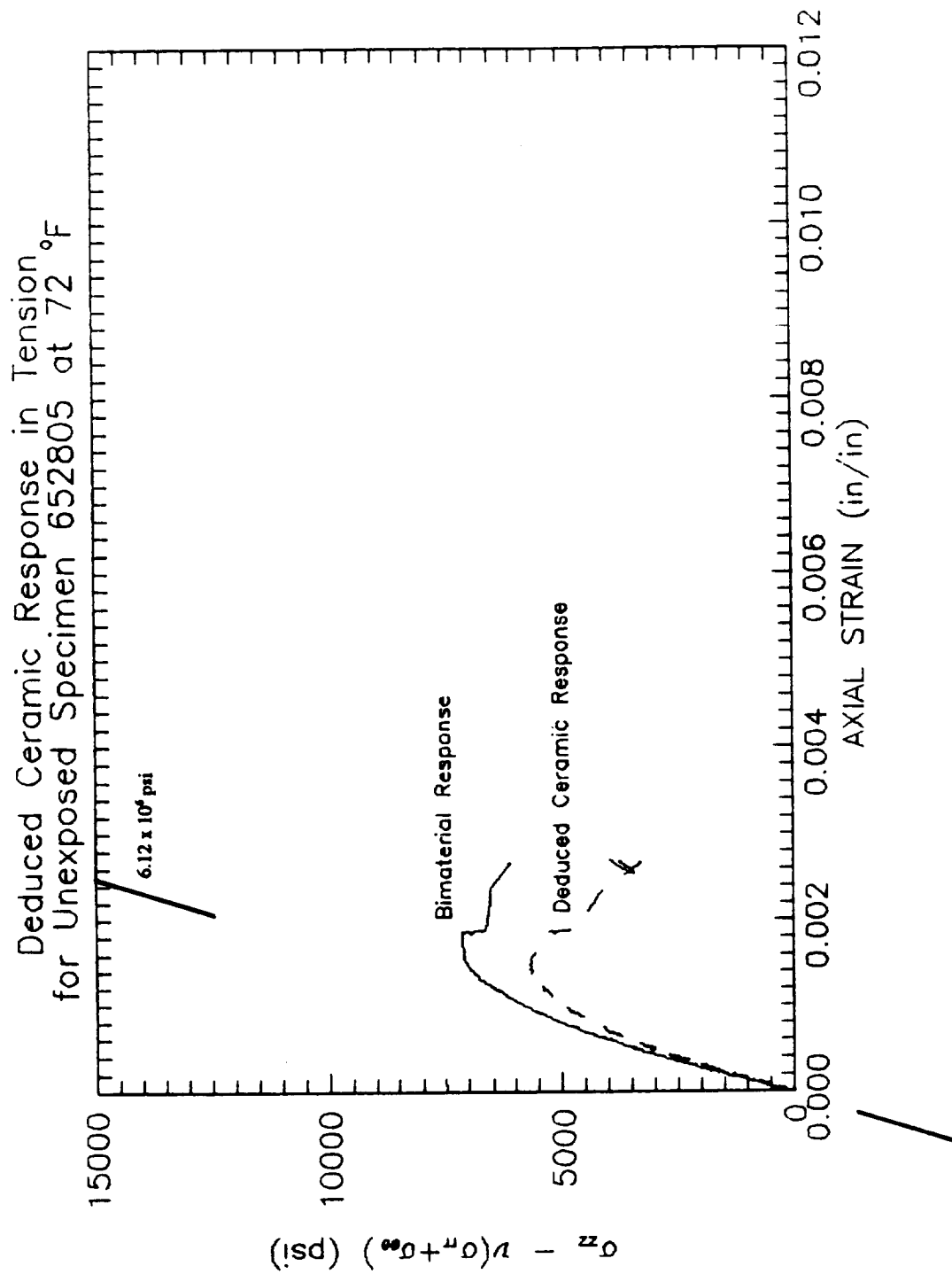


FIGURE 22. DEDUCED CERAMIC RESPONSE IN TENSION  
FOR UNEXPOSED SPECIMEN 652805 AT 72°F

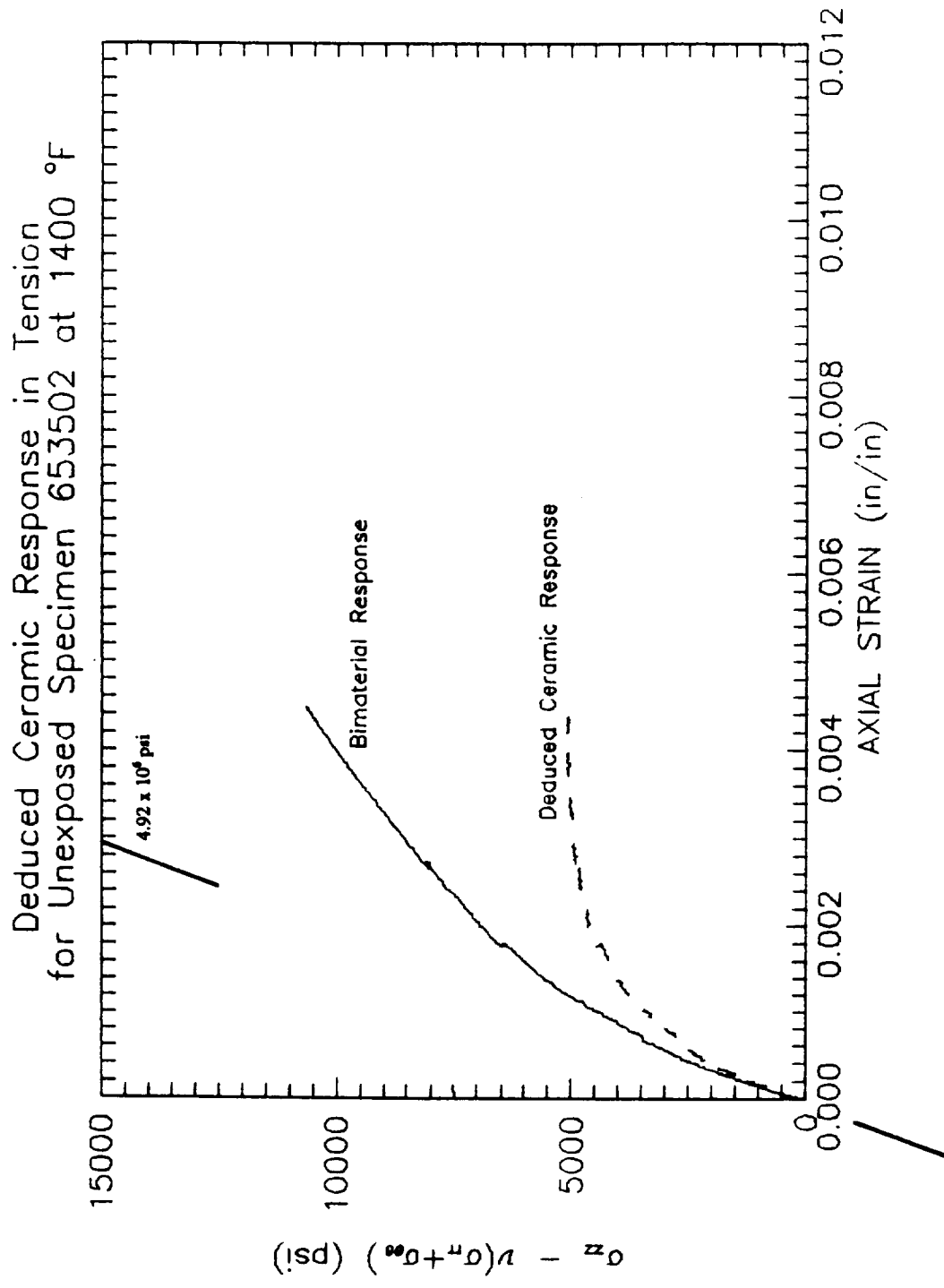


FIGURE 23. DEDUCED CERAMIC RESPONSE IN TENSION  
FOR UNEXPOSED SPECIMEN 653502 AT 1400°F

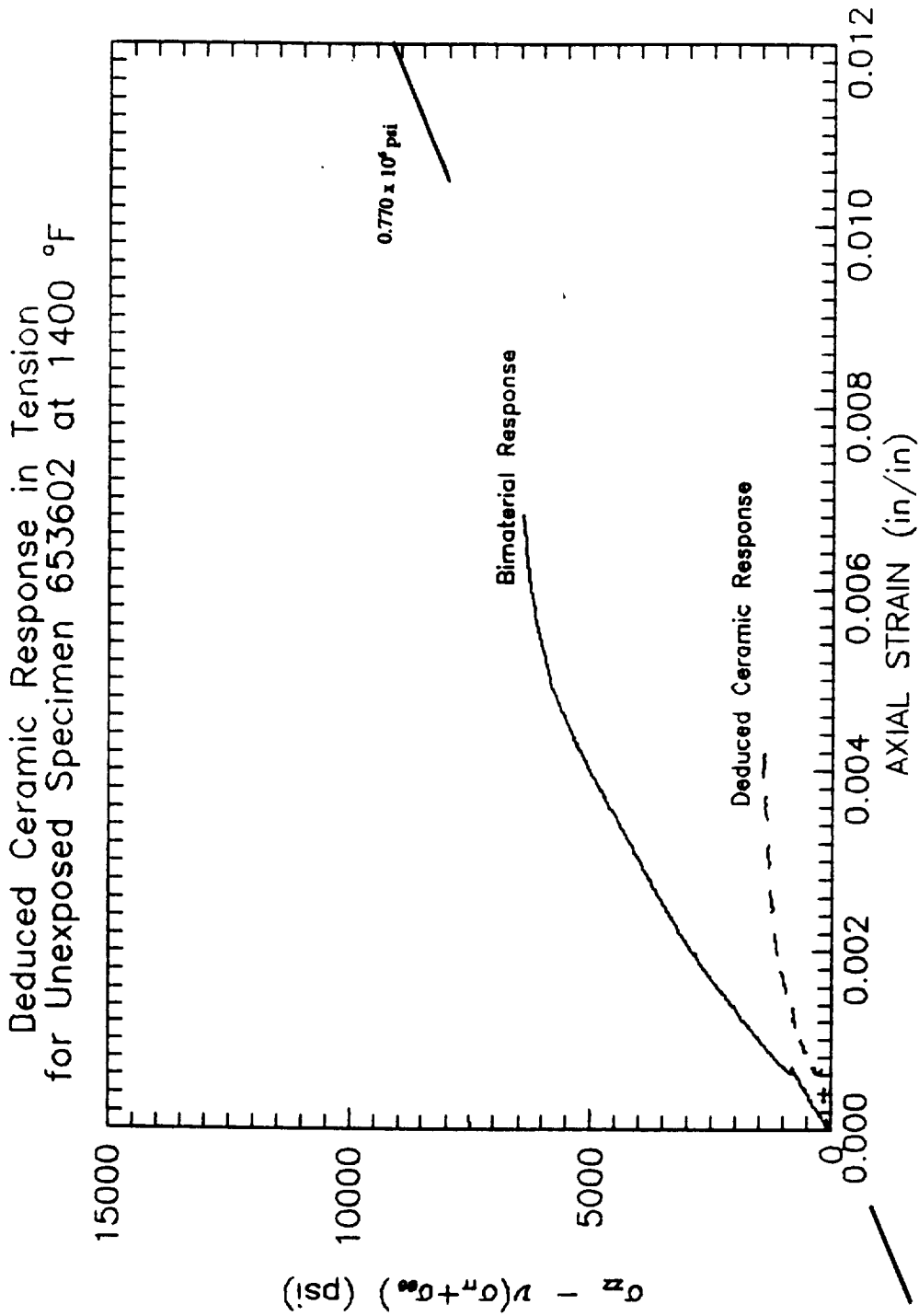


FIGURE 24. DEDUCED CERAMIC RESPONSE IN TENSION  
FOR UNEXPOSED SPECIMEN 653602 AT 1400°F

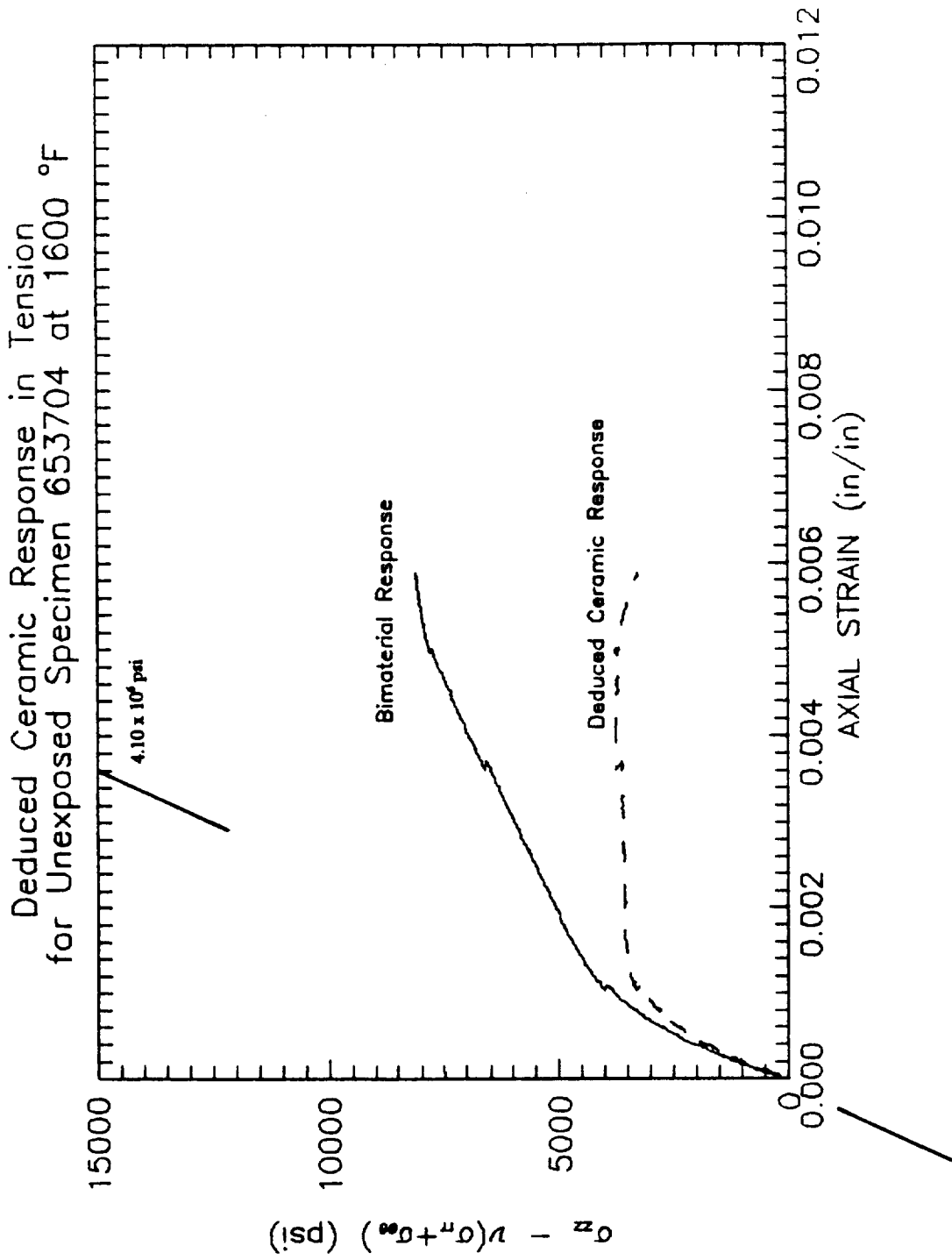


FIGURE 25. DEDUCED CERAMIC RESPONSE IN TENSION  
FOR UNEXPOSED SPECIMEN 653704 AT 1600°F



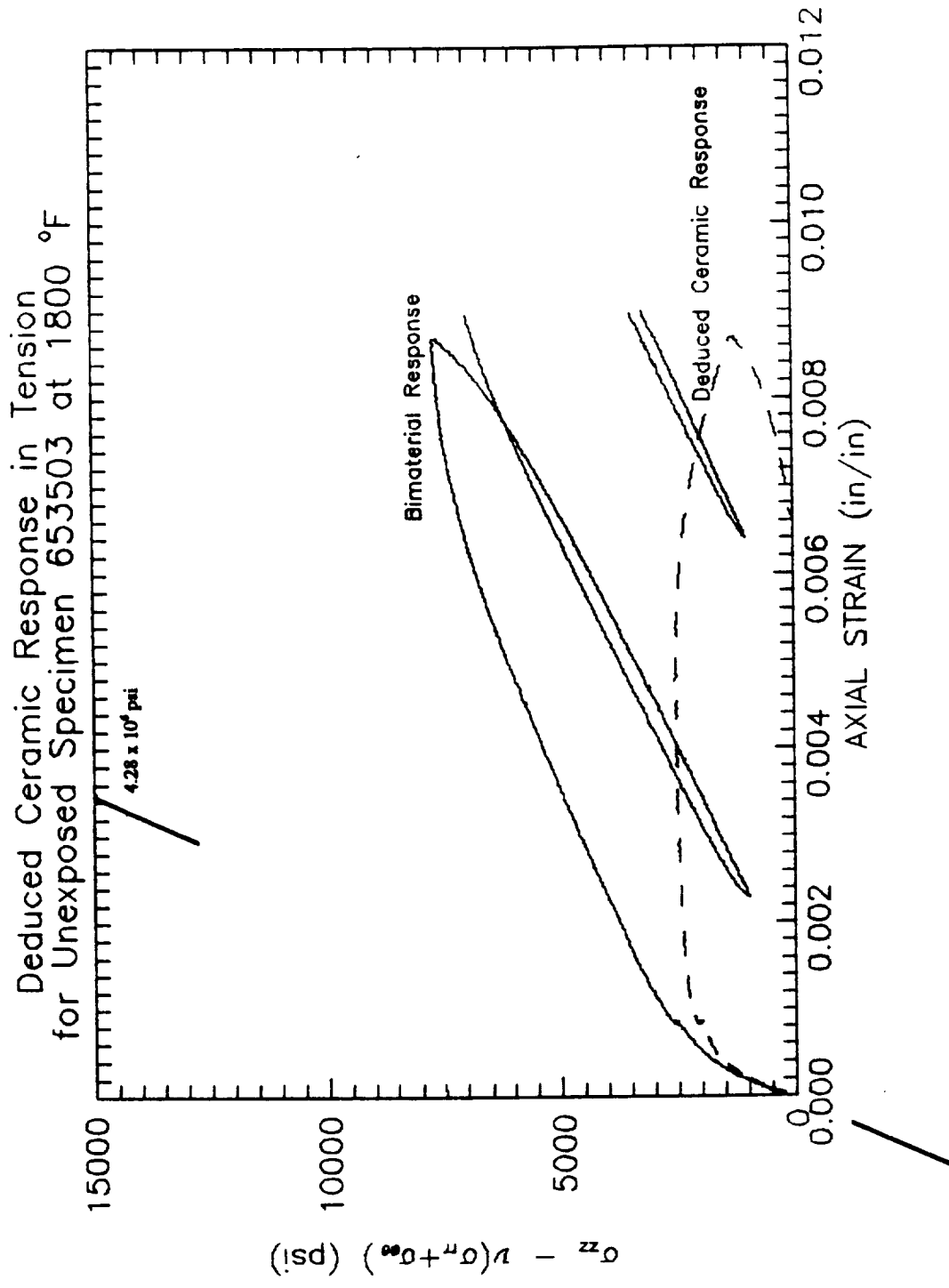


FIGURE 26. DEDUCED CERAMIC RESPONSE IN TENSION  
FOR UNEXPOSED SPECIMEN 653503 AT 1800°F

Deduced Ceramic Response in Tension  
for Unexposed Specimen 652802 at 1800 °F

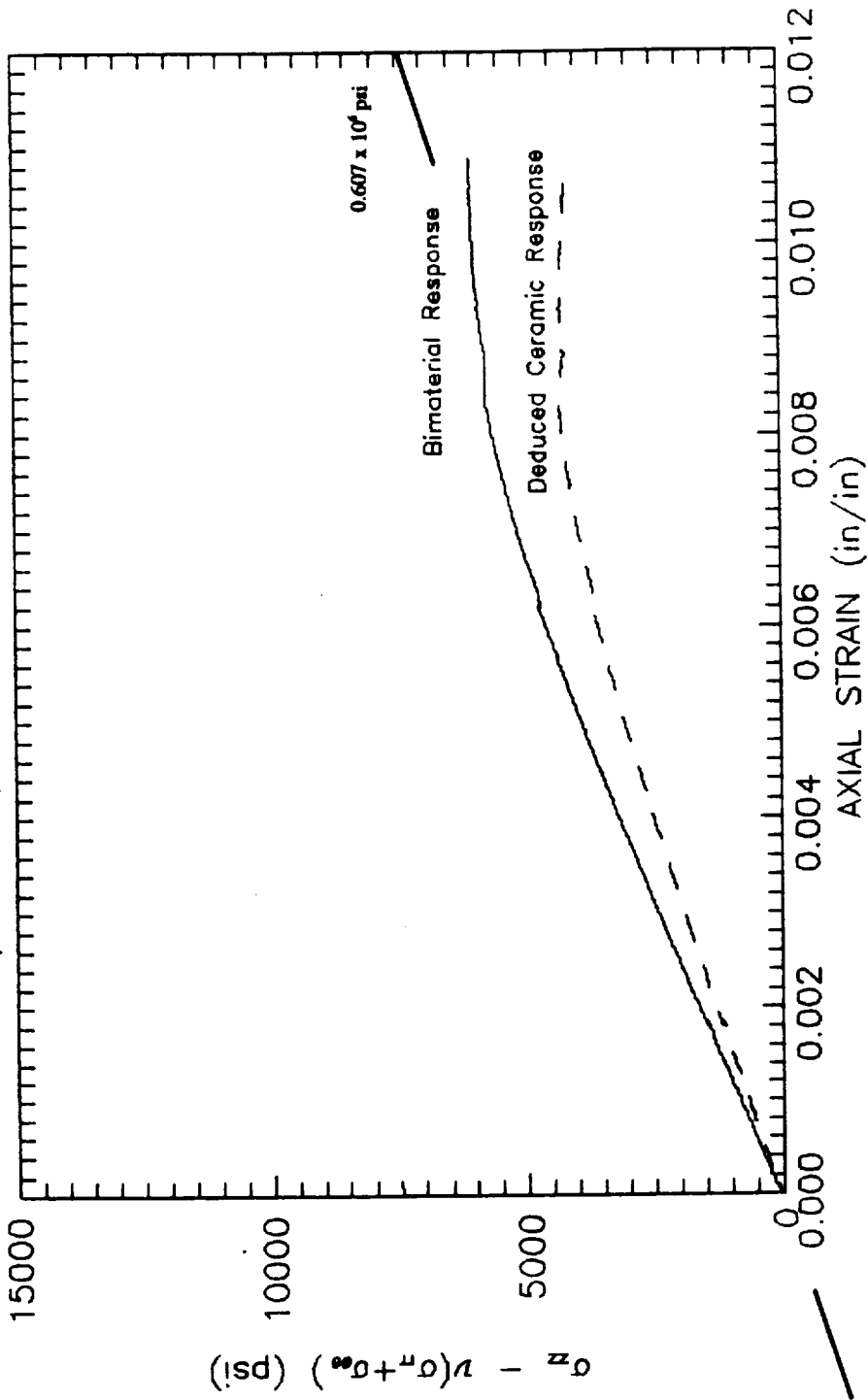


FIGURE 27. DEDUCED CERAMIC RESPONSE IN TENSION  
FOR UNEXPOSED SPECIMEN 652802 AT 1800°F

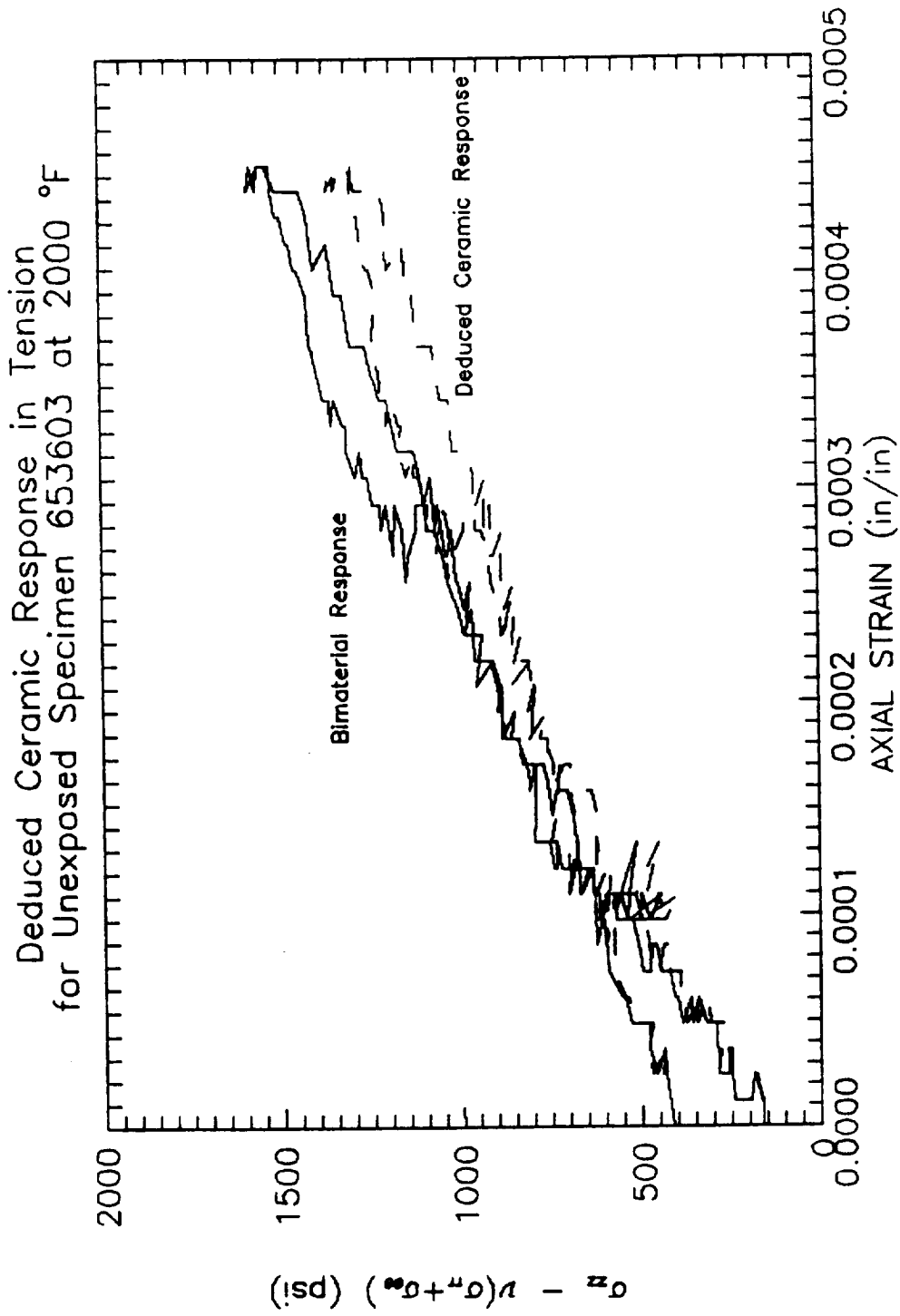


FIGURE 28. DEDUCED CERAMIC RESPONSE IN TENSION  
FOR UNEXPOSED SPECIMEN 653603 AT 2000°F

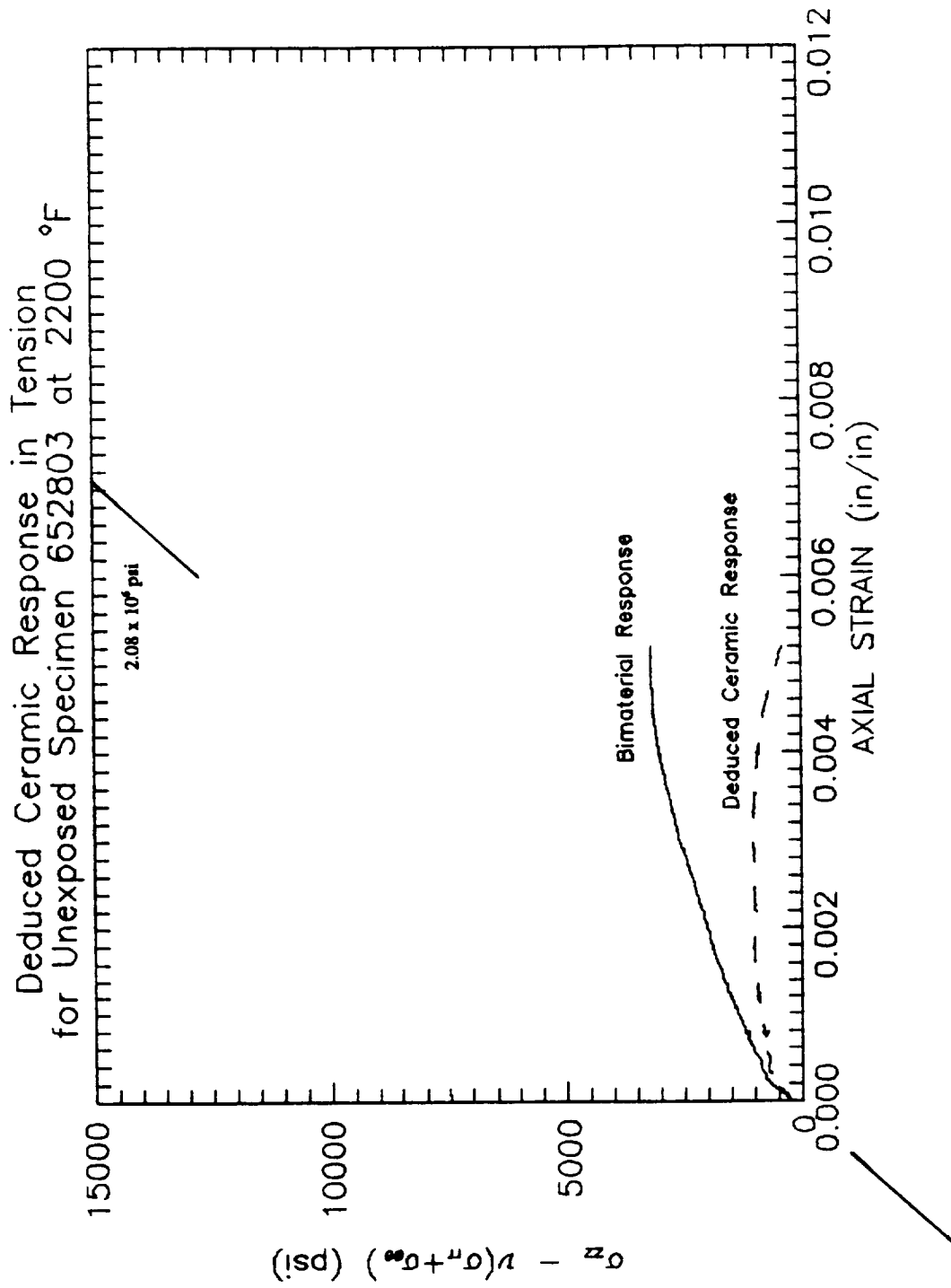


FIGURE 29. DEDUCED CERAMIC RESPONSE IN TENSION  
FOR UNEXPOSED SPECIMEN 652803 AT 2200°F

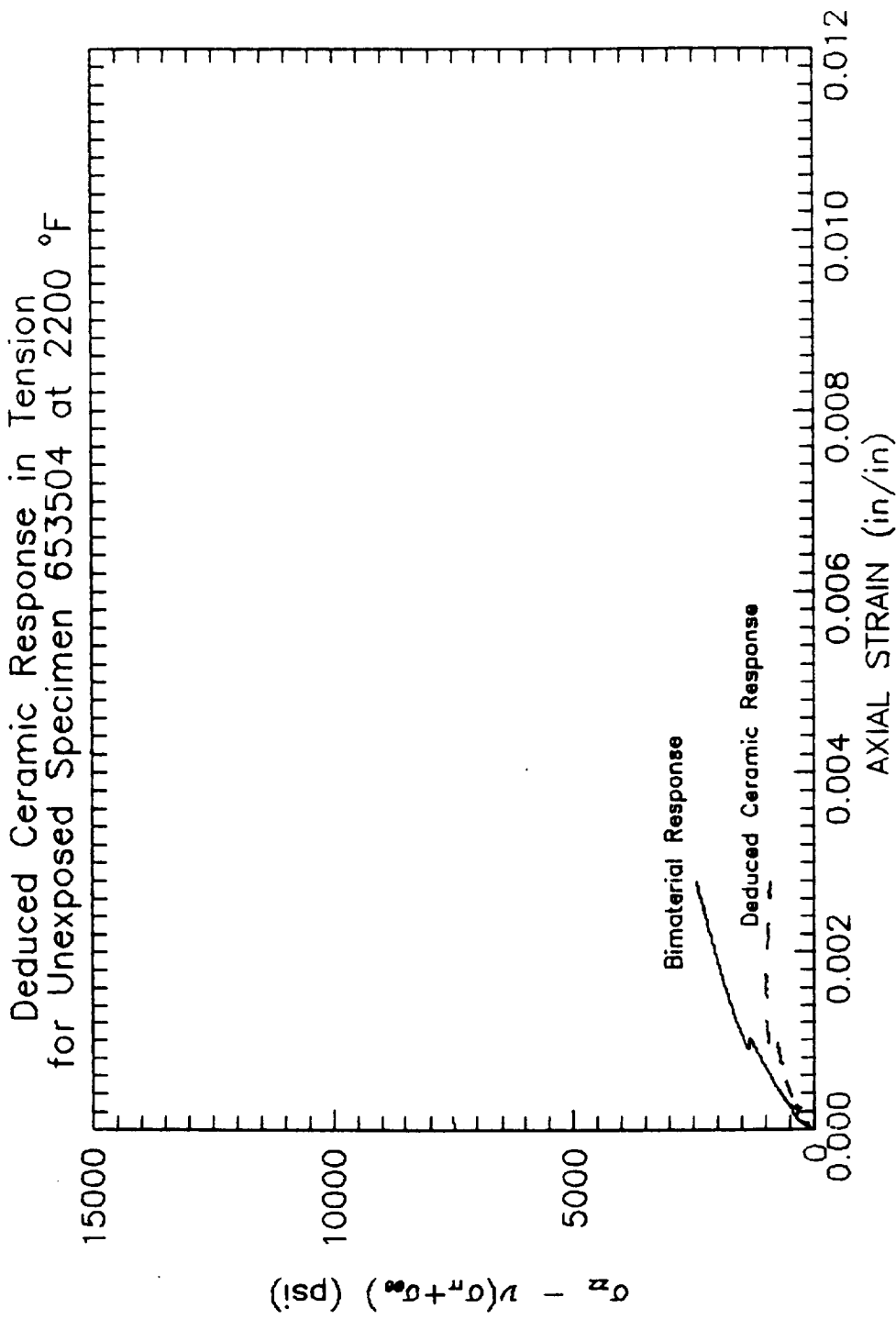


FIGURE 30. DEDUCED CERAMIC RESPONSE IN TENSION  
FOR UNEXPOSED SPECIMEN 653504 AT 2200°F

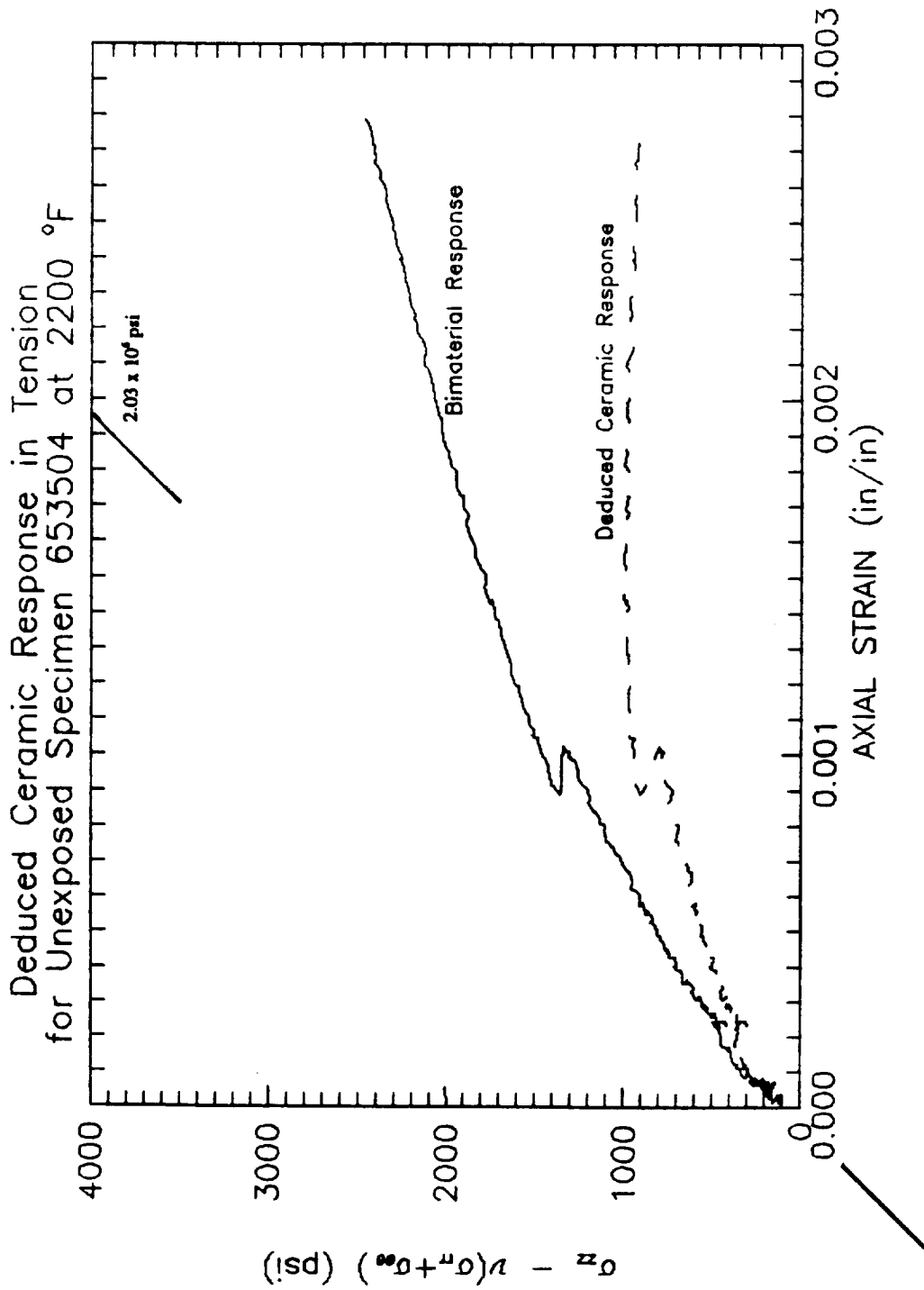


FIGURE 31. DEDUCED CERAMIC RESPONSE IN TENSION  
FOR UNEXPOSED SPECIMEN 653504 AT 2200°F

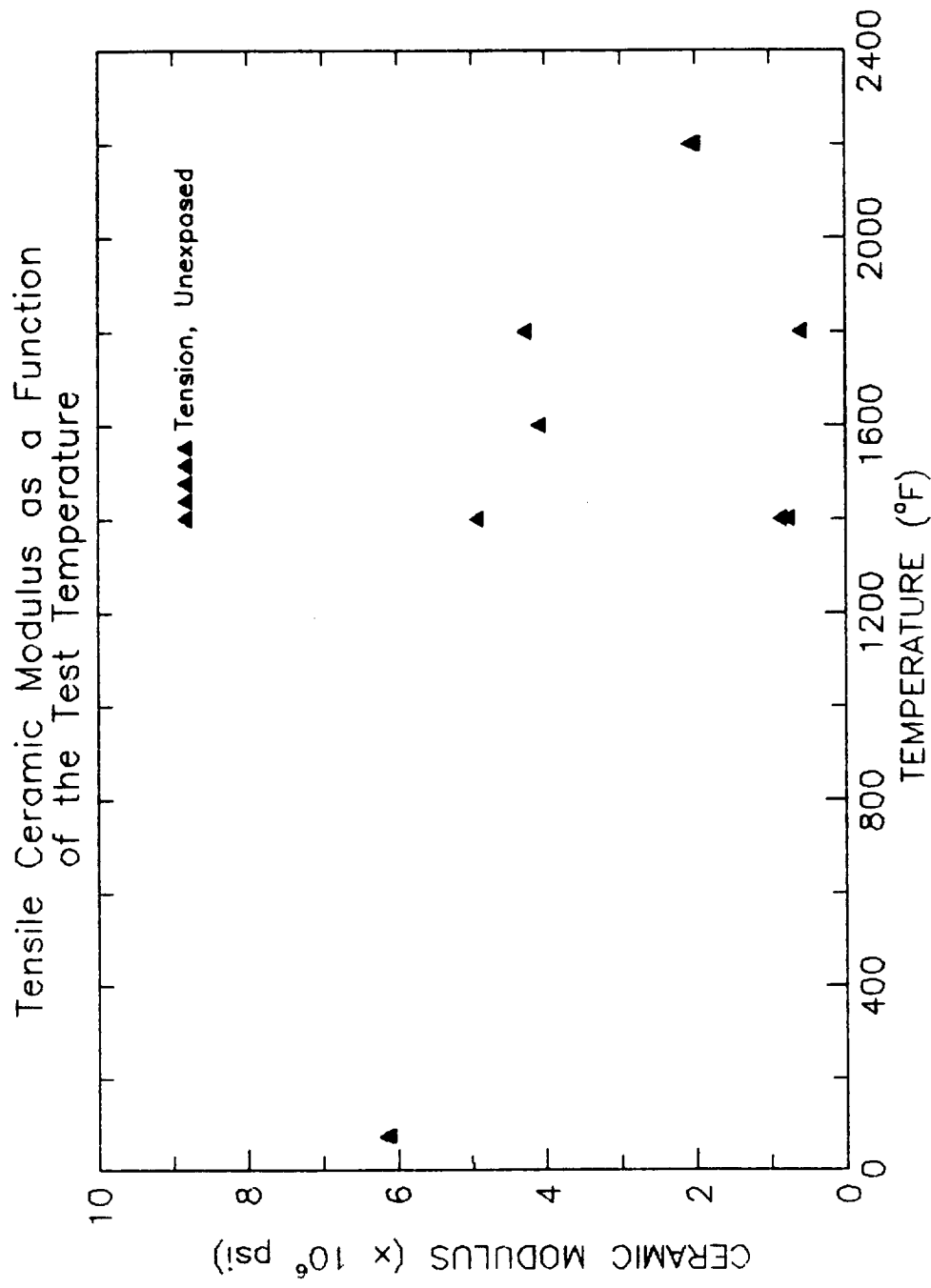


FIGURE 32. DEDUCED CERAMIC MODULUS AS A FUNCTION OF THE TEST TEMPERATURE

## 5 Appendix A: Elastic Bimaterial Model

The following is a detailed derivation of the linear elastic model used to deduce the ceramic response from the ceramic/substrate bimaterial system. Table A-1 defines the mathematical symbols used in the derivation that follows.

**Table A-1**  
**Definition of Mathematical Symbols**

Symbol	Definition
$a, b, c$	Inside, interface and outside radius, respectively
$A_C, A_S$	Cross-sectional area of the ceramic and substrate, respectively
$u_C, u_S$	Radial displacement of the ceramic and substrate, respectively
$\epsilon_{zz}^C, \epsilon_{zz}^S$	Axial strain in the ceramic and substrate, respectively
$P_T, \epsilon_{zz}$	Total applied load and corresponding axial strain
$P_C, P_S$	Axial load in the ceramic and substrate, respectively
$E_C, E_S$	Elastic modulus of the ceramic and substrate, respectively
$\nu_C, \nu_S$	Poisson's ratio of the ceramic and substrate, respectively
$\sigma_{zz}^C, \sigma_{zz}^S$	Axial stress in the ceramic and substrate, respectively
$\sigma_{rr}^C, \sigma_{rr}^S$	Radial stress in the ceramic and substrate, respectively
$\sigma_{\theta\theta}^C, \sigma_{\theta\theta}^S$	Circumferential stress in the ceramic and substrate, respectively
$\epsilon_{crit}, P_{flow}$	Critical strain denoting plastic substrate behavior and the corresponding axial load

Figure 8 defines the cross-sectional area of the ceramic and substrate which are given by

$$A_C = \pi(c^2 - b^2) \quad (A - 1a)$$

$$A_S = \pi(b^2 - a^2) \quad (A - 1b)$$

From the thick-walled cylinder solution [1,2], the radial displacements of the ceramic and substrate are given by



$$u_c = \frac{r}{E_c(c^2 - b^2)} \left[ (1 - 2\nu_c)pb^2 + \frac{(1 + \nu_c)}{r^2}c^2b^2p - \nu_c \frac{P_c}{\pi} \right] \quad (A-2a)$$

$$u_s = \frac{r}{E_s(b^2 - a^2)} \left[ (1 - 2\nu_s)(-pb^2) + \frac{(1 + \nu_s)}{r^2}b^2a^2(-p) - \nu_s \frac{P_s}{\pi} \right] \quad (A-2b)$$

The radial displacements at the ceramic/substrate interface are given from Equations (A-2a) and (A-2b) by taking  $r = b$ . Thus,

$$u_c = \frac{b}{E_c(c^2 - b^2)} \left[ (1 - 2\nu_c)pb^2 + (1 + \nu_c)pc^2 - \nu_c \frac{P_c}{\pi} \right] \quad (A-3a)$$

$$u_s = \frac{b}{E_s(b^2 - a^2)} \left[ (1 - 2\nu_s)(-pb^2) + (1 + \nu_s)(-pa^2) - \nu_s \frac{P_s}{\pi} \right] \quad (A-3b)$$

Assuming no debonding at the ceramic/substrate interface, the radial displacements must be equal. Equating Equations (A-3a) and (A-3b) and solving for the interfacial pressure,  $p$ , gives

$$p = \frac{\nu_c E_s A_s P_c - \nu_s E_c A_c P_s}{\pi \{ E_s A_s [(1 - 2\nu_c)b^2 + (1 + \nu_c)c^2] + E_c A_c [(1 - 2\nu_s)b^2 + (1 + \nu_s)a^2] \}} \quad (A-4)$$

The axial strains from 3-D Hooke's law are given by

$$\epsilon_{xx}^c = \frac{1}{E_c} [\sigma_{xx}^c - \nu_c (\sigma_{rr}^c + \sigma_{\theta\theta}^c)] \quad (A-5a)$$

$$\epsilon_{xx}^s = \frac{1}{E_s} [\sigma_{xx}^s - \nu_s (\sigma_{rr}^s + \sigma_{\theta\theta}^s)] \quad (A-5b)$$

The normal stresses in the ceramic are given as

$$\sigma_{xx}^c = \frac{P_c}{\pi(c^2 - b^2)} + \frac{pb^2}{(c^2 - b^2)} \quad (A-6a)$$

$$\sigma_{rr}^c = \frac{pb^2}{c^2 - b^2} - \frac{pc^2b^2}{r^2(c^2 - b^2)} \quad (A-6b)$$

$$\sigma_{\theta\theta}^c = \frac{pb^2}{c^2 - b^2} + \frac{pc^2b^2}{r^2(c^2 - b^2)} \quad (A-6c)$$

Similarly, the normal stresses in the substrate are given as

$$\sigma_{zz}^s = \frac{P_s}{\pi(b^2 - a^2)} + \frac{pb^2}{(b^2 - a^2)} \quad (A-7a)$$

$$\sigma_{rr}^s = \frac{-pb^2}{b^2 - a^2} + \frac{pb^2a^2}{r^2(b^2 - a^2)} \quad (A-7b)$$

$$\sigma_{\theta\theta}^s = \frac{-pb^2}{b^2 - a^2} - \frac{pb^2a^2}{r^2(b^2 - a^2)} \quad (A-7c)$$

Substituting Equations (A-6) and (A-7) into Equations (A-5a) and (A-5b), respectively, gives

$$\epsilon_{zz}^c = \frac{1}{E_c A_c} [P_c + \pi(1 - 2\nu_c)pb^2] \quad (A-8a)$$

$$\epsilon_{zz}^s = \frac{1}{E_s A_s} [P_s - \pi(1 - 2\nu_s)pb^2] \quad (A-8b)$$

Noting that the axial strain in the ceramic must equal the axial strain in the substrate, equating the axial strains given in Equations (A-8a) and (A-8b) and solving for the load in the ceramic yields

$$P_c = \left( \frac{E_c A_c}{E_s A_s} \right) [P_s - \pi(1 - 2\nu_s)pb^2] - \pi(1 - 2\nu_c)pb^2 \quad (A-9)$$

Substituting Equation (A-4) into (A-9) and simplifying gives

$$P_c = \frac{1}{D E_s A_s} \{ D E_c A_c P_s + b^2 [E_c A_c (1 - 2\nu_s) + E_s A_s (1 - 2\nu_c)] (\nu_s E_c A_c P_s - \nu_c E_s A_s P_c) \} \quad (A-10)$$

where, for convenience, D is defined as

$$D = E_s A_s [(1 - 2\nu_c)b^2 + (1 + \nu_c)c^2] + E_c A_c [(1 - 2\nu_s)b^2 + (1 + \nu_s)a^2] \quad (A-11)$$

From equilibrium,

$$P_T = P_c + P_s \quad (A-12)$$

Or, equivalently

$$P_s = P_T - P_c \quad (A-13)$$

Substituting Equation (A-13) into (A-10), it can be shown that

$$P_c = K(E_c)P_T \quad (A-14)$$

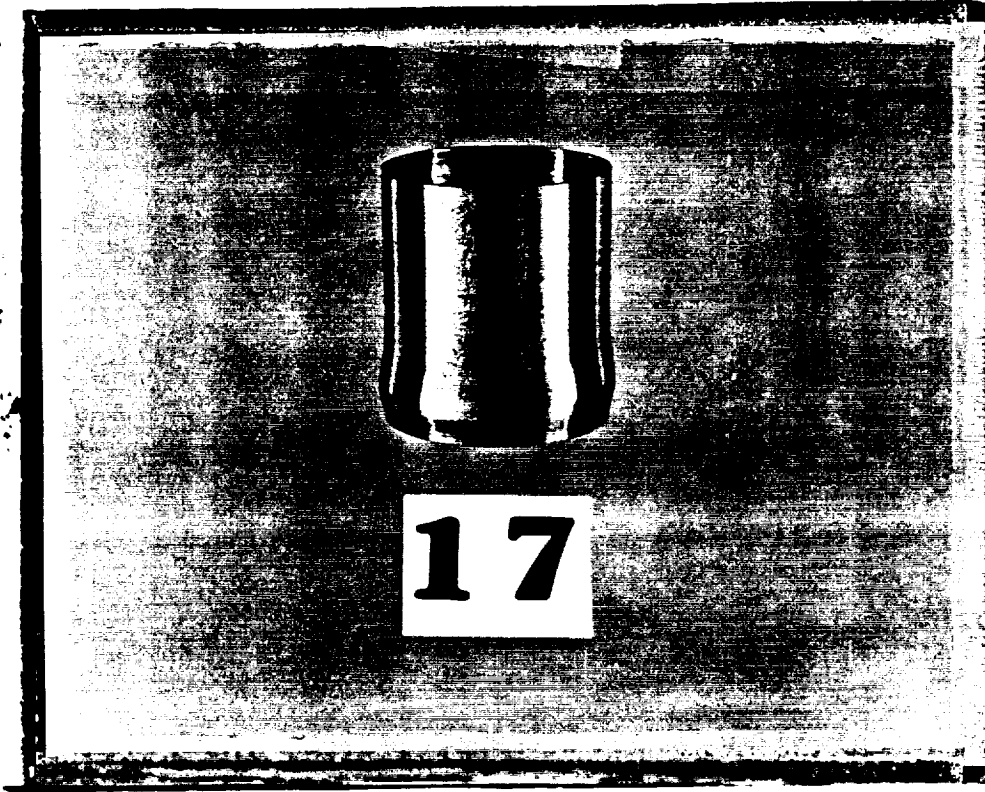
where

$$K(E_c) = \frac{b^2 [E_c A_c (1 - 2\nu_s) + E_s A_s (1 - 2\nu_c)] \nu_s E_c A_c + D E_c A_c}{D E_s A_s + b^2 [E_c A_c (1 - 2\nu_s) + E_s A_s (1 - 2\nu_c)] (\nu_s E_c A_c + \nu_c E_s A_s) + D E_c A_c} \quad (A-15)$$

Finally, substituting Equations (A-4), (A-13) and (A-14) into Equation (A-8a) yields

$$\epsilon_{xx}^c = \frac{P_T}{E_c A_c} \left\{ K(E_c) + b^2 \left[ \frac{\nu_c E_s A_s K(E_c) - \nu_s E_c A_c (1 - K(E_c))}{D} \right] (1 - 2\nu_c) \right\} \quad (A - 16)$$

## **6 Appendix B: Failed Specimen Photographs**



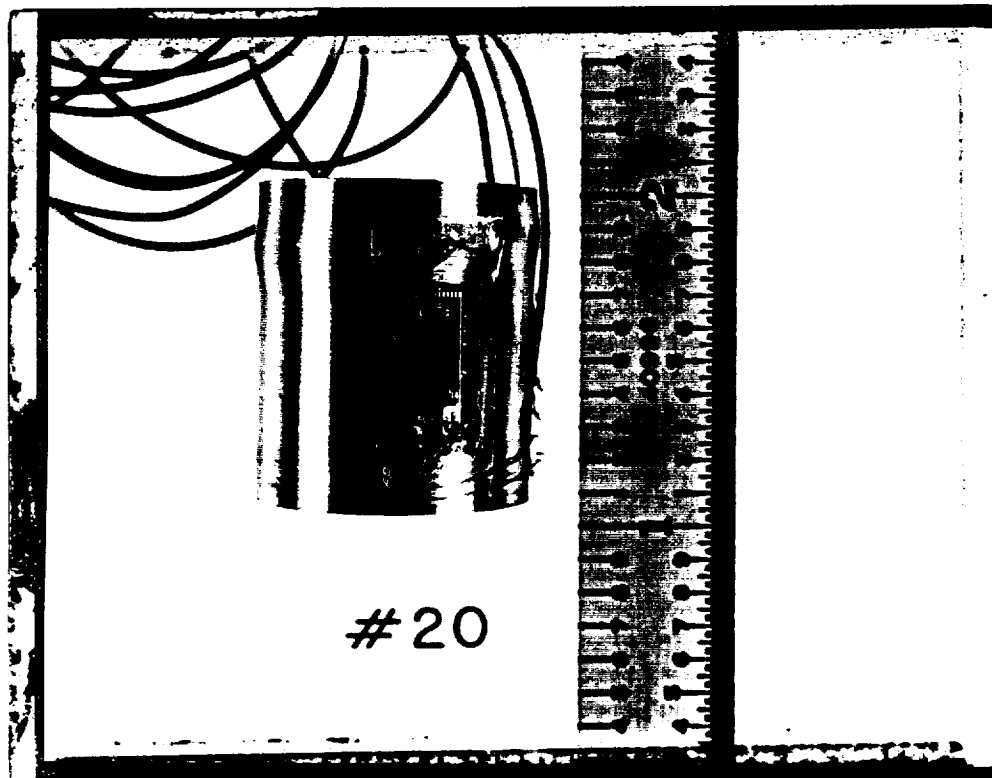
COMPRESSION SPECIMEN NO. 17, PHOTO NO. 40668



COMPRESSION SPECIMEN NO. 18, PHOTO NO. 40669



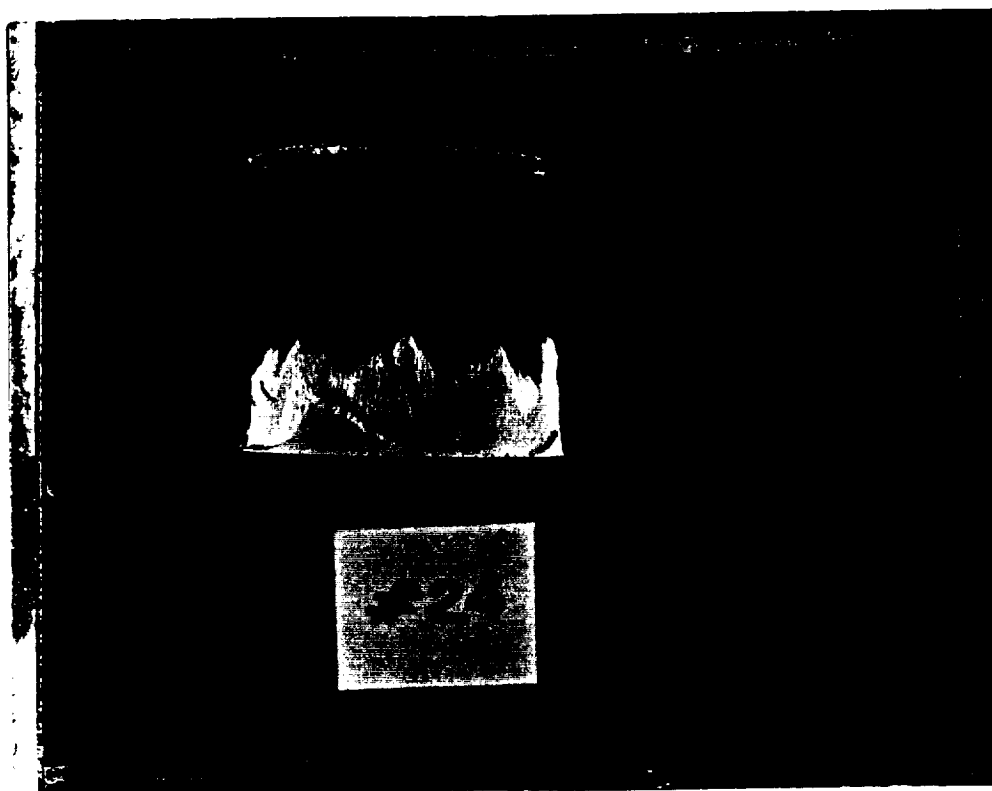
COMPRESSION SPECIMEN NO. 19, PHOTO NO. 40670



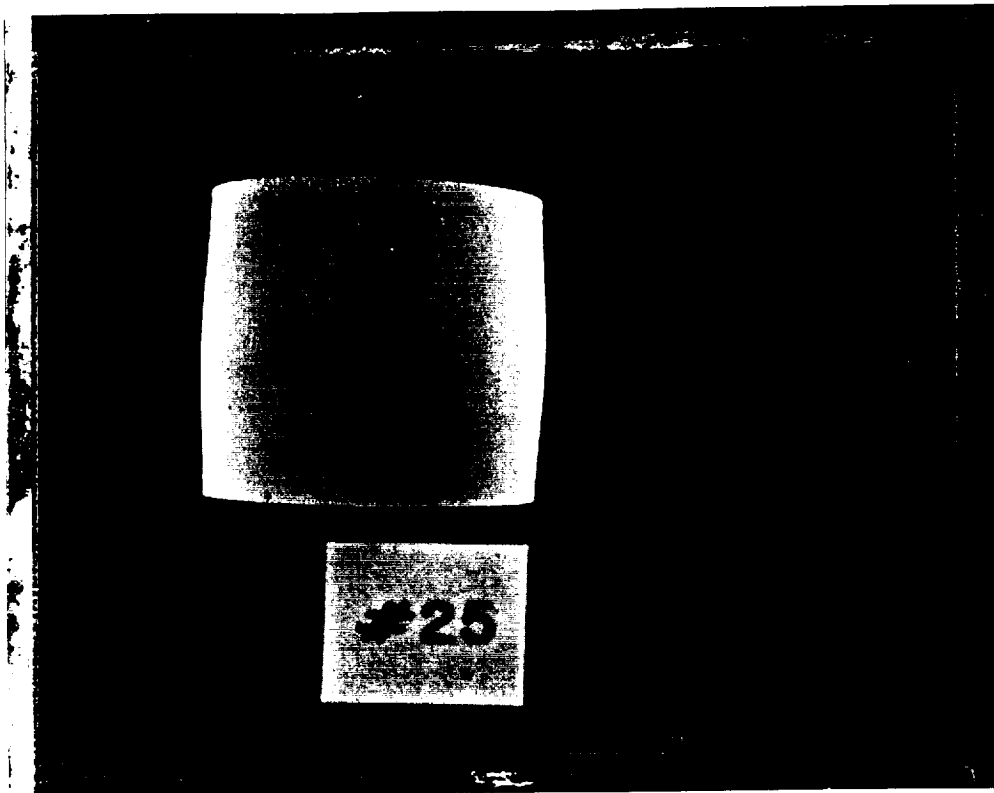
COMPRESSION SPECIMEN NO. 20, PHOTO NO. 37271



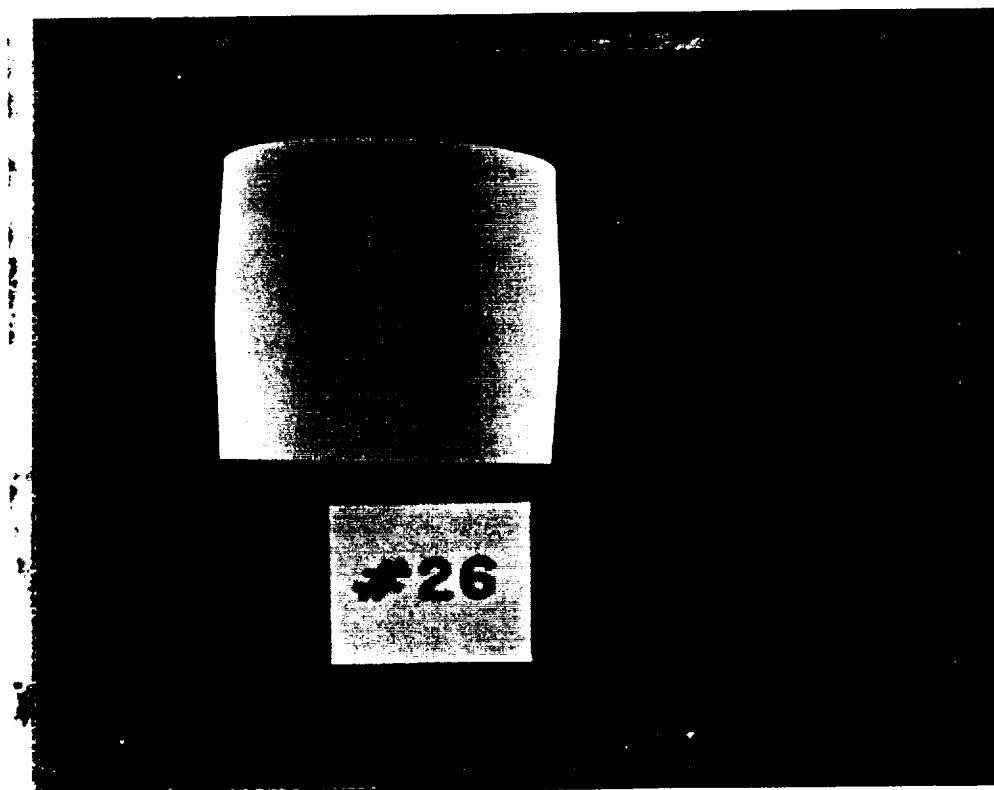
COMPRESSION SPECIMEN NO. 21, PHOTO NO. 40671



COMPRESSION SPECIMEN NO. 24, PHOTO NO. 37271



COMPRESSION SPECIMEN NO. 25, PHOTO NO. 31770

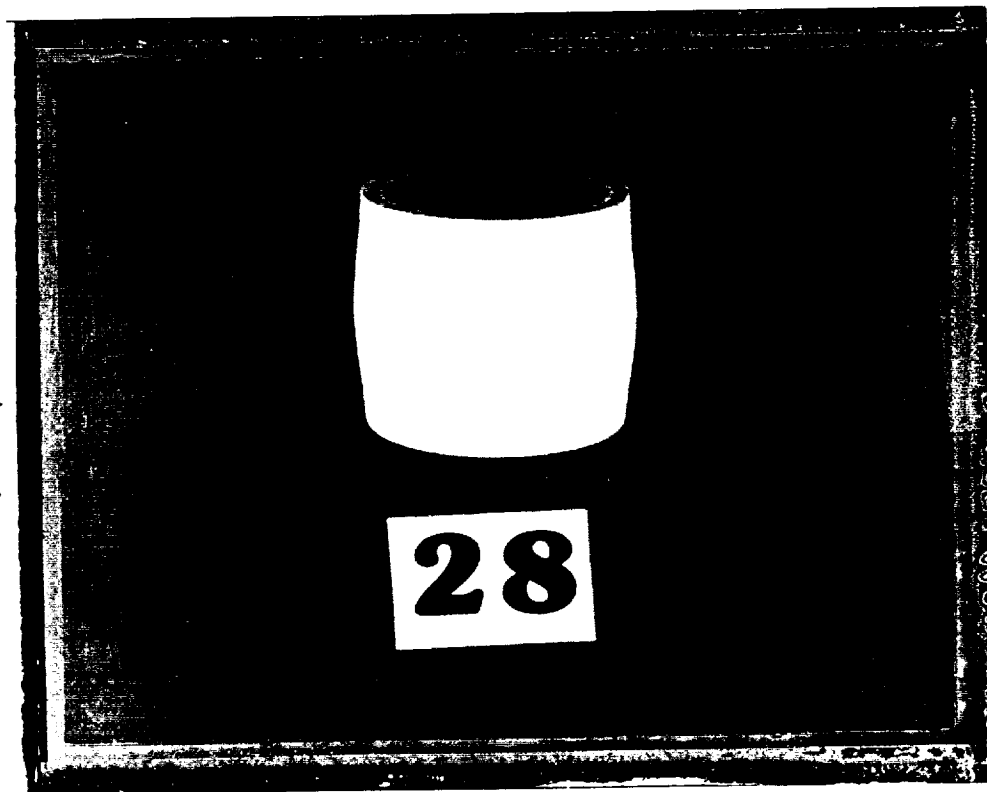


COMPRESSION SPECIMEN NO. 26, PHOTO NO. 37269

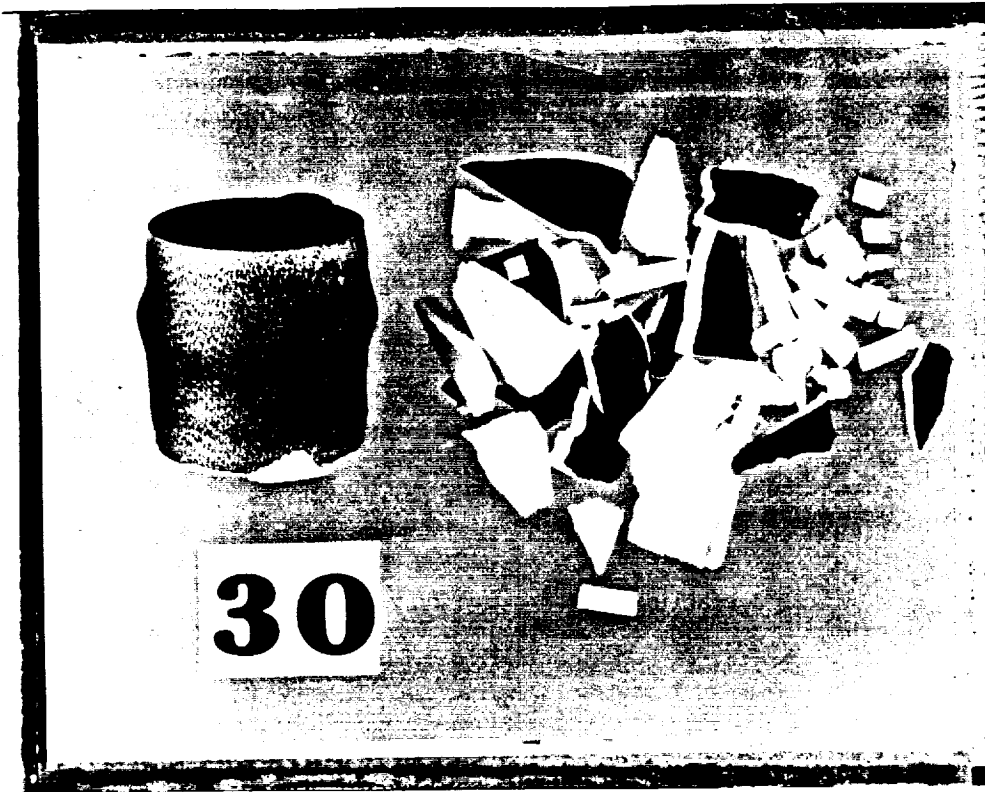




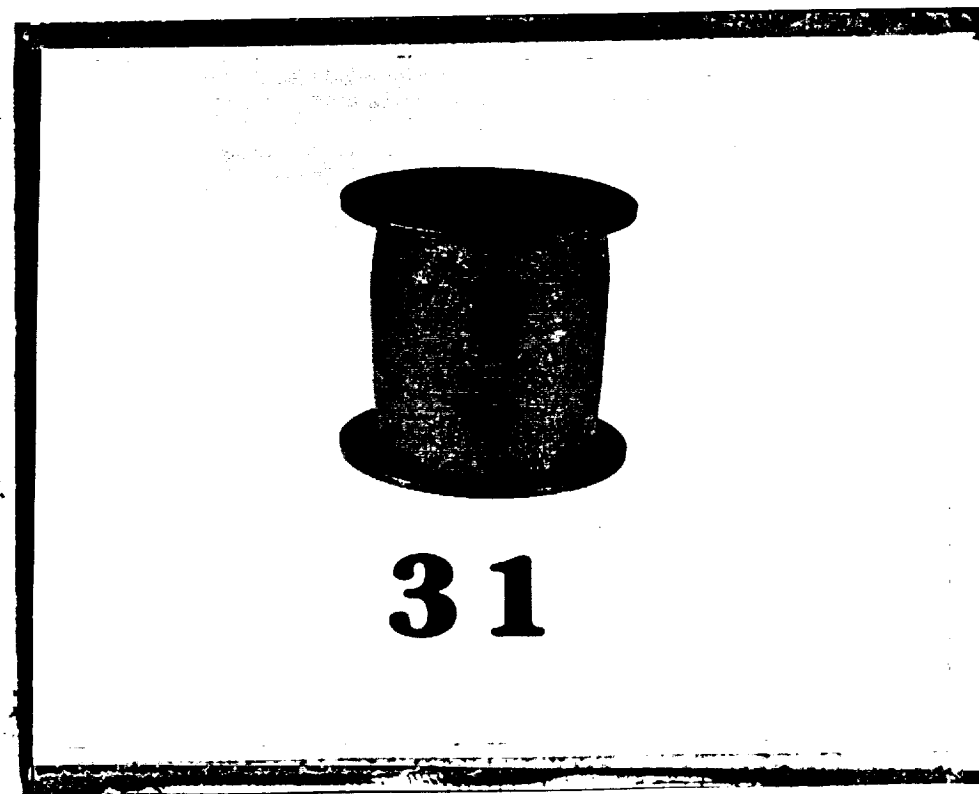
COMPRESSION SPECIMEN NO. 27, PHOTO NO. 40672



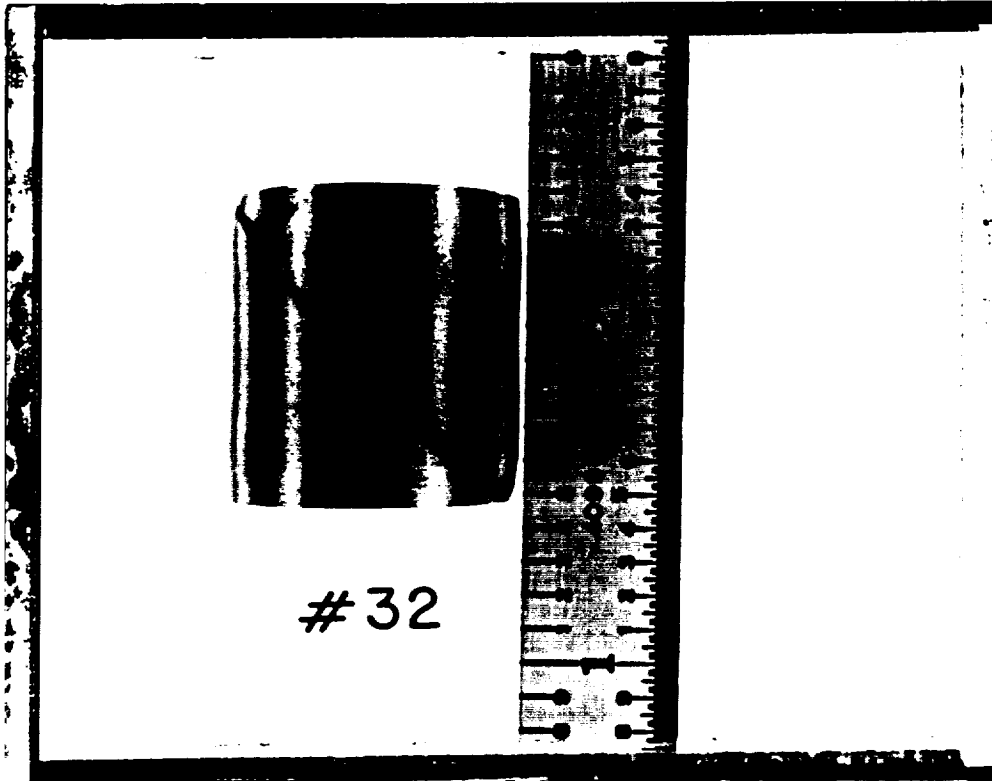
COMPRESSION SPECIMEN NO. 28, PHOTO NO. 40673



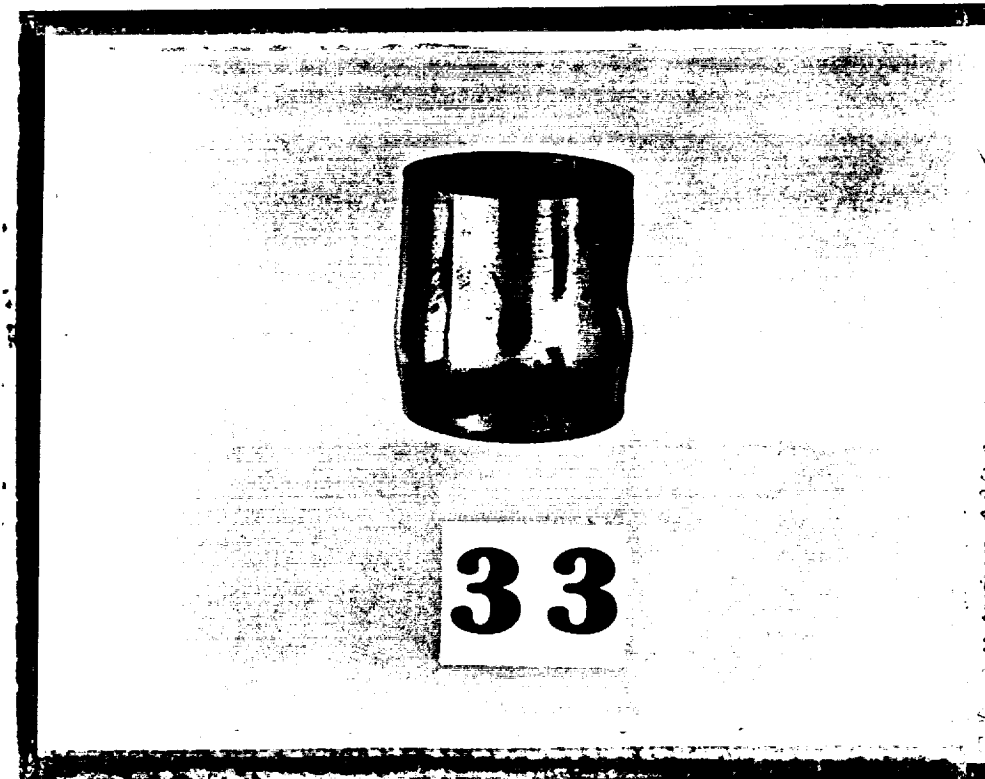
COMPRESSION SPECIMEN NO. 30, PHOTO NO. 40674



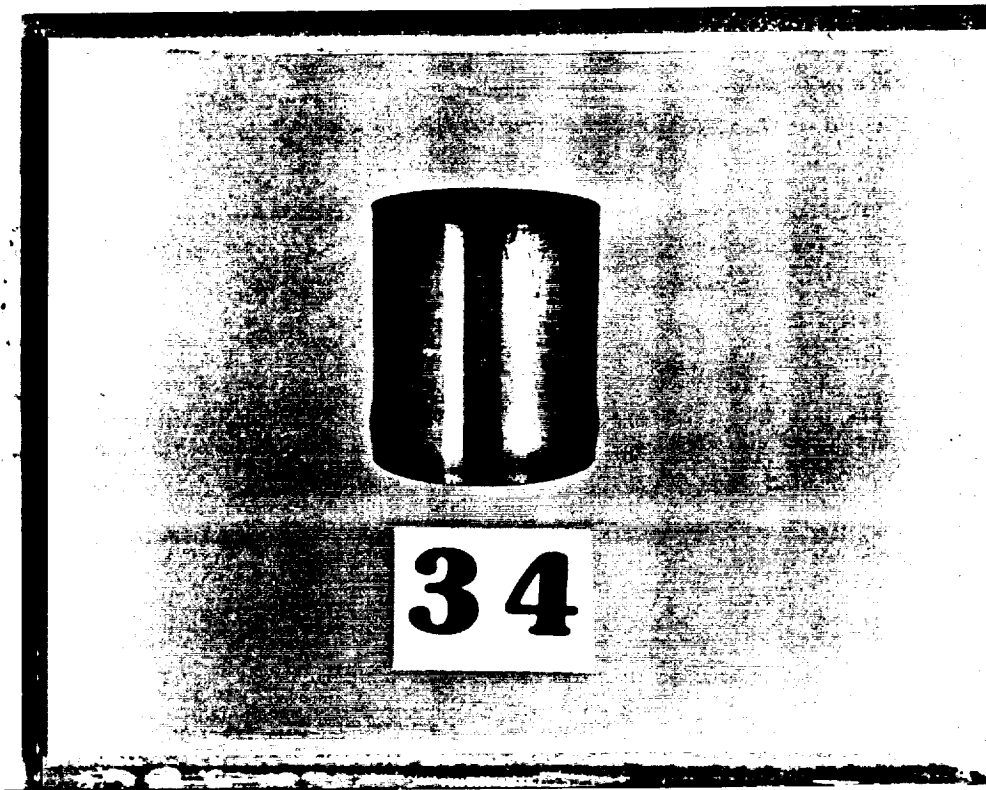
COMPRESSION SPECIMEN NO. 31, PHOTO NO. 40675



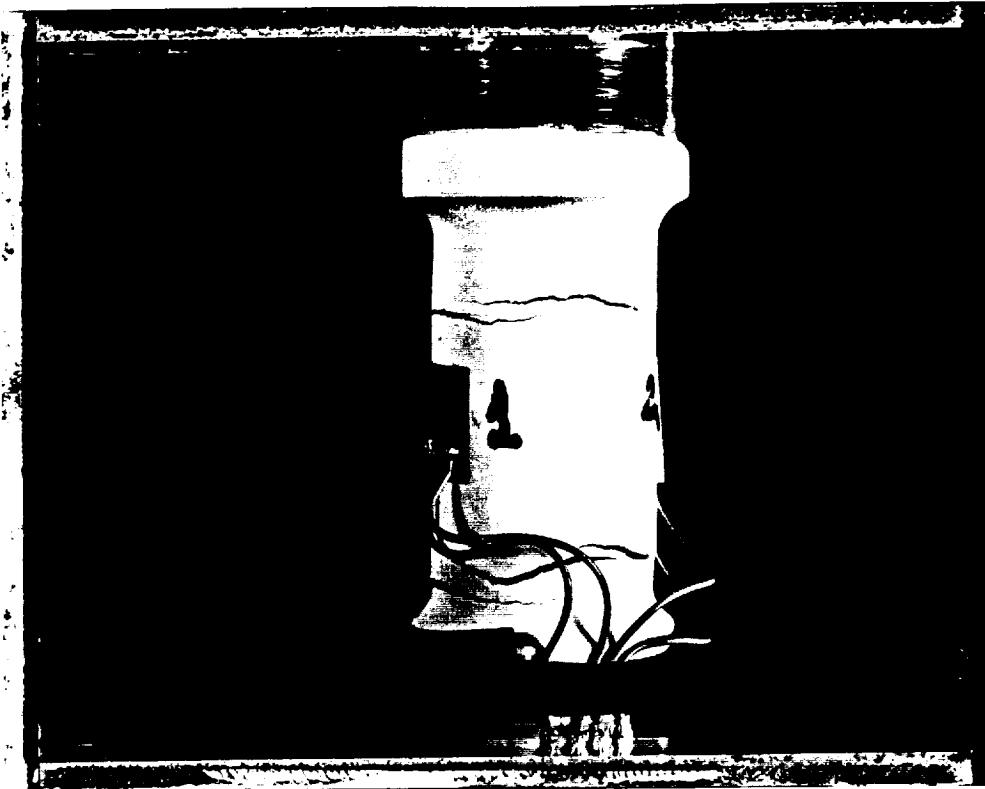
COMPRESSION SPECIMEN NO. 32, PHOTO NO. 37268



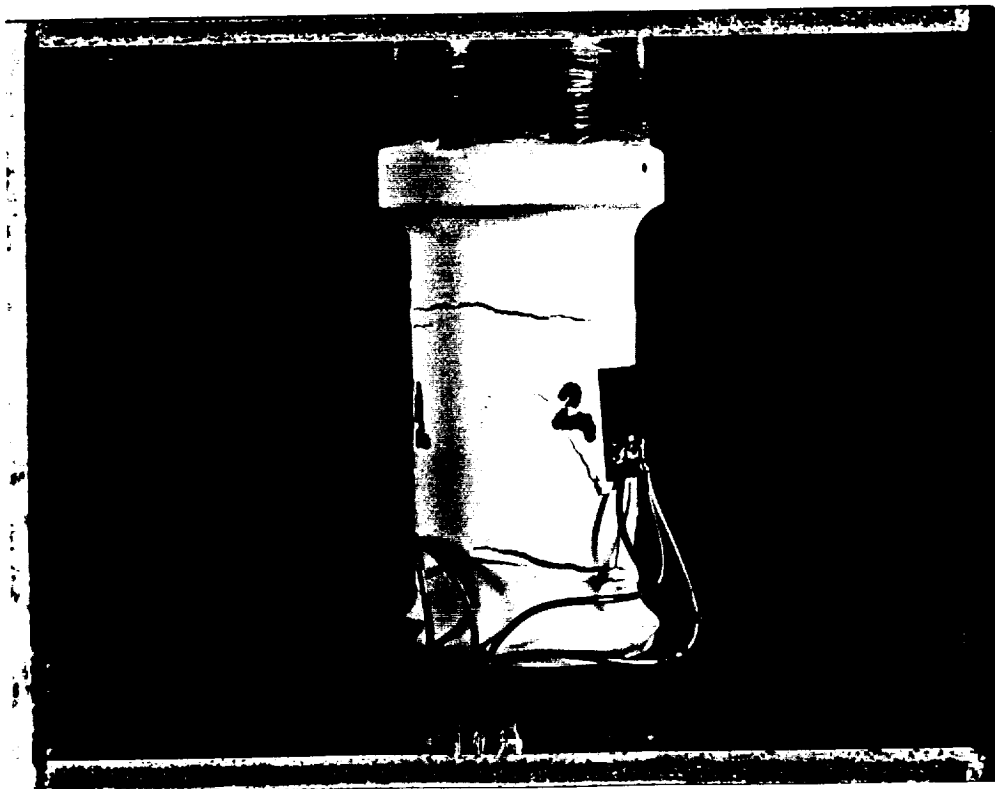
COMPRESSION SPECIMEN NO. 33, PHOTO NO. 40676



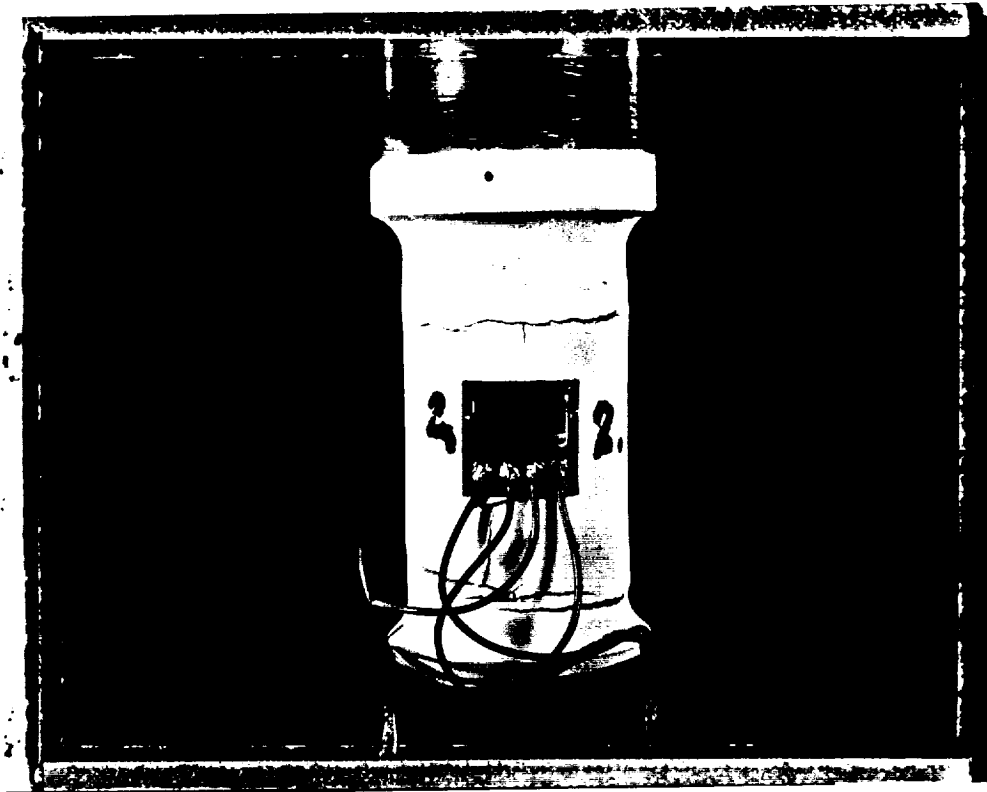
COMPRESSION SPECIMEN NO. 34, PHOTO NO. 40677



TENSION SPECIMEN NO. 652801, VIEW NO. 1, PHOTO NO. 40731



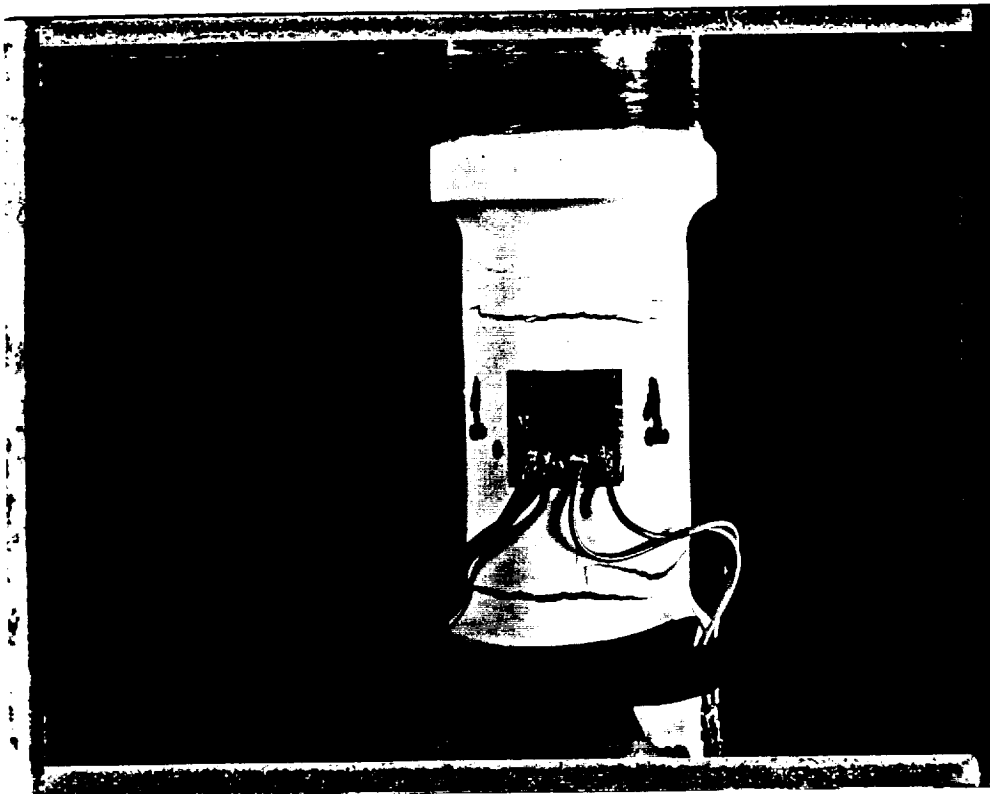
TENSION SPECIMEN NO. 652801, VIEW NO. 2, PHOTO NO. 40732



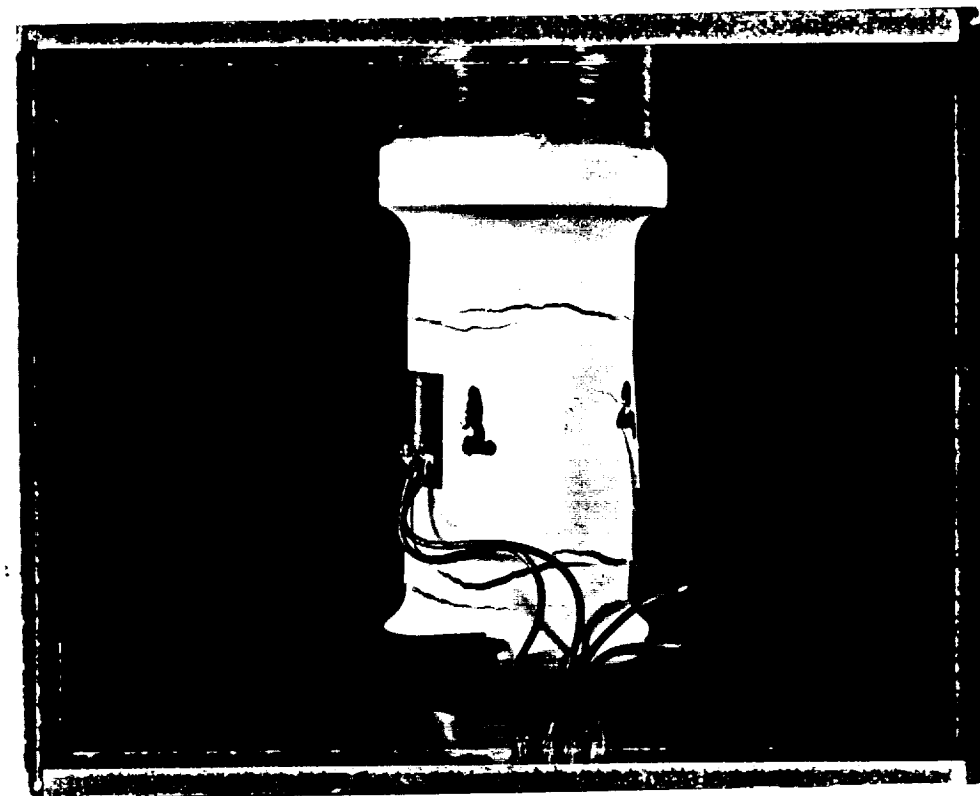
TENSION SPECIMEN NO. 652801, VIEW NO. 3, PHOTO NO. 40733



TENSION SPECIMEN NO. 652801, VIEW NO. 4, PHOTO NO. 40734



TENSION SPECIMEN NO. 652801, VIEW NO. 5, PHOTO NO. 40730

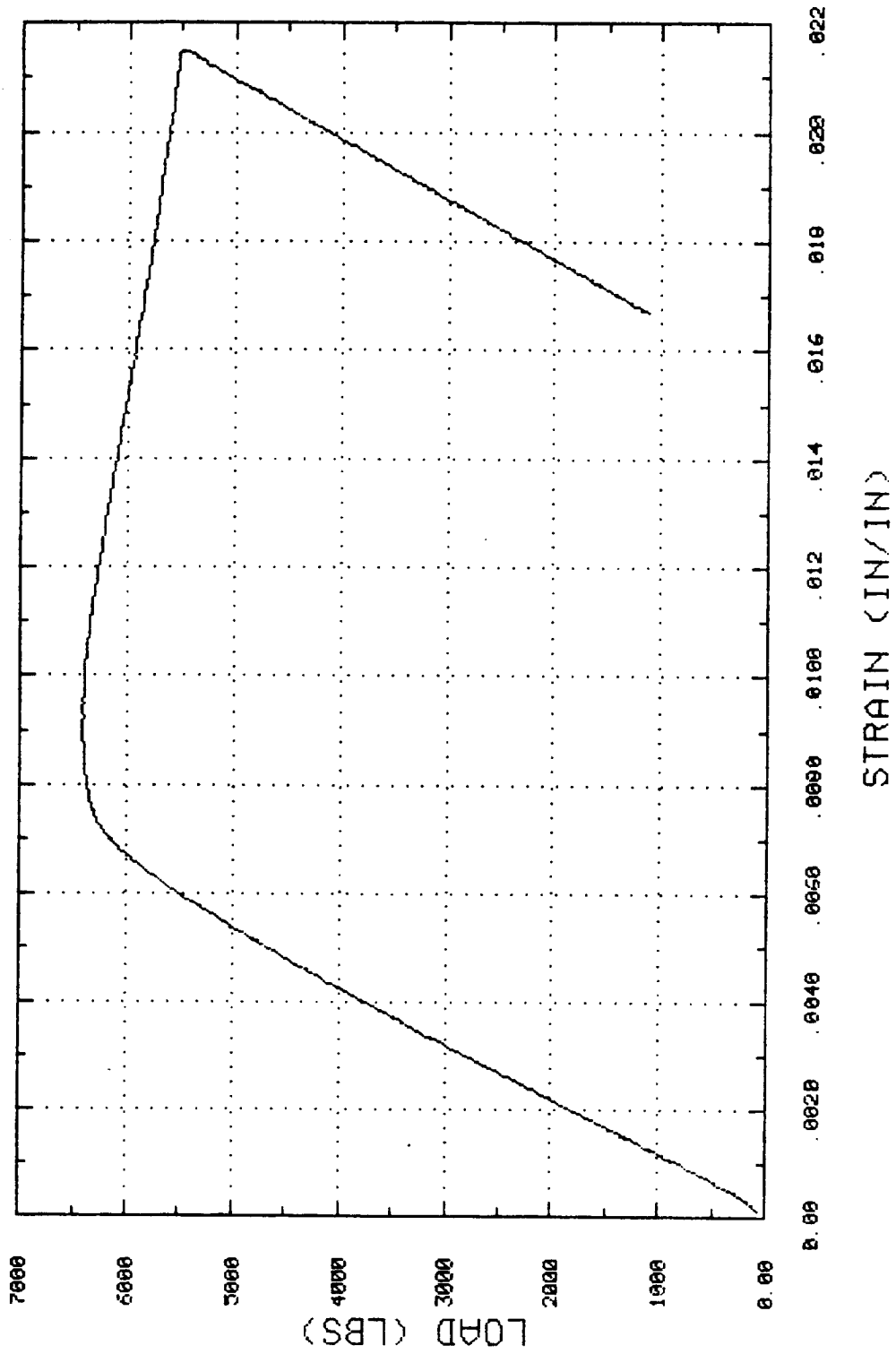


TENSION SPECIMEN NO. 652801, VIEW NO. 6, PHOTO NO. 40735

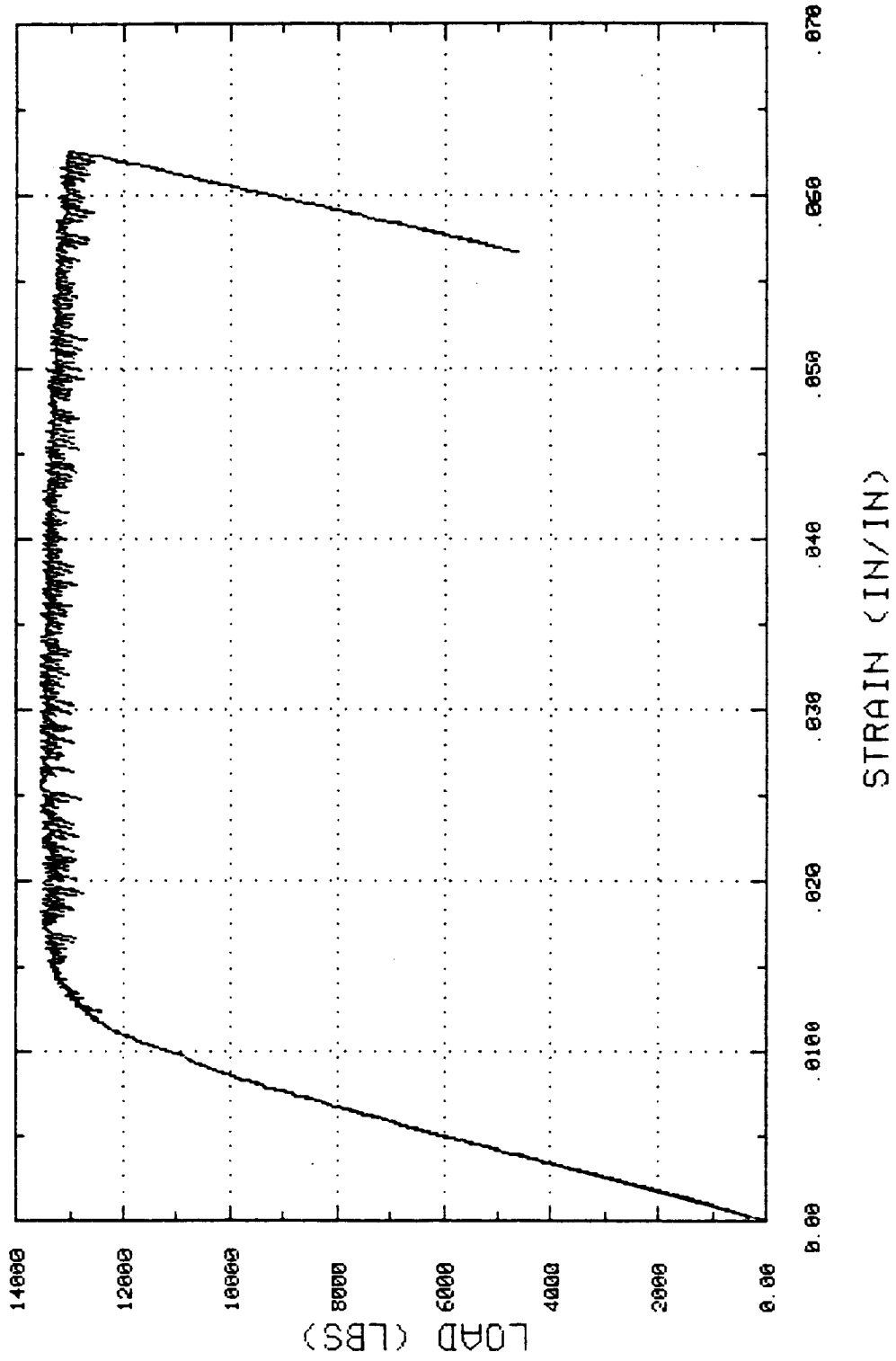
## **7 Appendix C: Computer Plots of Compression Tests**



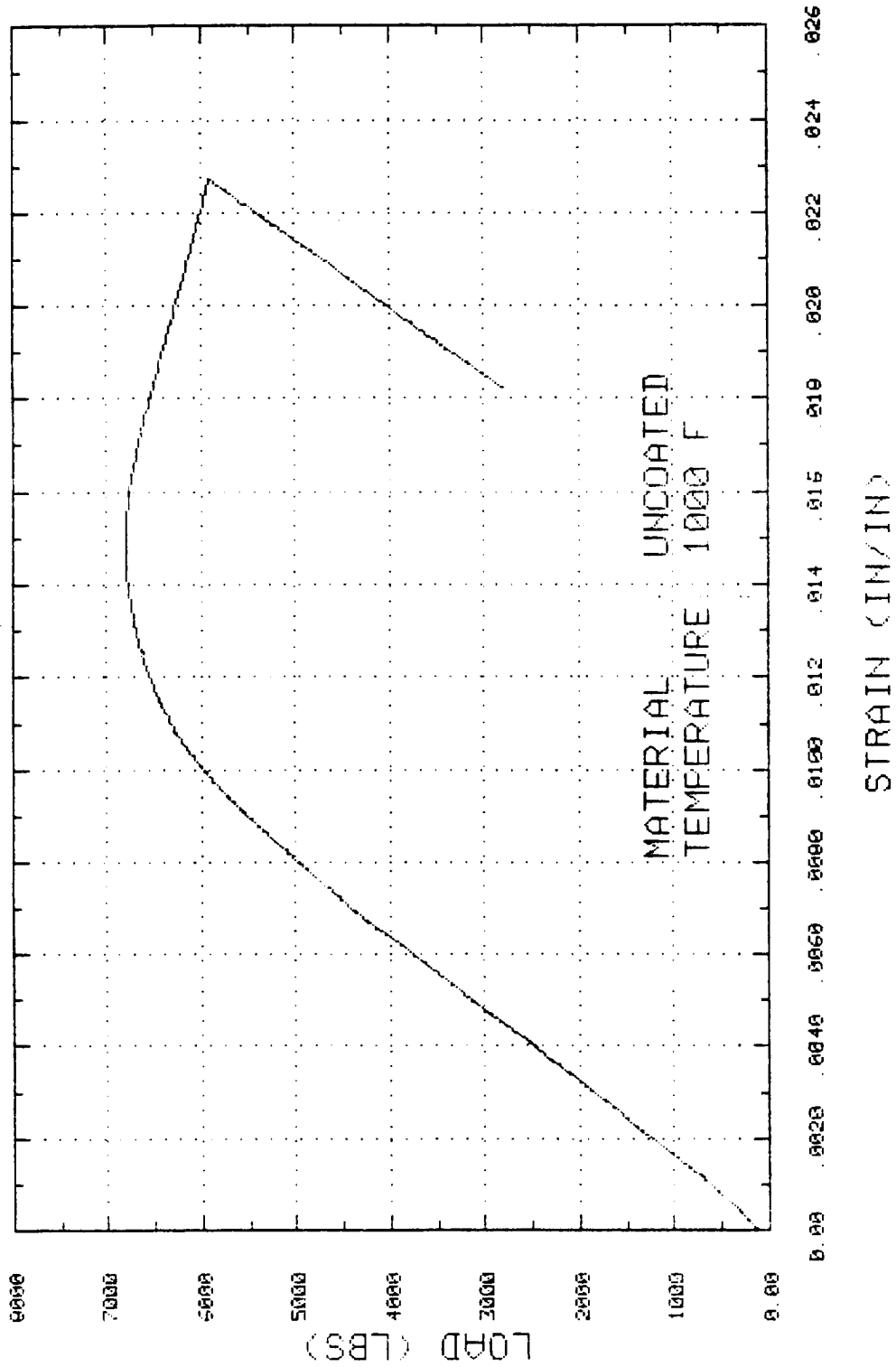
06-1778 PROJECT  
SPECIMEN 20



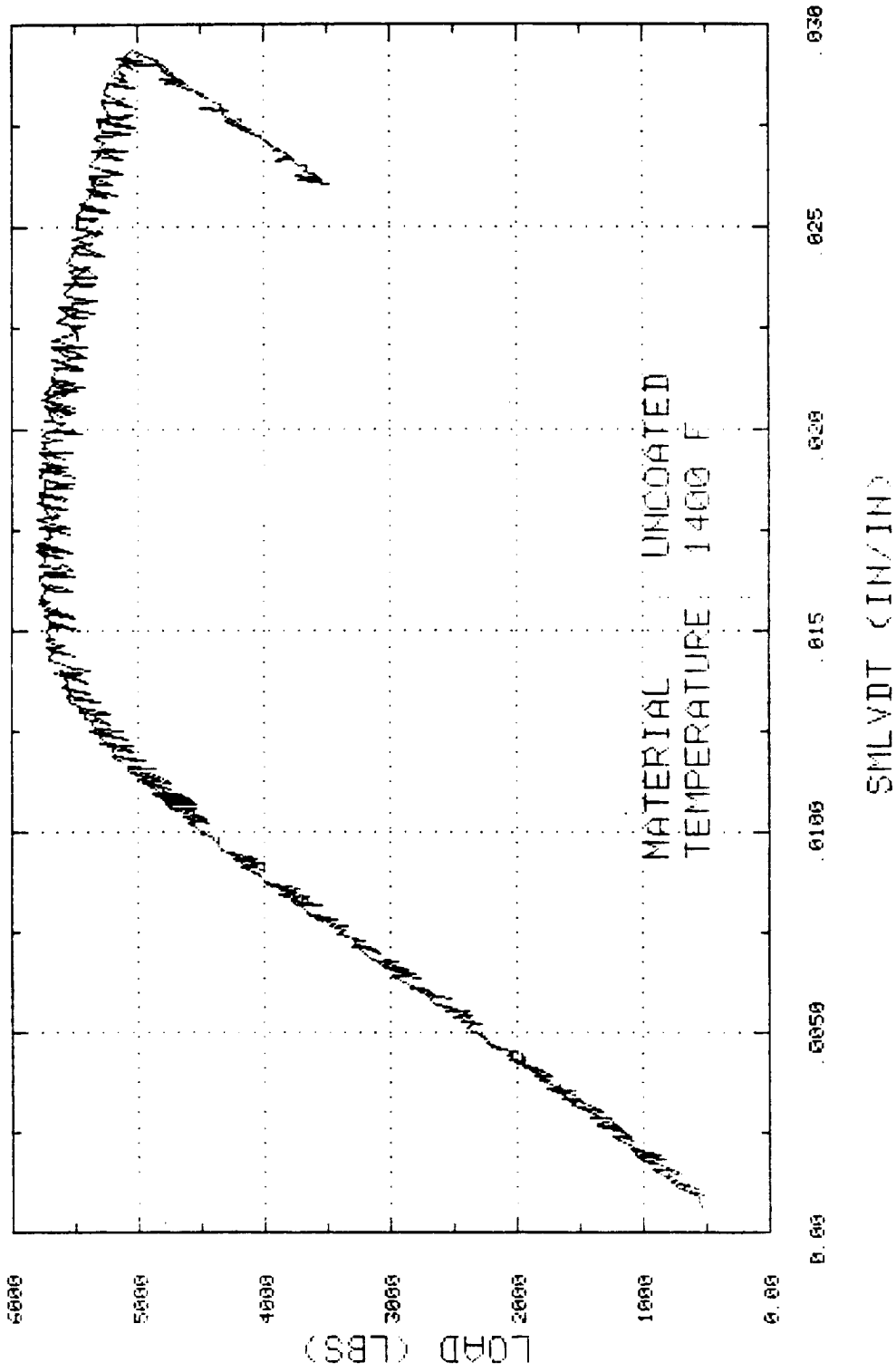
06-1778 PROJECT  
SPECIMEN 33



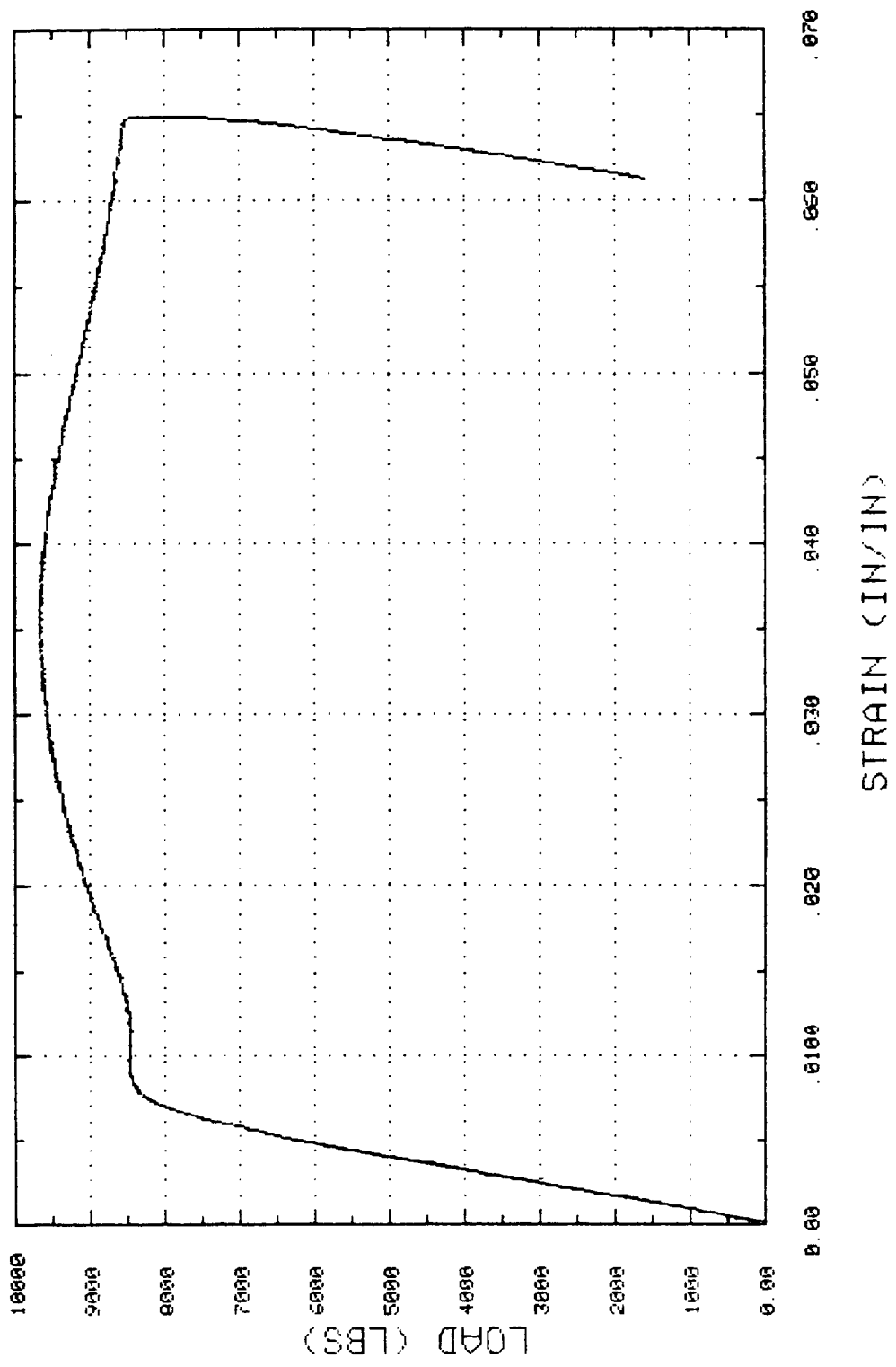
06-1778 PROJECT  
SPECIMEN 34



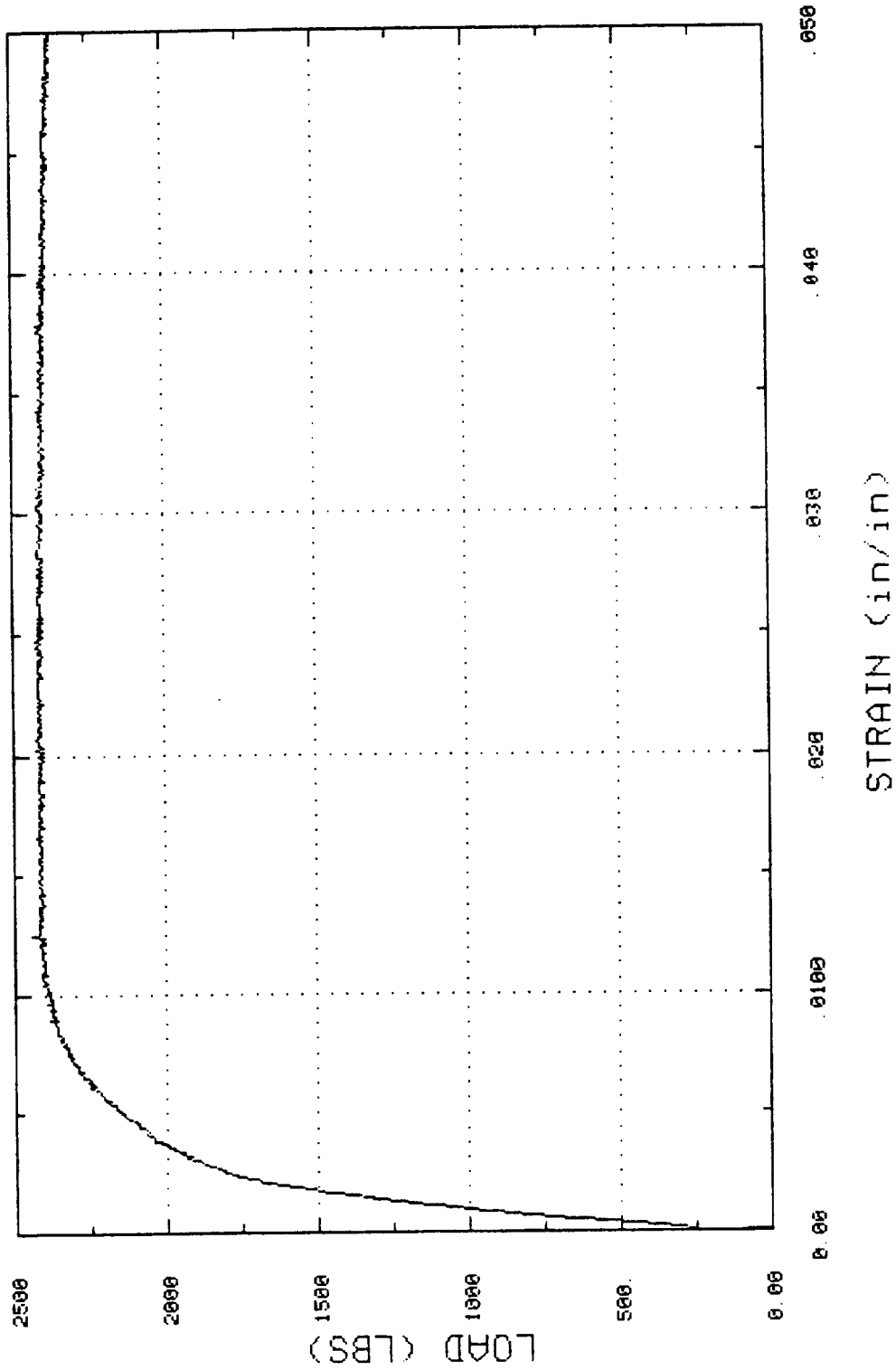
06-1778 PROJECT  
SPECIMEN 17



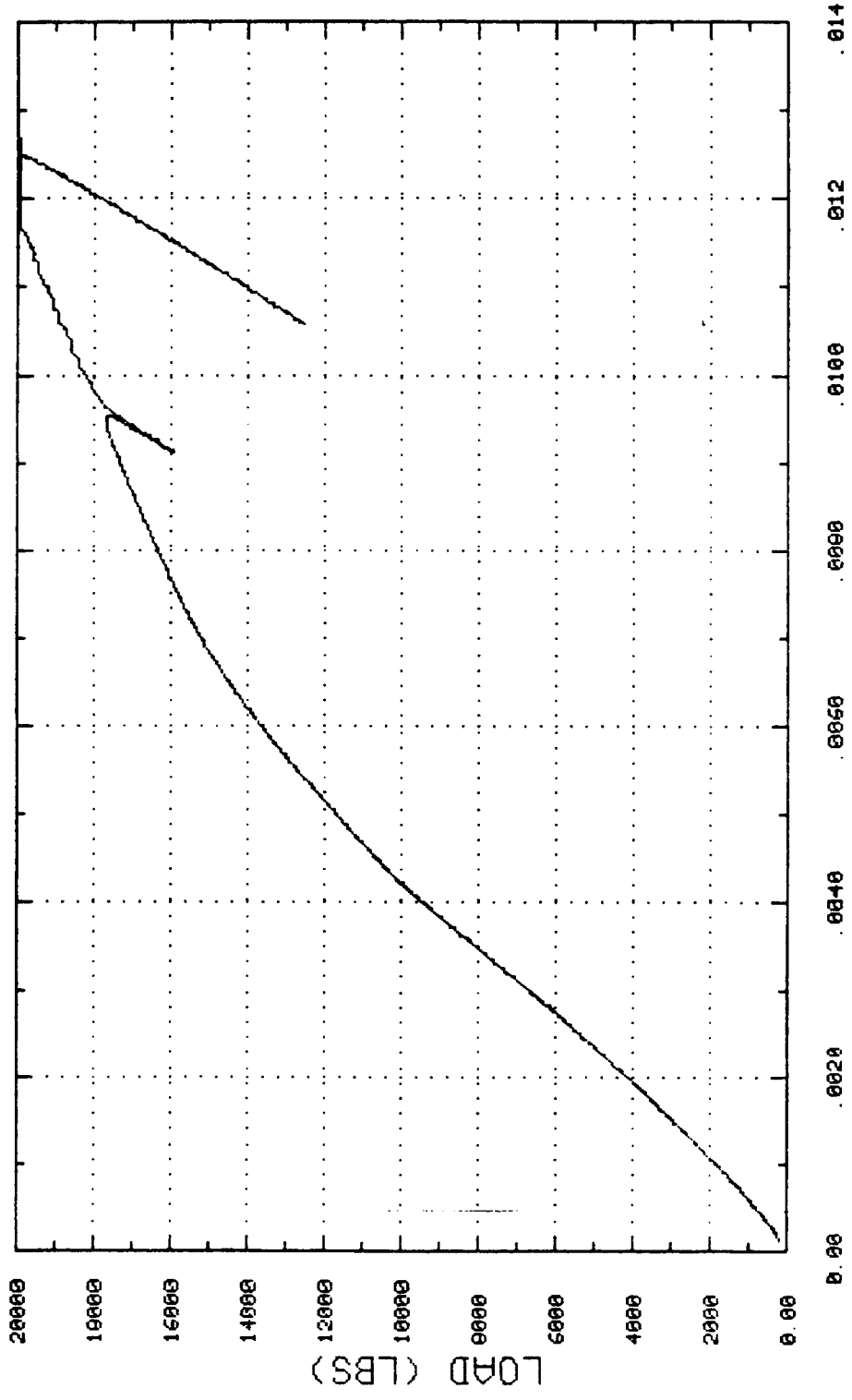
06-1778 PROJECT  
SPECIMEN 32



06-1778 PROJECT  
SPECIMEN 31

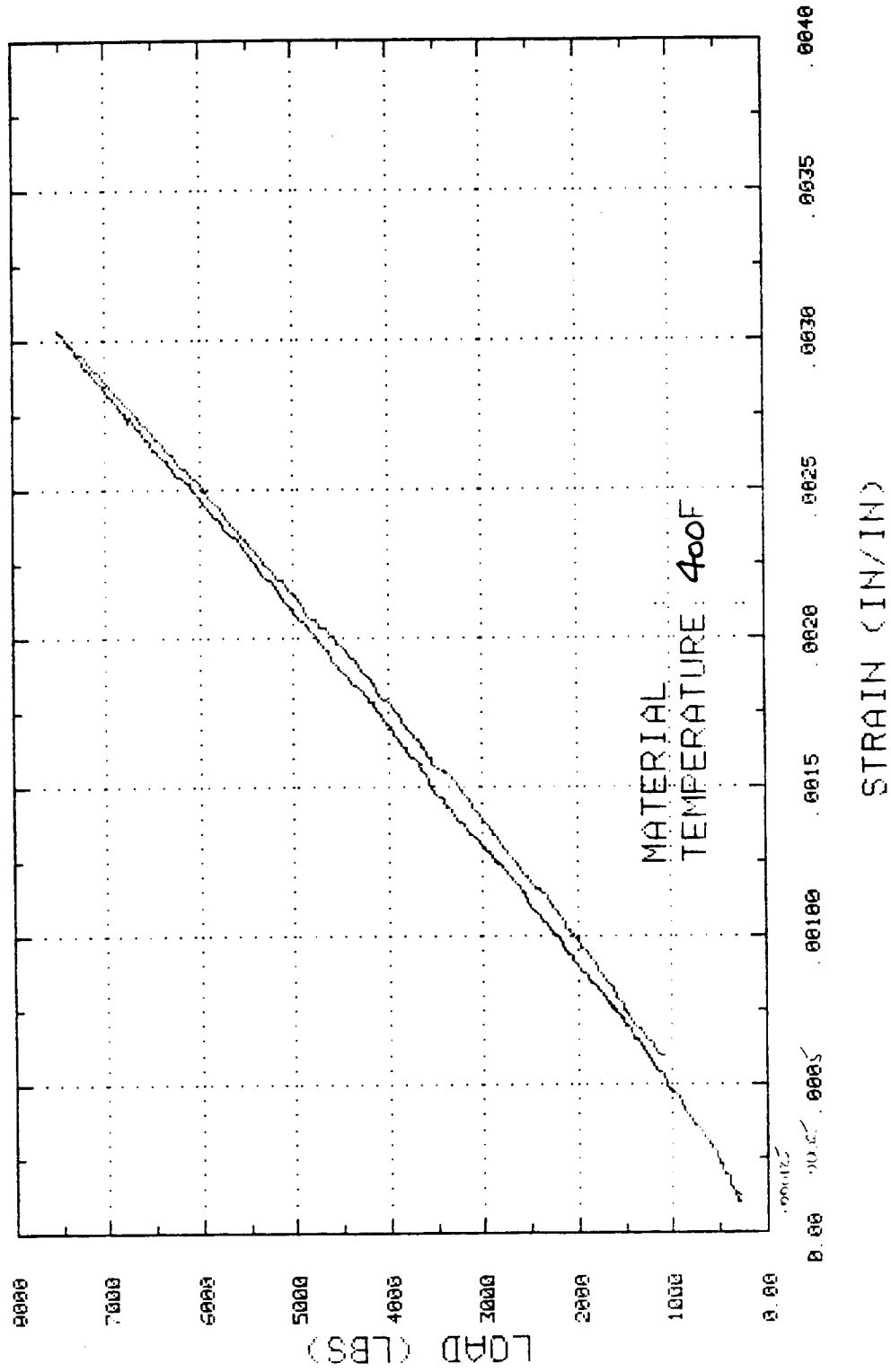


06-1778 PROJECT  
SPECIMEN 18A



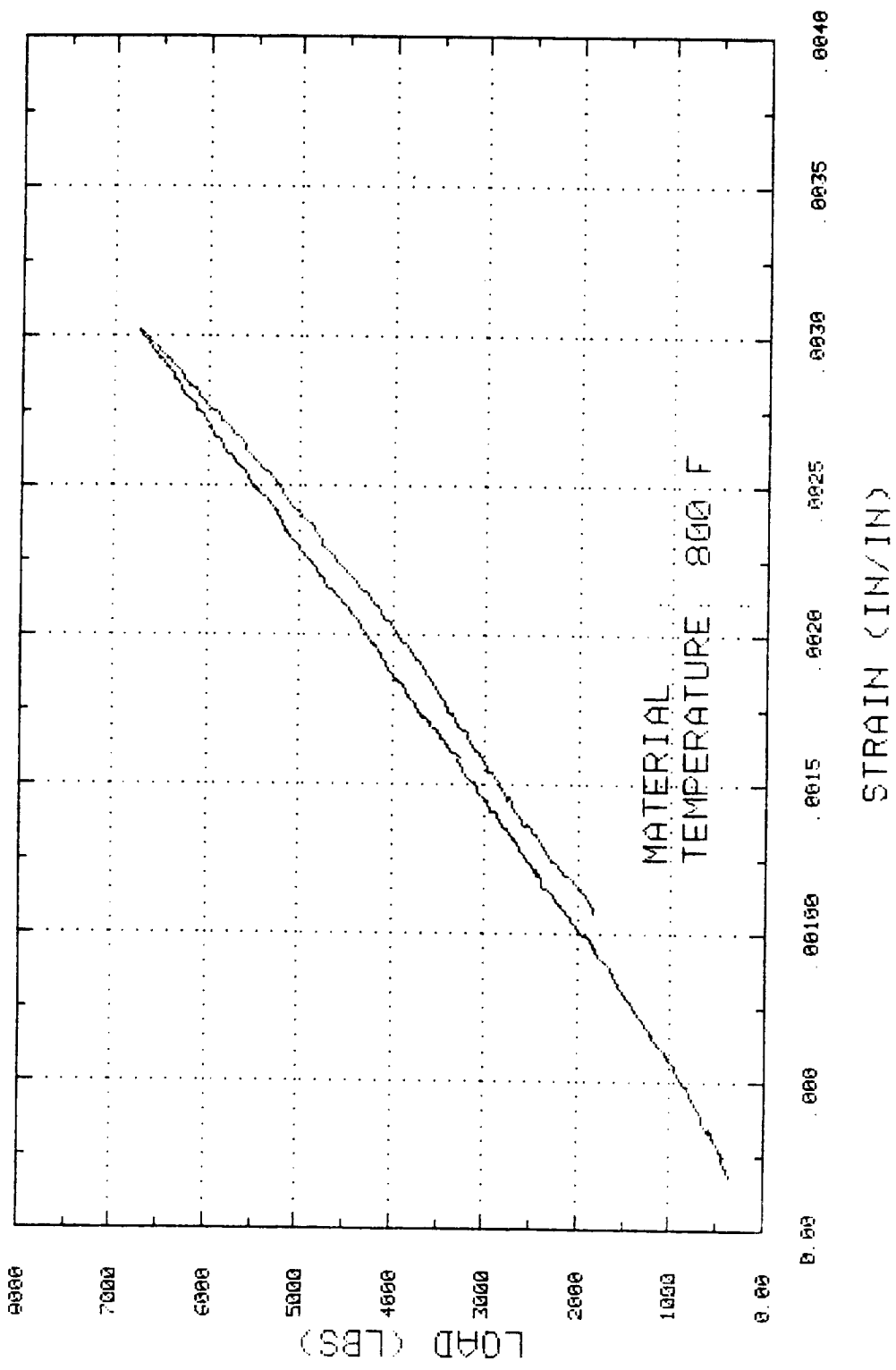
STRAIN (IN/IN)

06-1778 PROJECT  
SPECIMEN 27A1

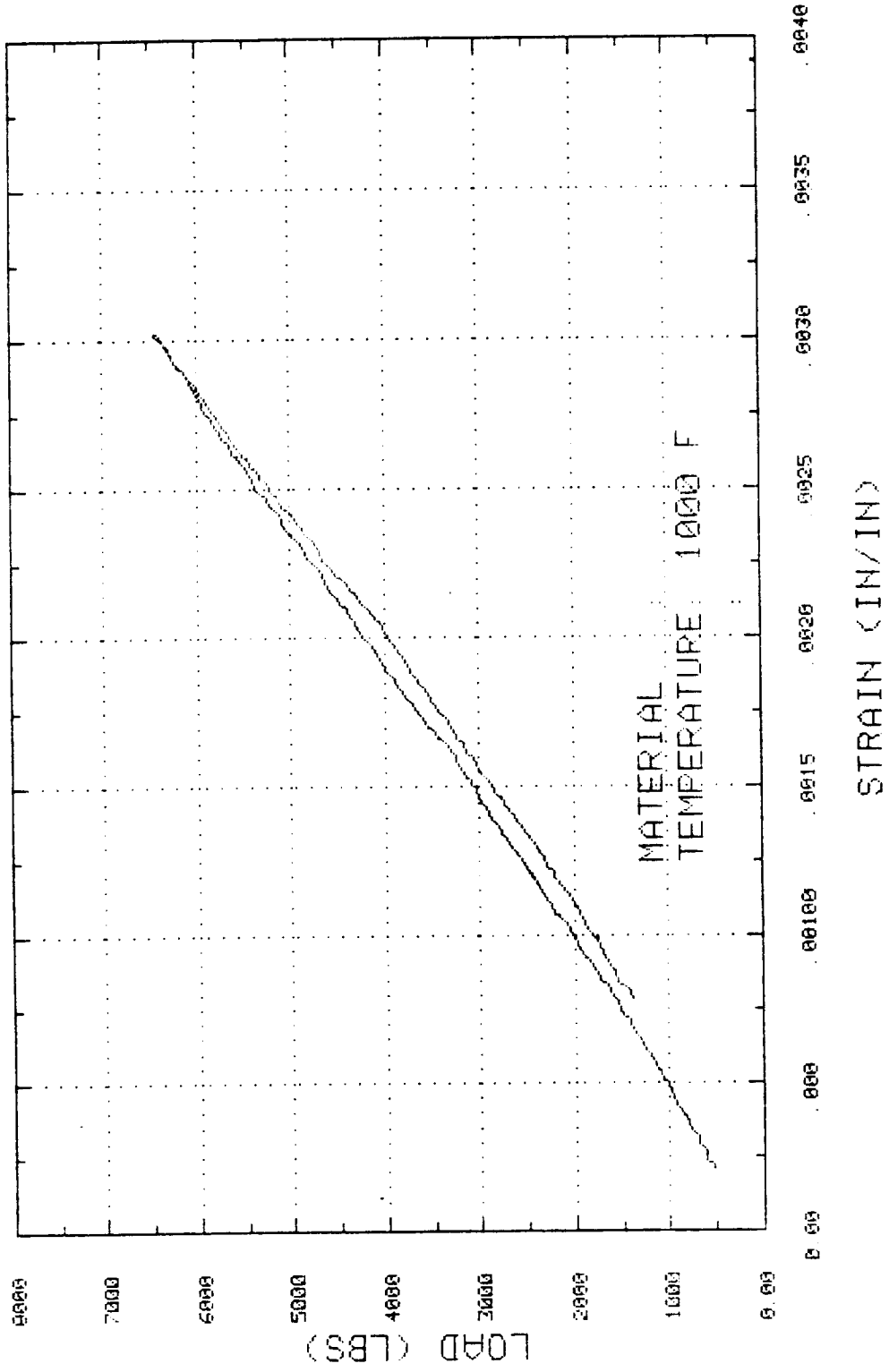




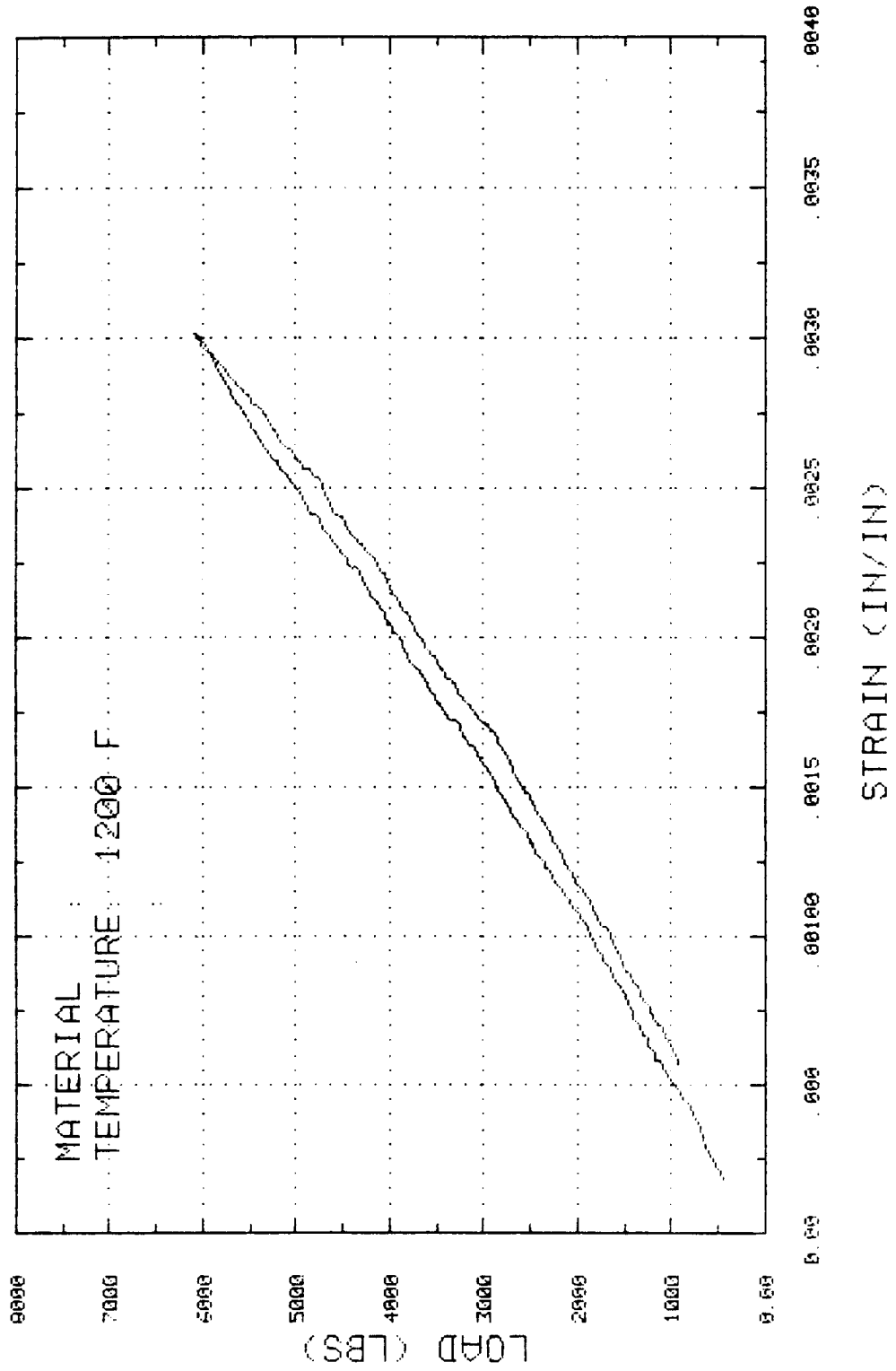
06-1778 PROJECT  
SPECIMEN 27B1



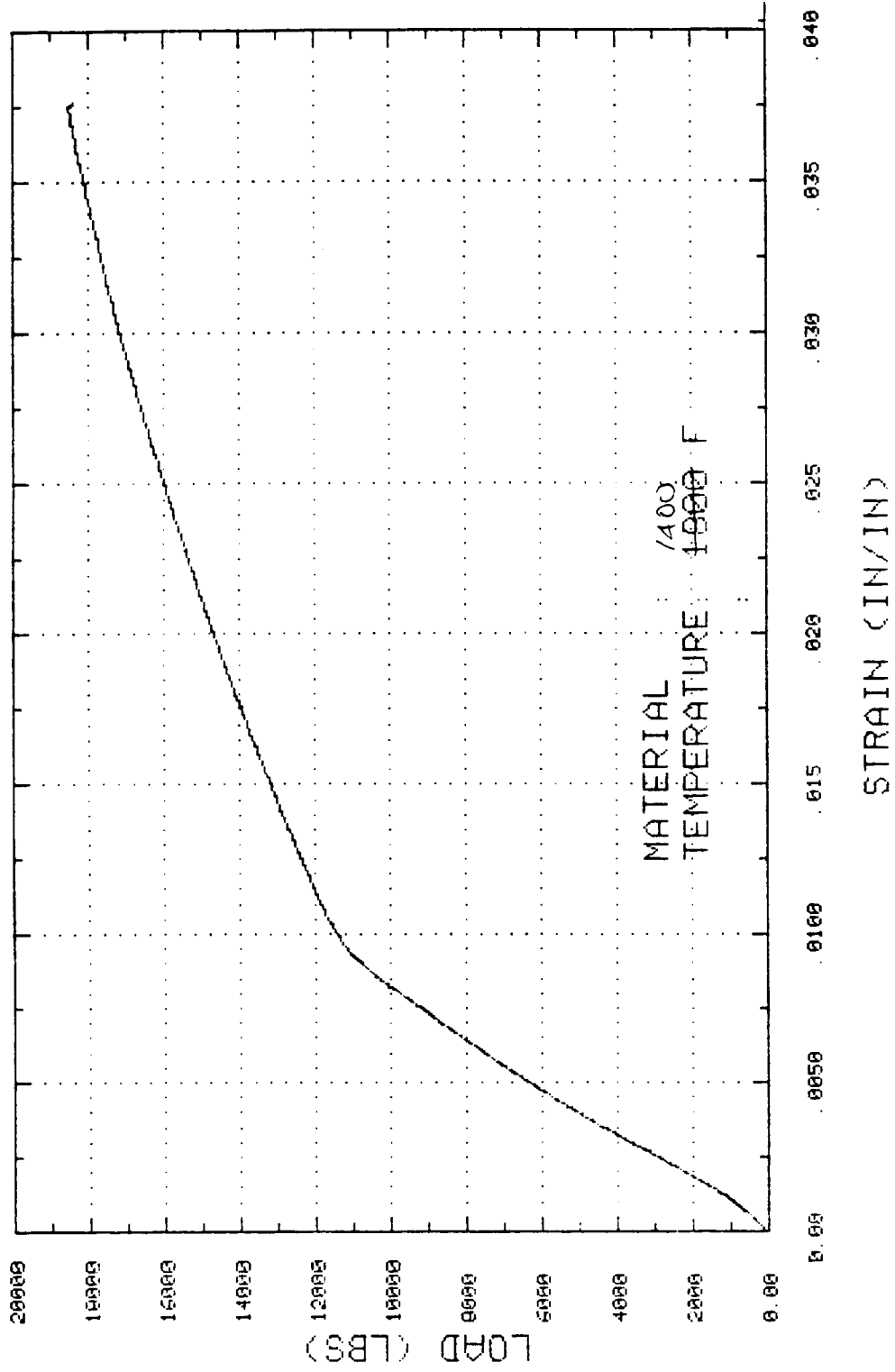
06-1778 PROJECT  
SPECIMEN 2702



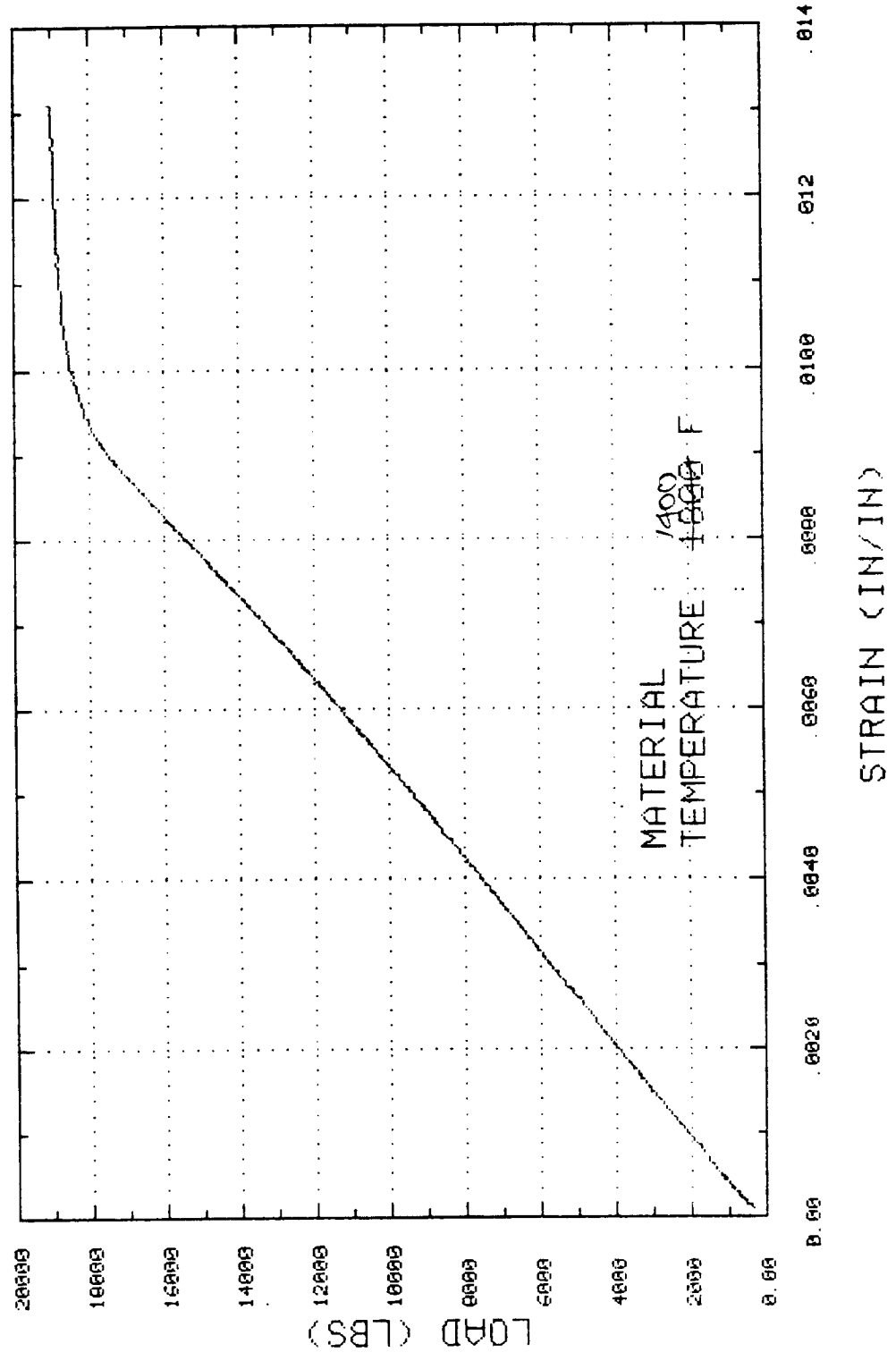
06-1778 PROJECT  
SPECIMEN 27D2



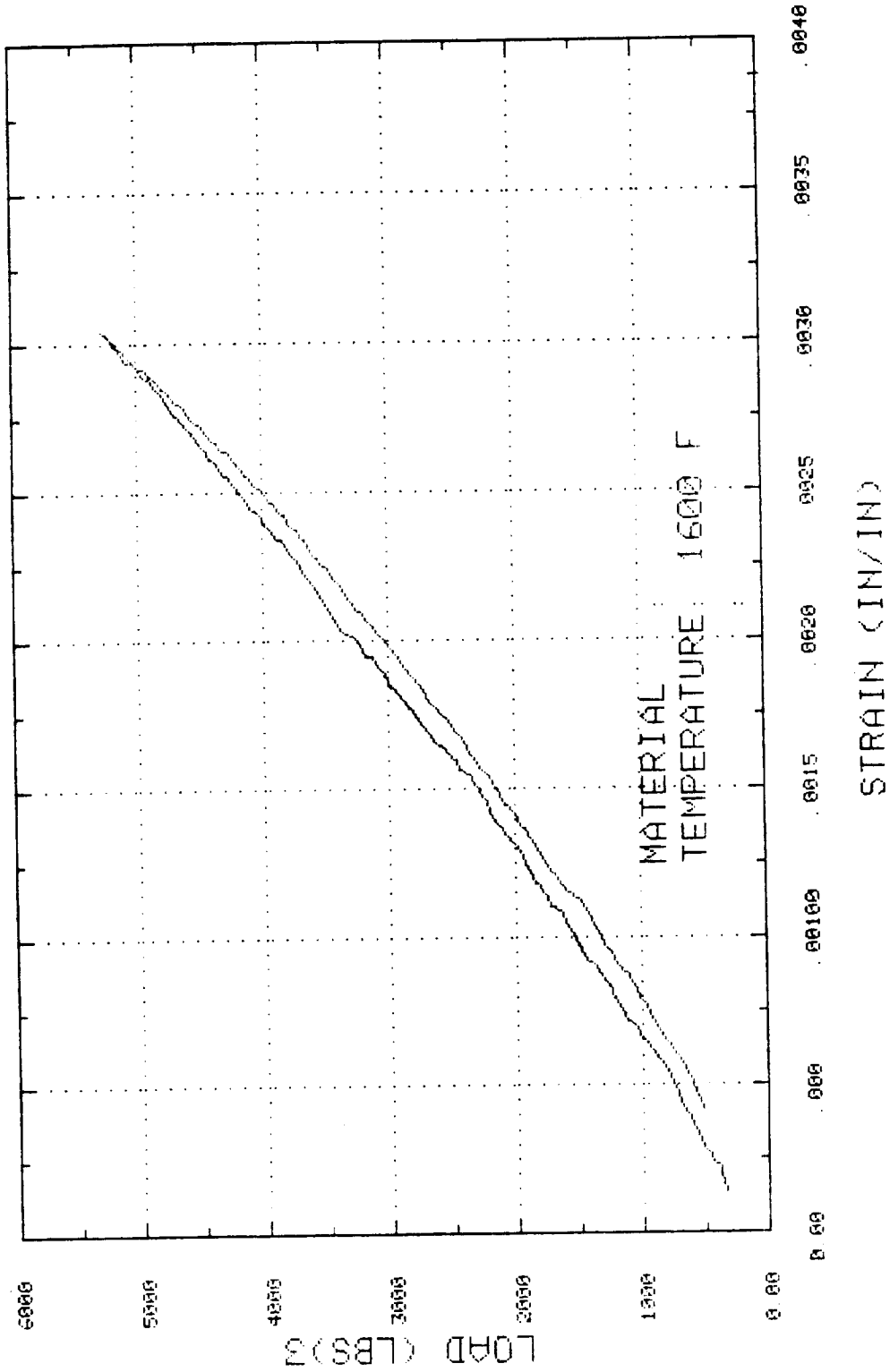
06-1778 PROJECT  
SPECIMEN 21D



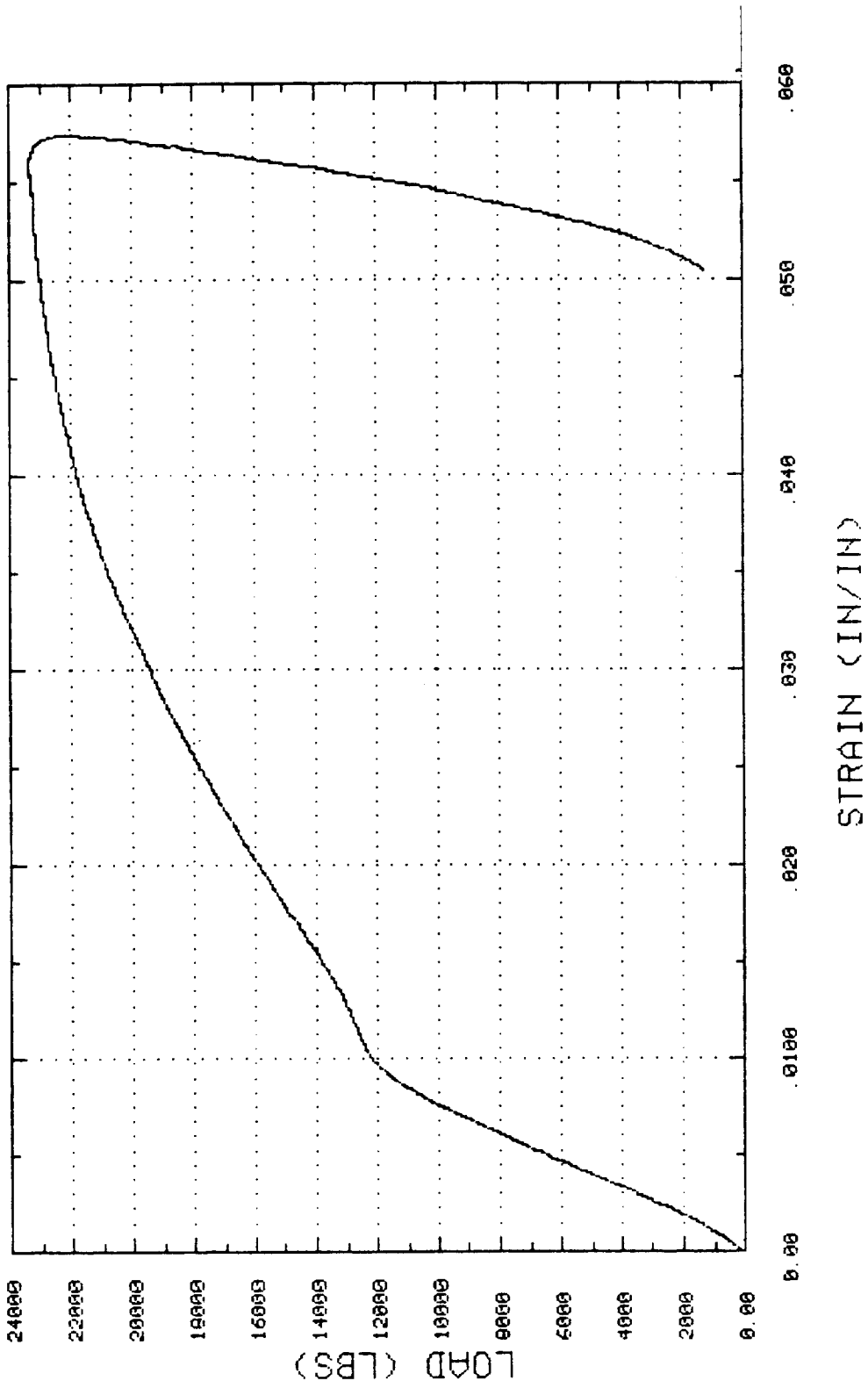
06-1778 PROJECT  
SPECIMEN 21E



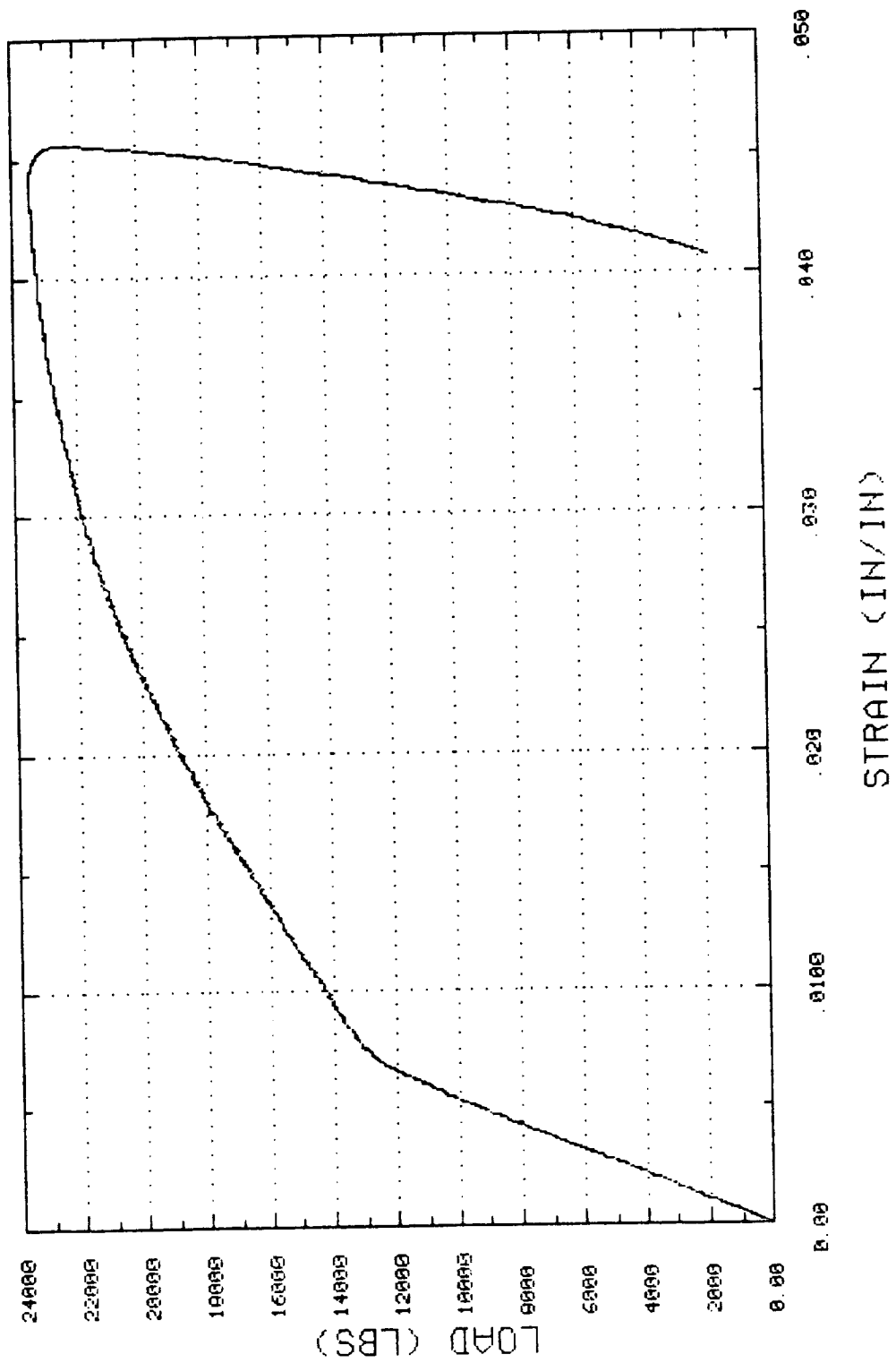
06-1778 PROJECT  
SPECIMEN 27E2



06-1778 PROJECT  
SPECIMEN 26

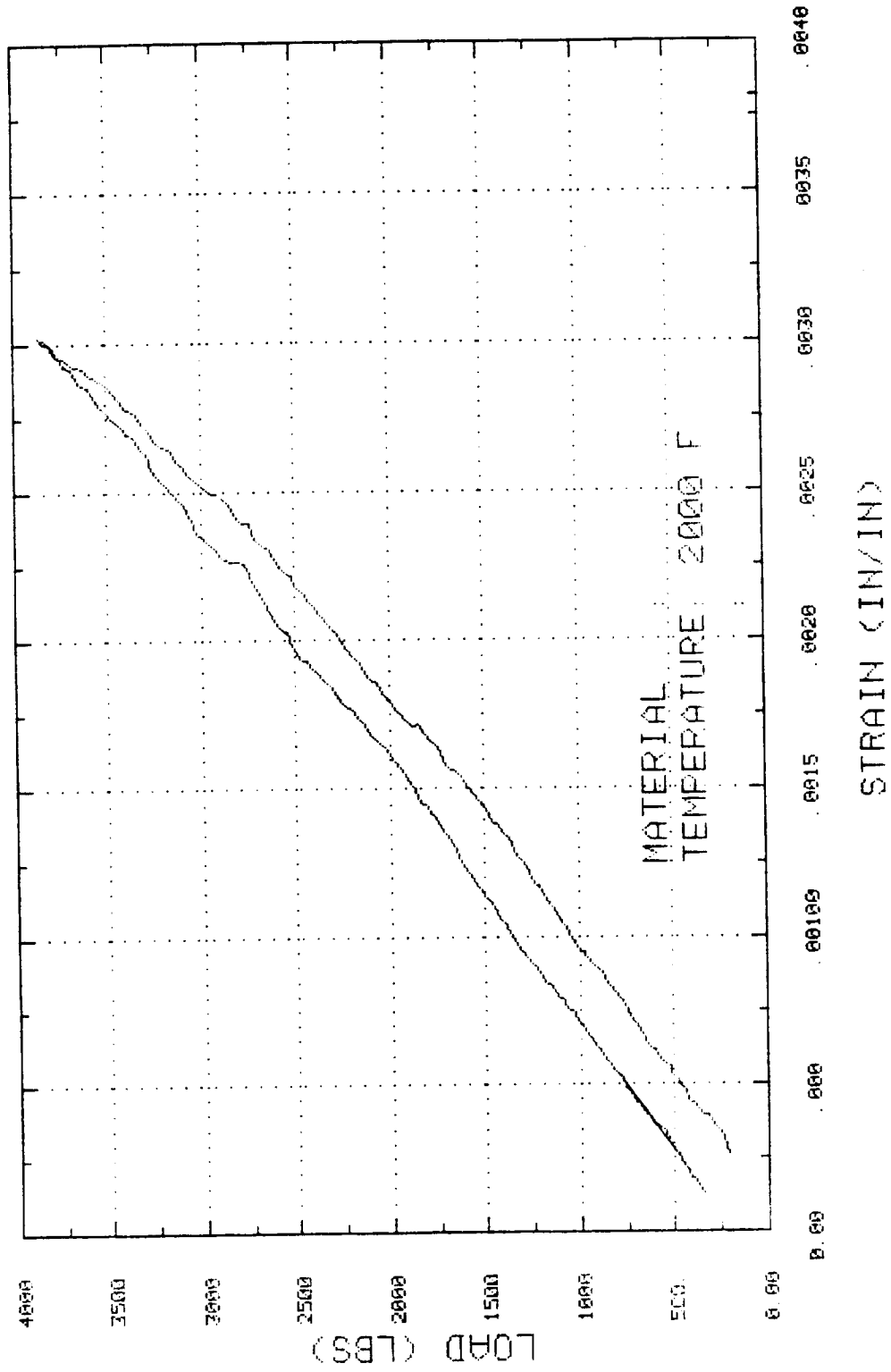


06-1778 PROJECT  
SPECIMEN 25

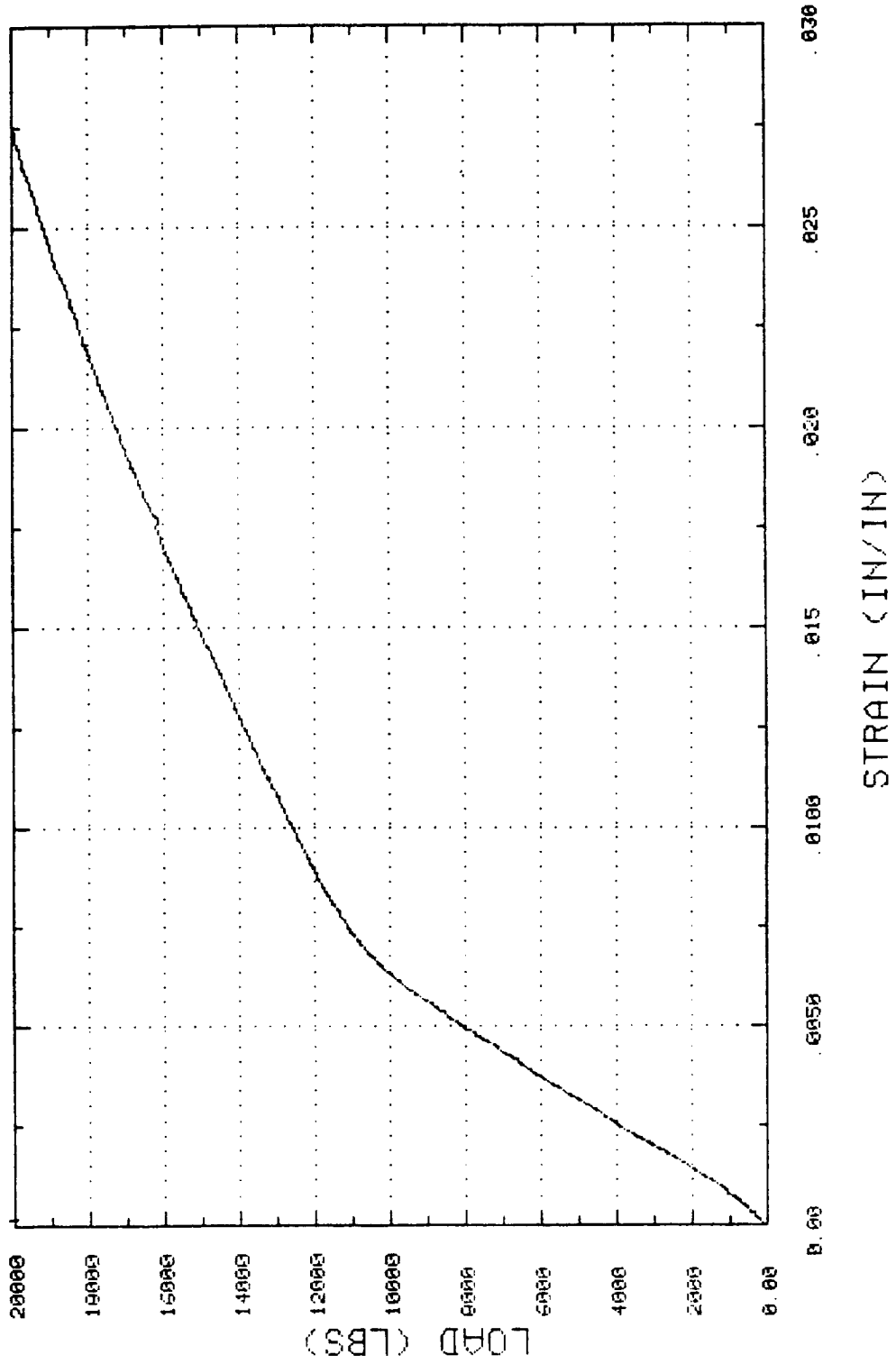




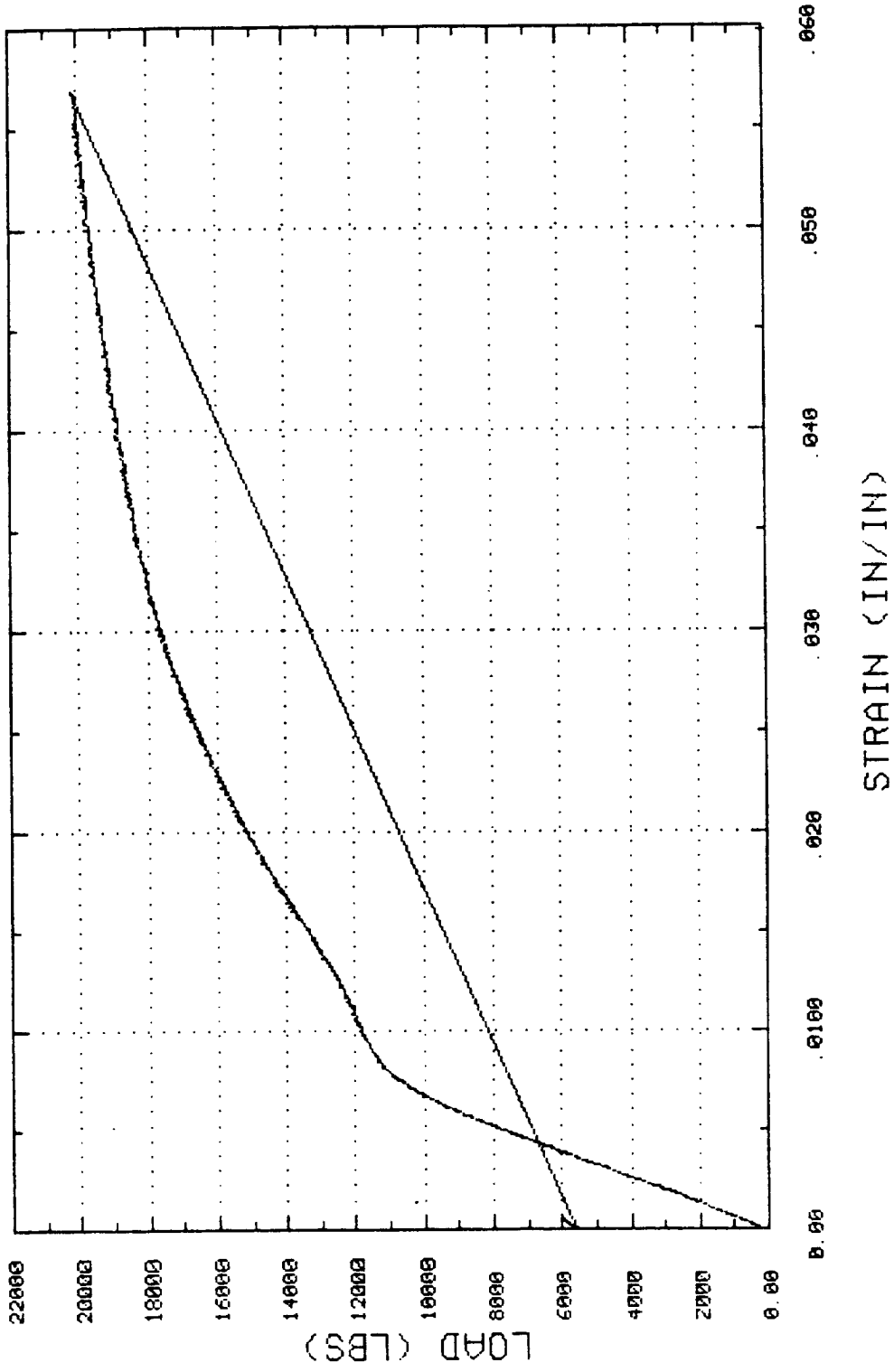
06-1778 PROJECT  
SPECIMEN 27f2



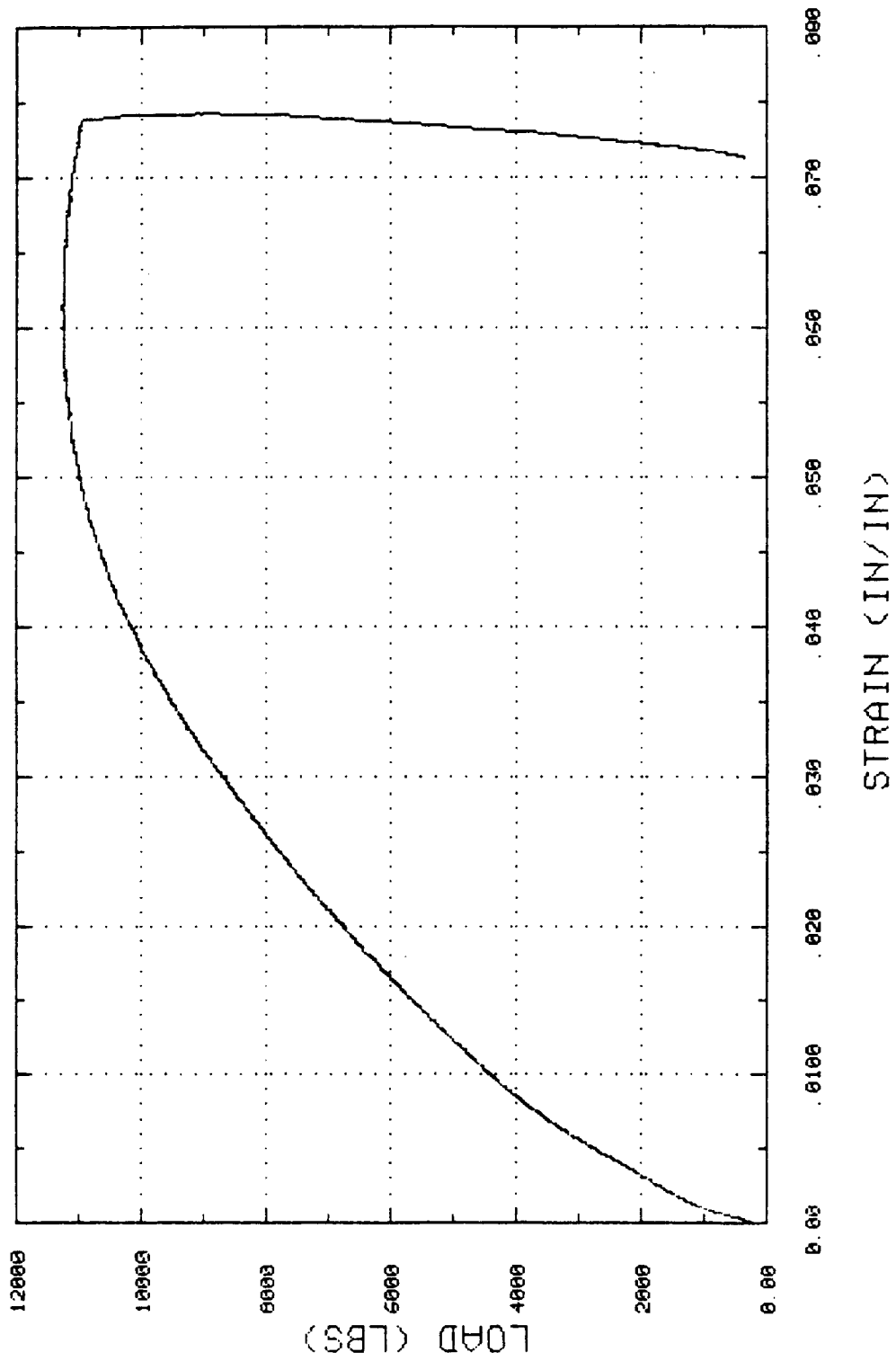
06-1778 PROJECT  
SPECIMEN 30



06-1778 PROJECT  
SPECIMEN 24

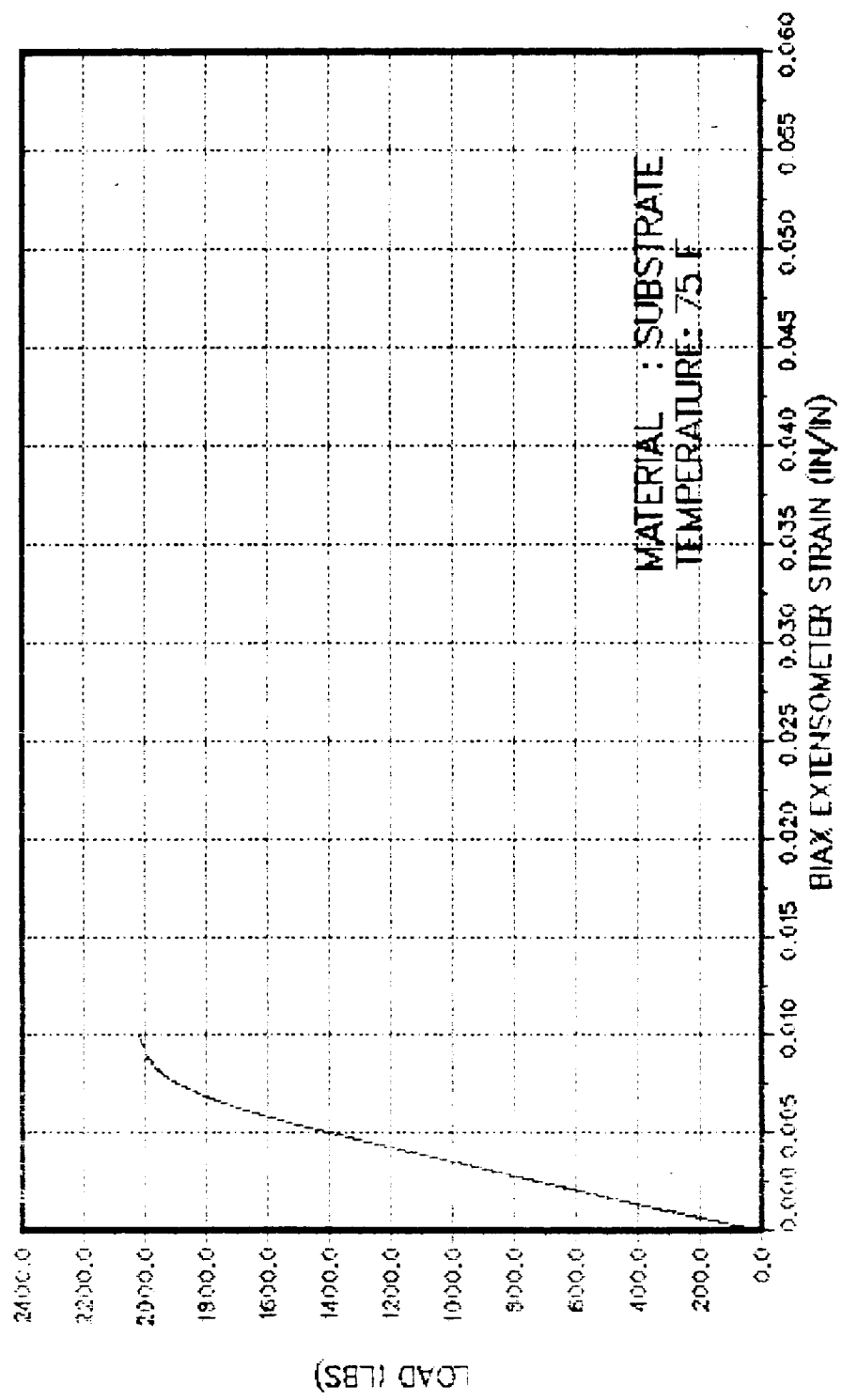


06-1778 PROJECT  
SPECIMEN 28

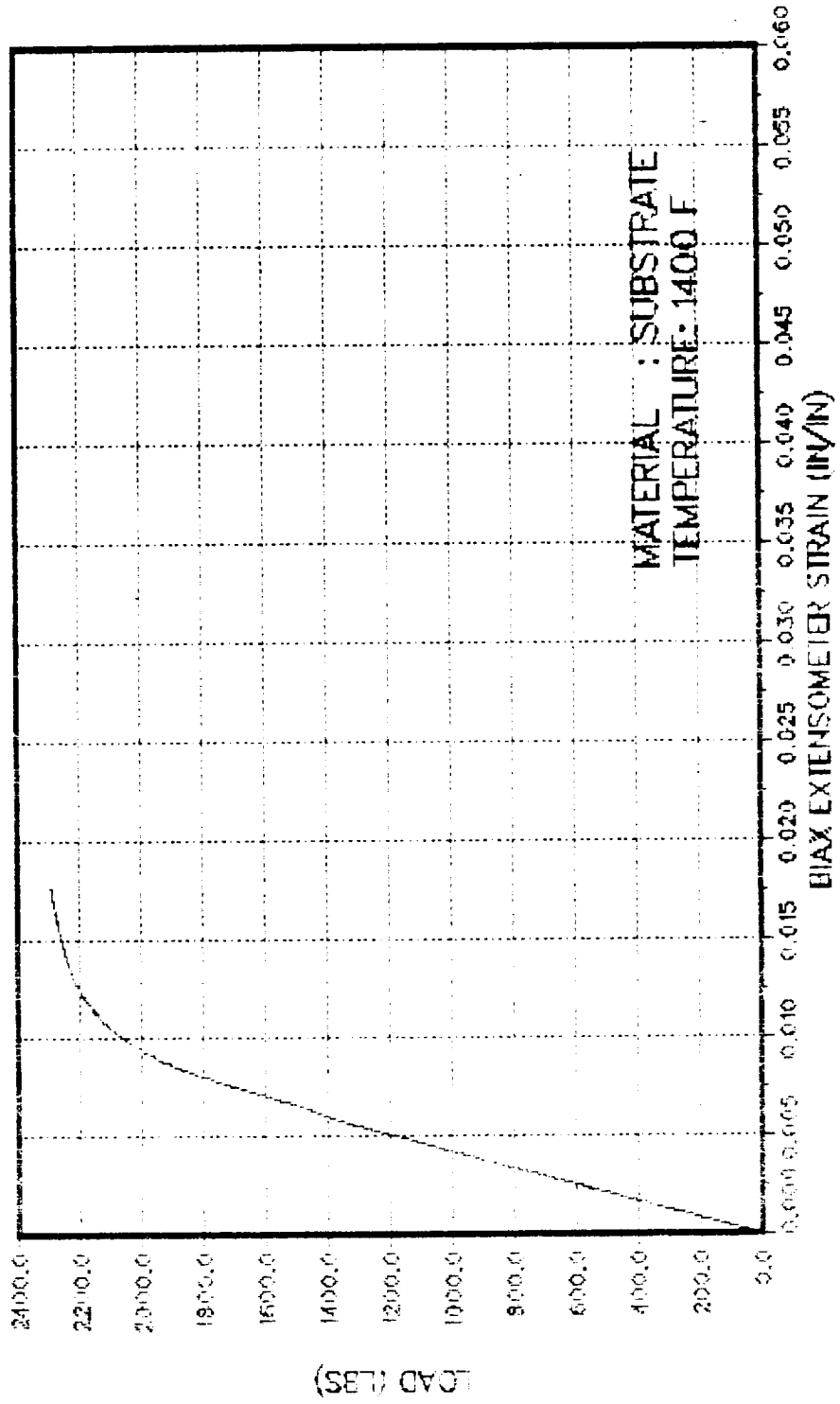


## 8 Appendix D: Computer Plots of Tension Tests

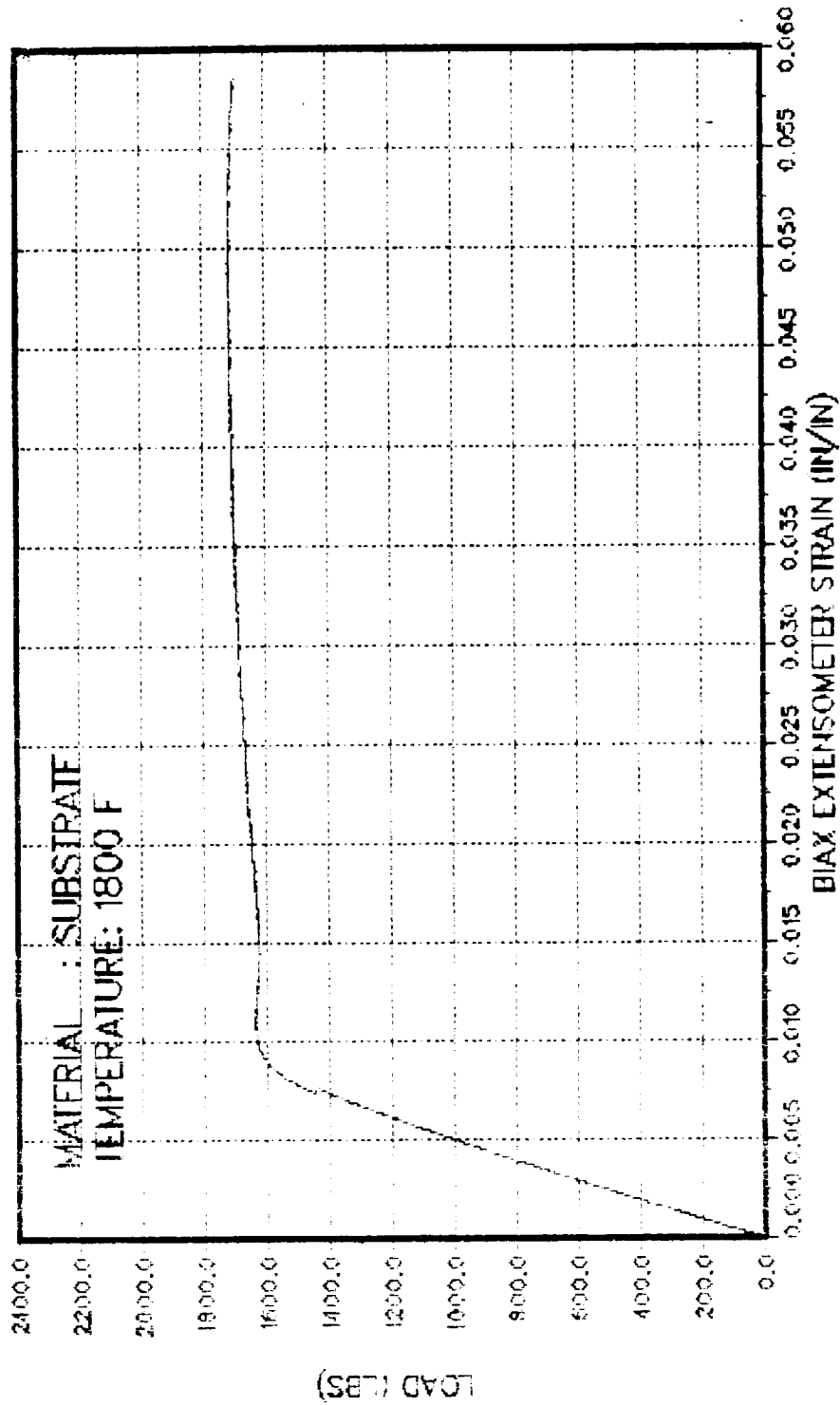
8-MAR-90 22:50 VIRPLX-1.2 Frame# 1  
PROJECT 06-1778  
SPECIMEN 653601



8-MAR-90 22:54 VIRPLX-1.2 Frame# 1  
PROJECT 06-1778  
SPECIMEN 653605

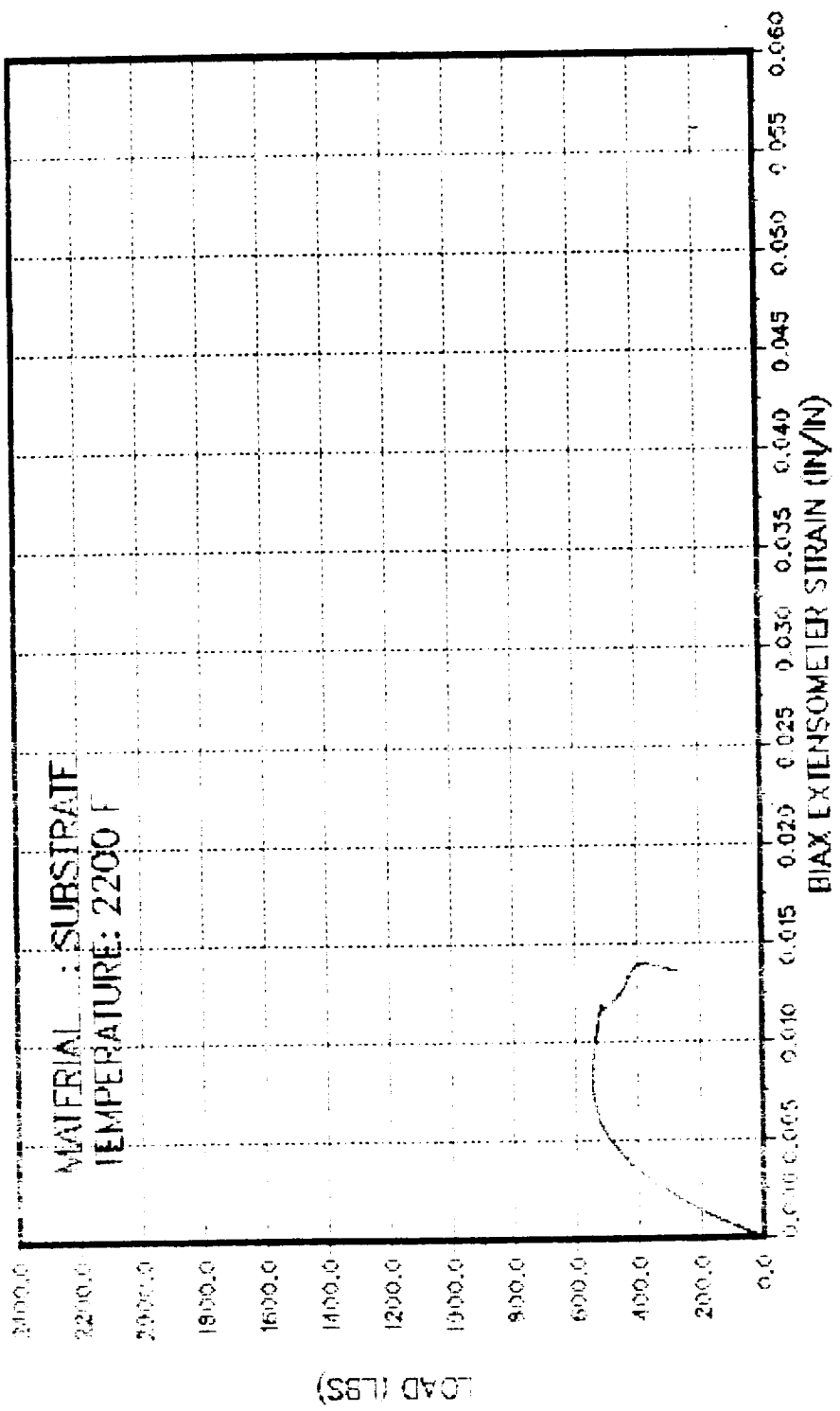


8-MAR-90 22:58 VIRPLX-1.2 Frame# 1  
PROJECT 06-1778  
SPECIMEN 653701





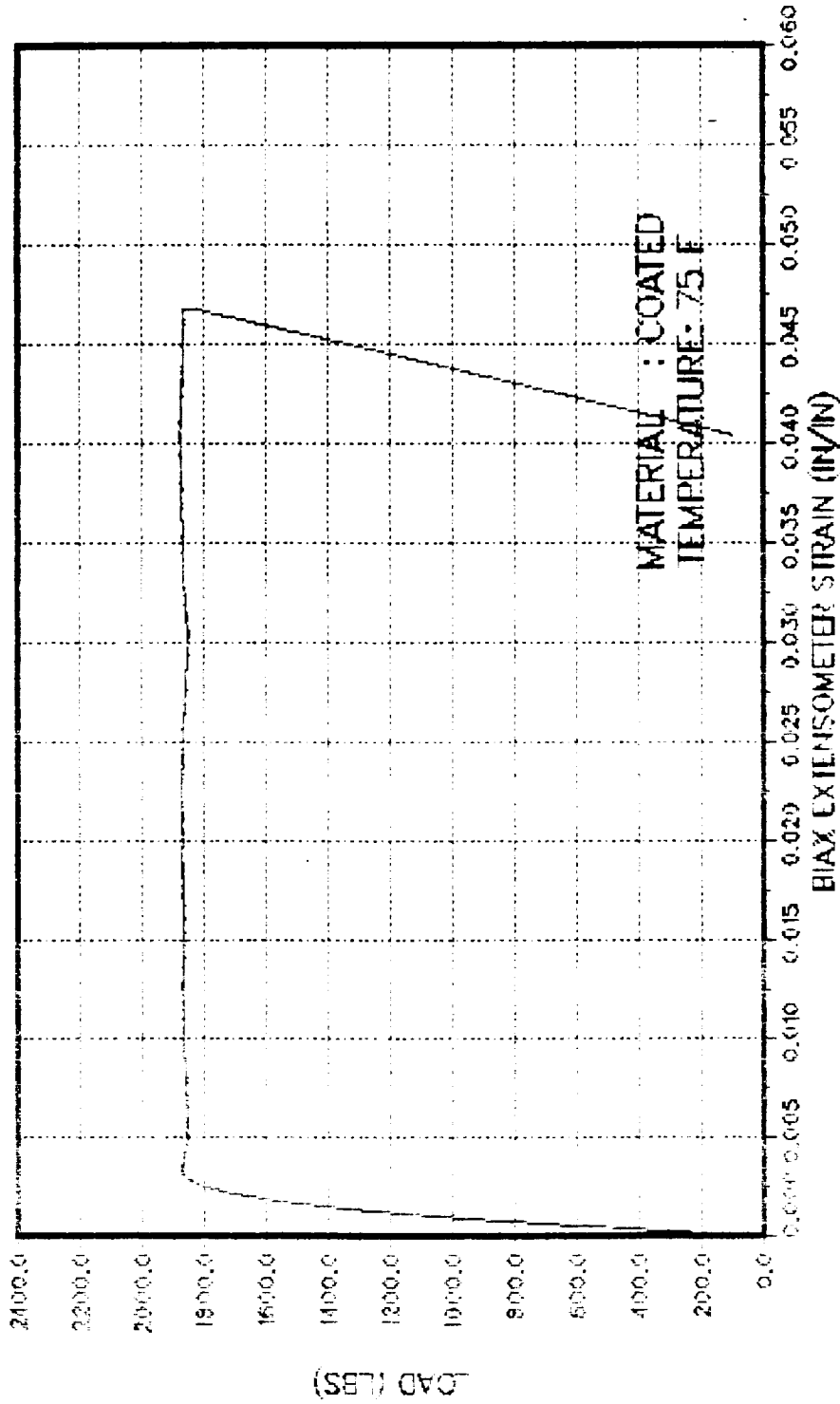
8-MAR-90 23:02 VIRELX-1.2 Frame# 1  
PROJECT 06-1778  
SPECIMEN 653702



8-MAR-90 23:06 VIRPLX-1.2 Frame# 1

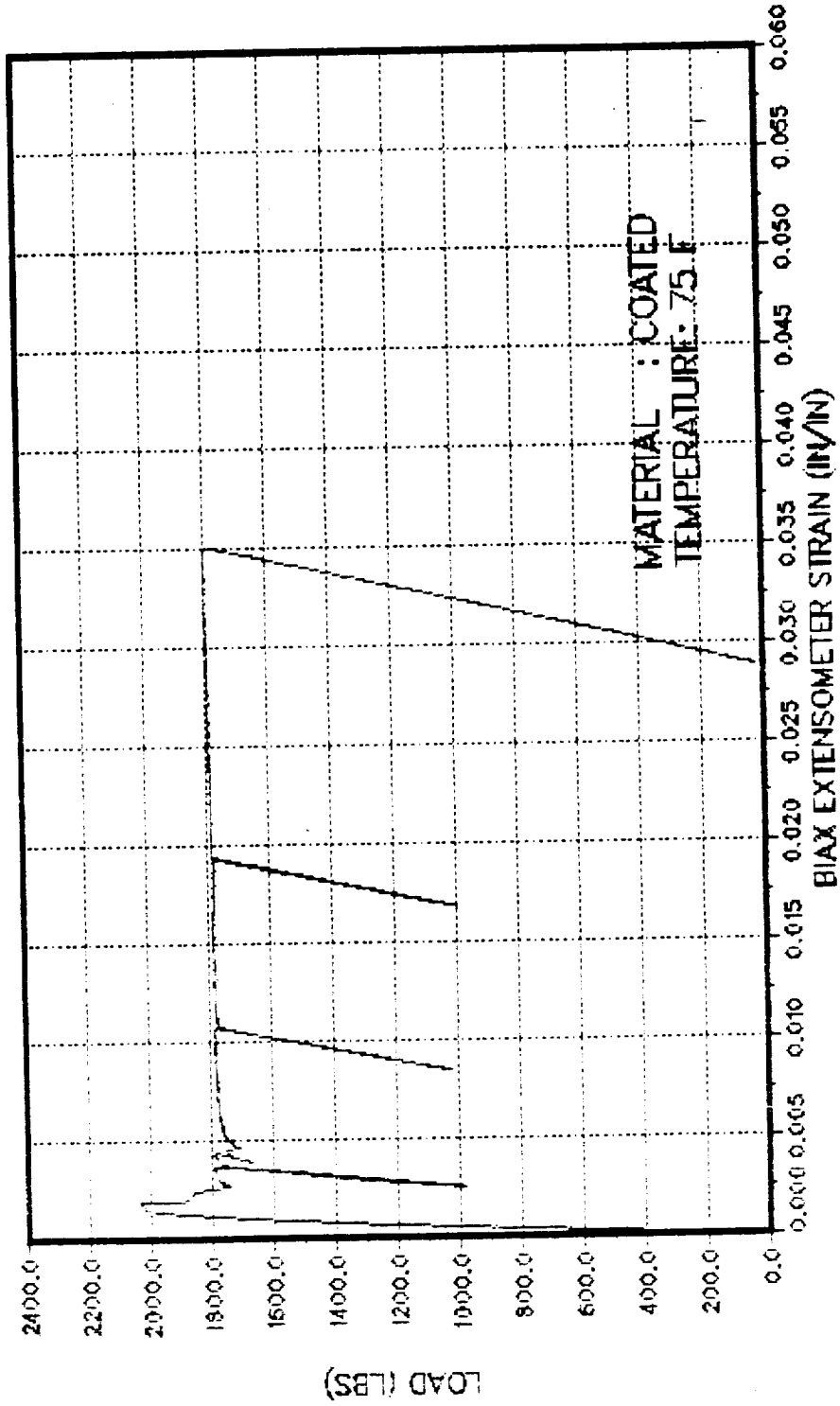
PROJECT 06-1778

SPECIMEN 652801



C2

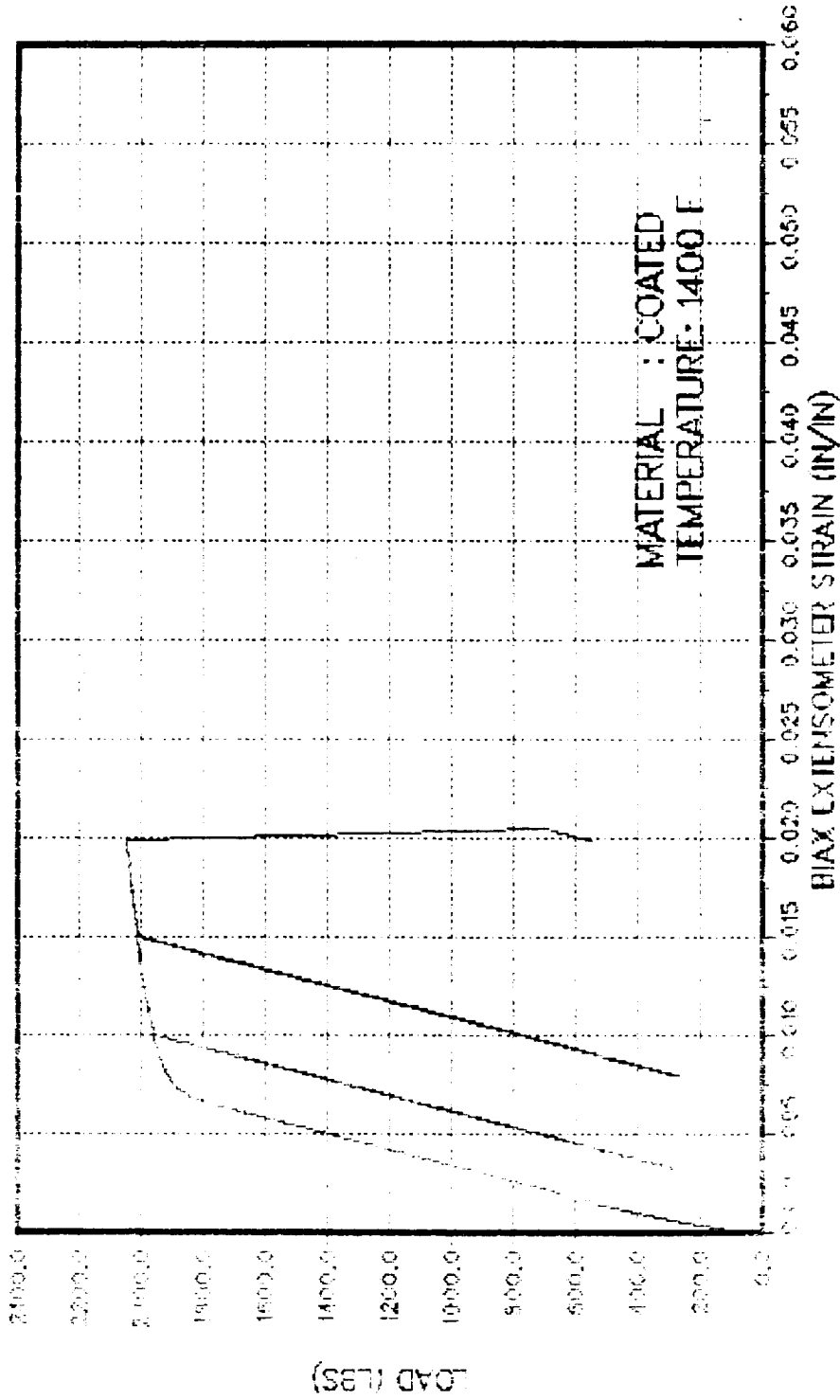
8-MAR-90 23:12 VIRPLX-1.2 frame# 1  
PROJECT 06-1778  
SPECIMEN 652805



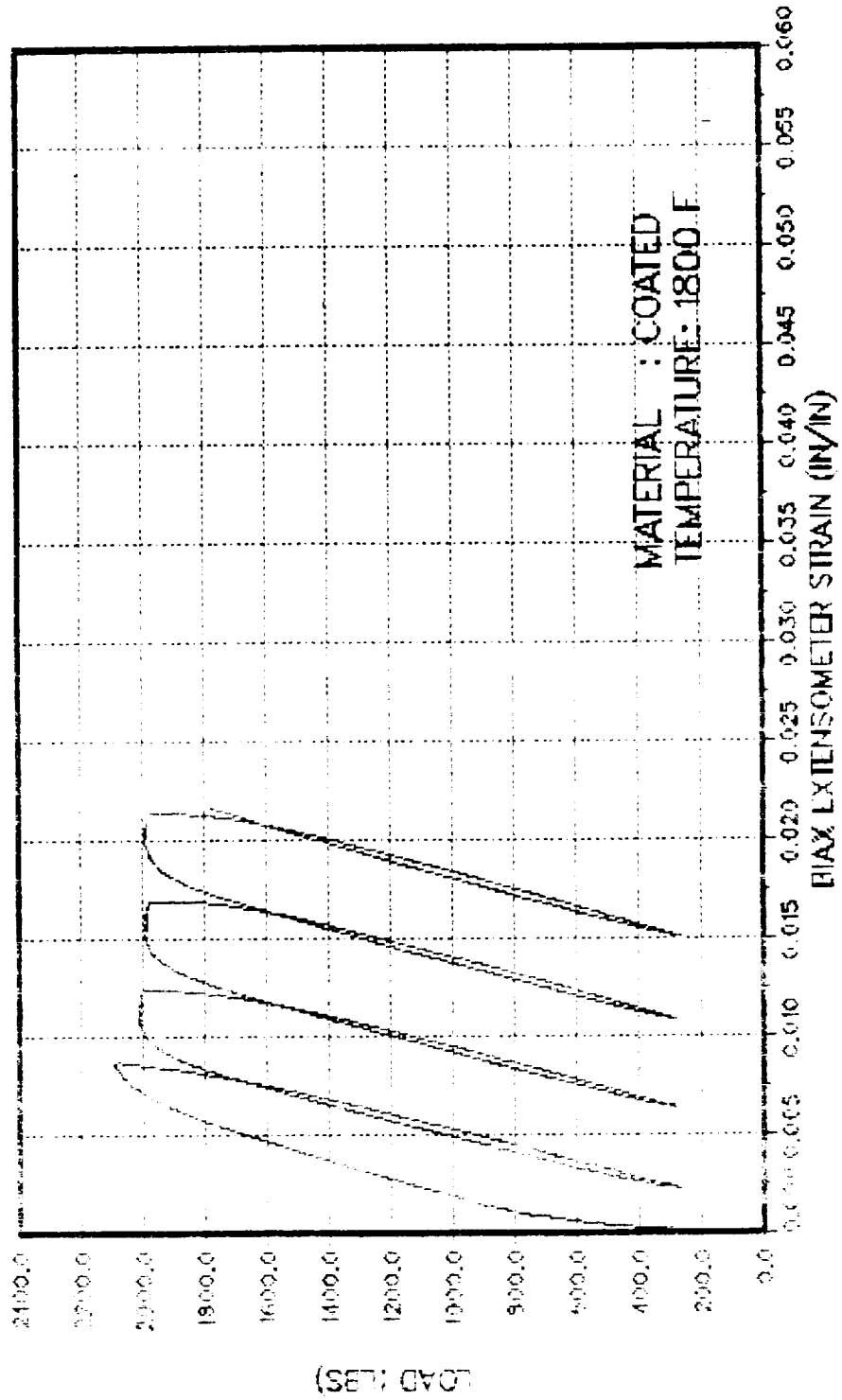
S-MAR-90 2:32:21 VIRPLX-1.2 Frame# 1

PROJECT 06-1778

SPECIMEN 652902



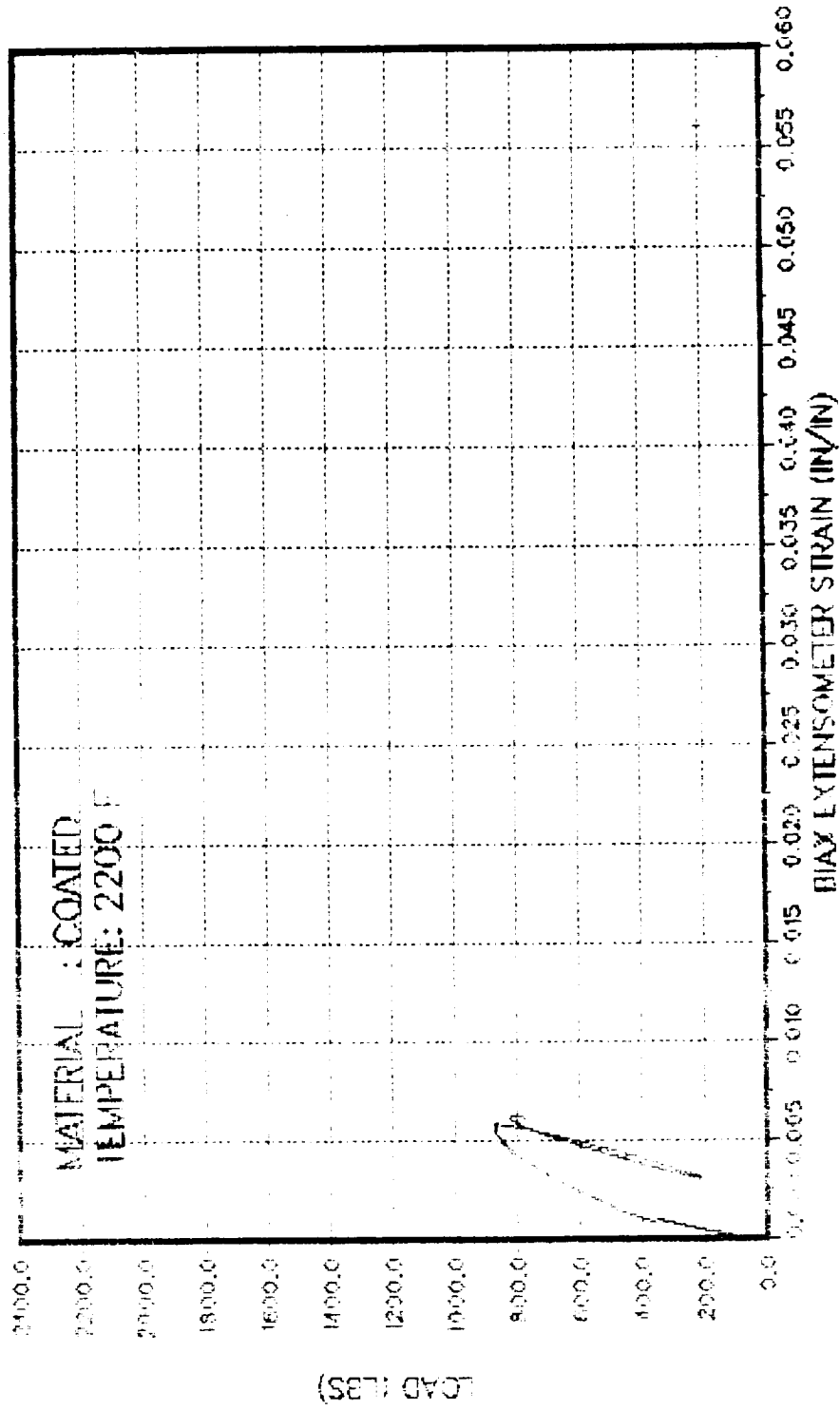
8-MAR-90 23:27 VIRFLA-1.2 Frame# 1  
PROJECT 06-1778  
SPECIMEN 653503



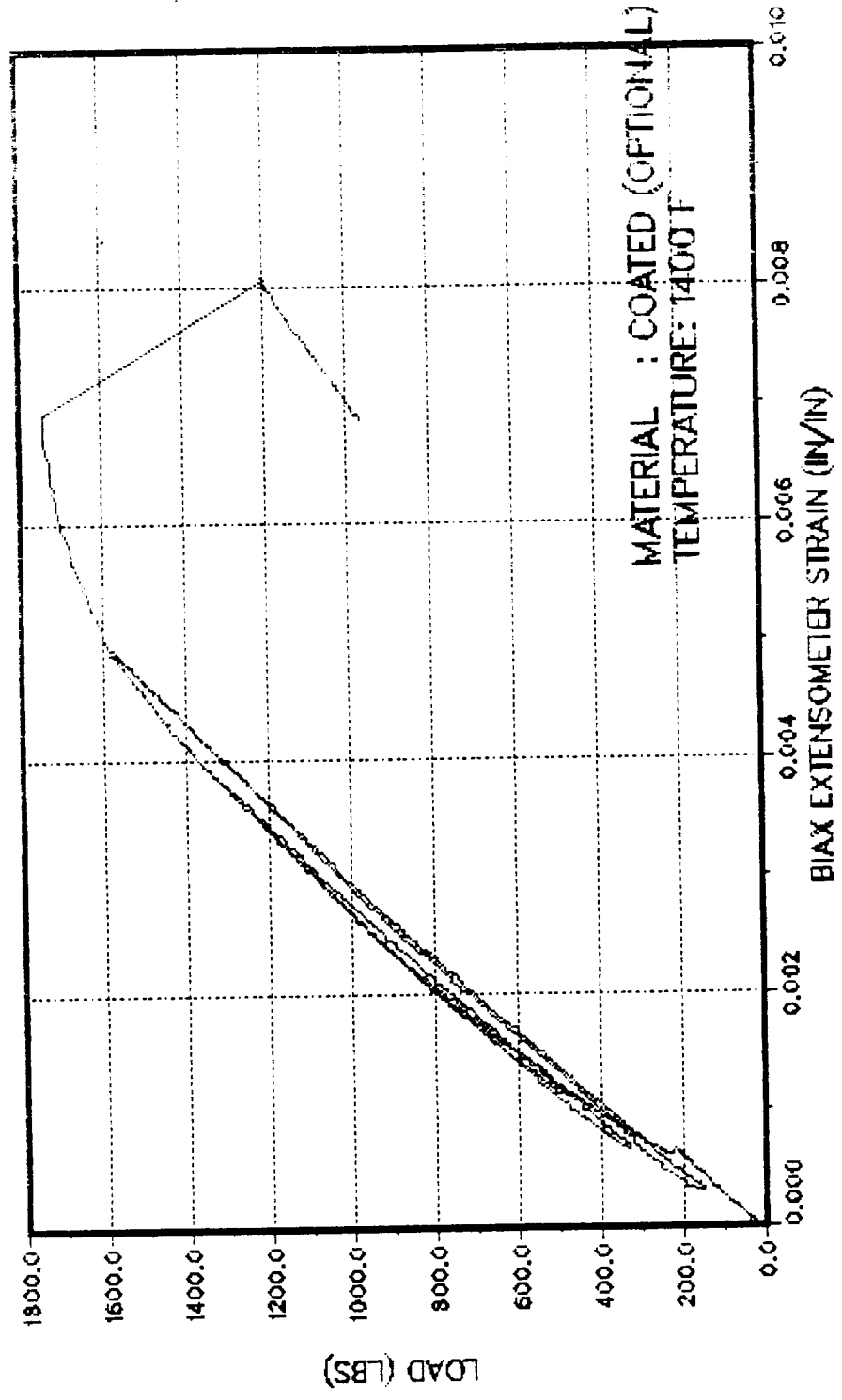
S-MAR-90 2:5:54 VIRFLX-1.2 Frame# 1

PROJECT 06-1778

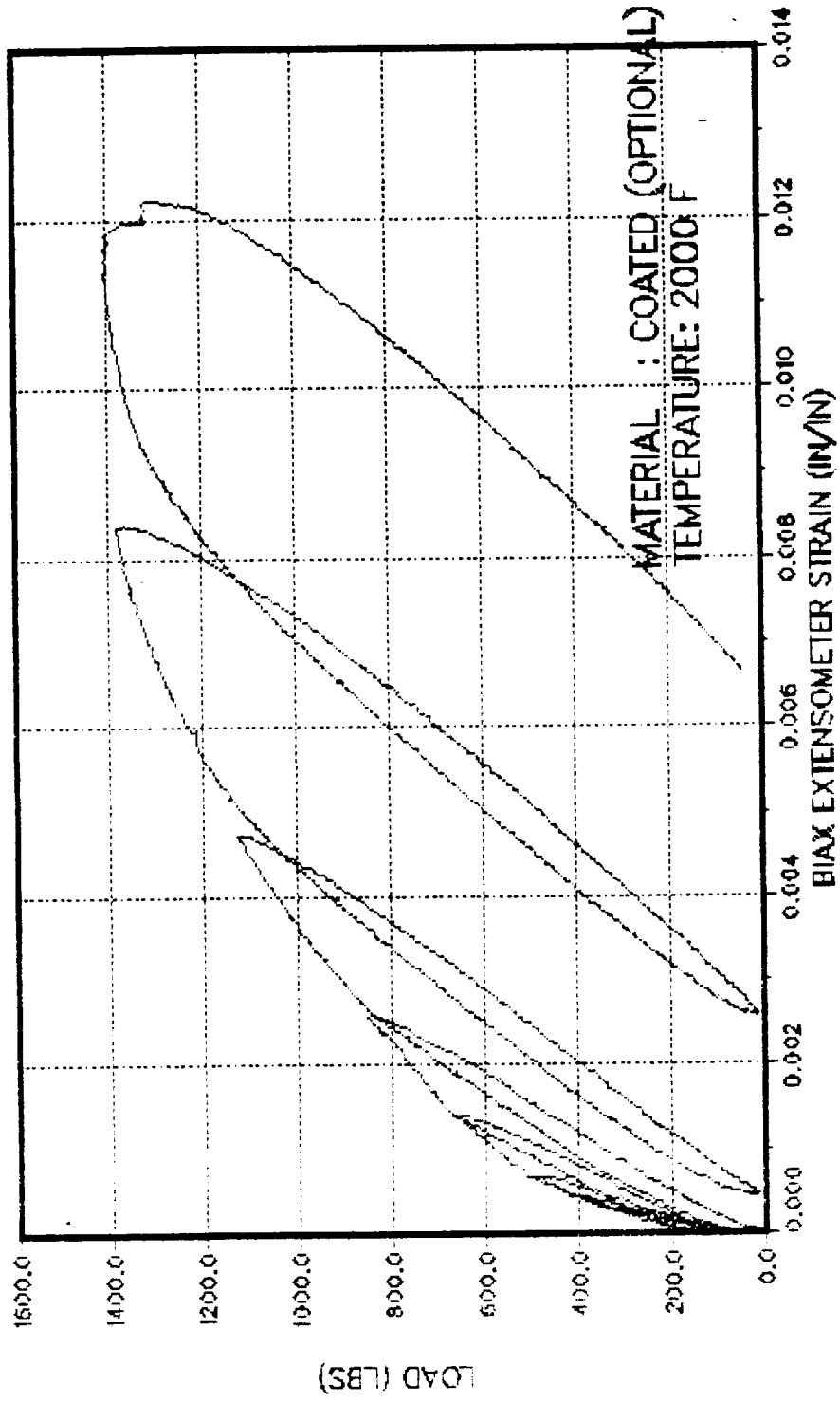
SPECIMEN 653504



25-MAY-90 07:28 VIRPLX-1.2 Frame# 1  
PROJECT 06-1778  
SPECIMEN 653602

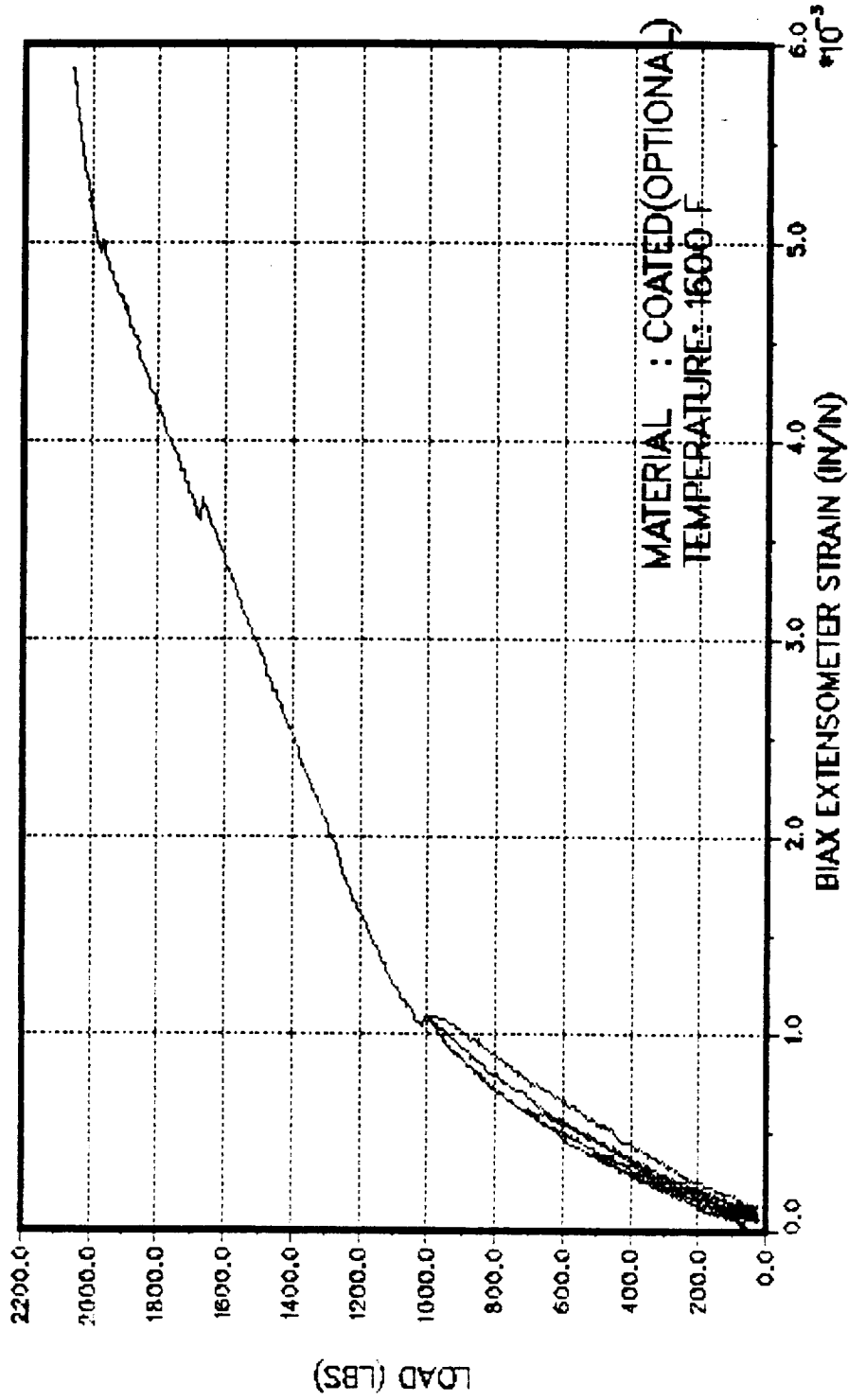


13-MAR-90 17:07 VIRPLX-1.2 Frame# 1  
PROJECT 06-1778  
SPECIMEN 653603

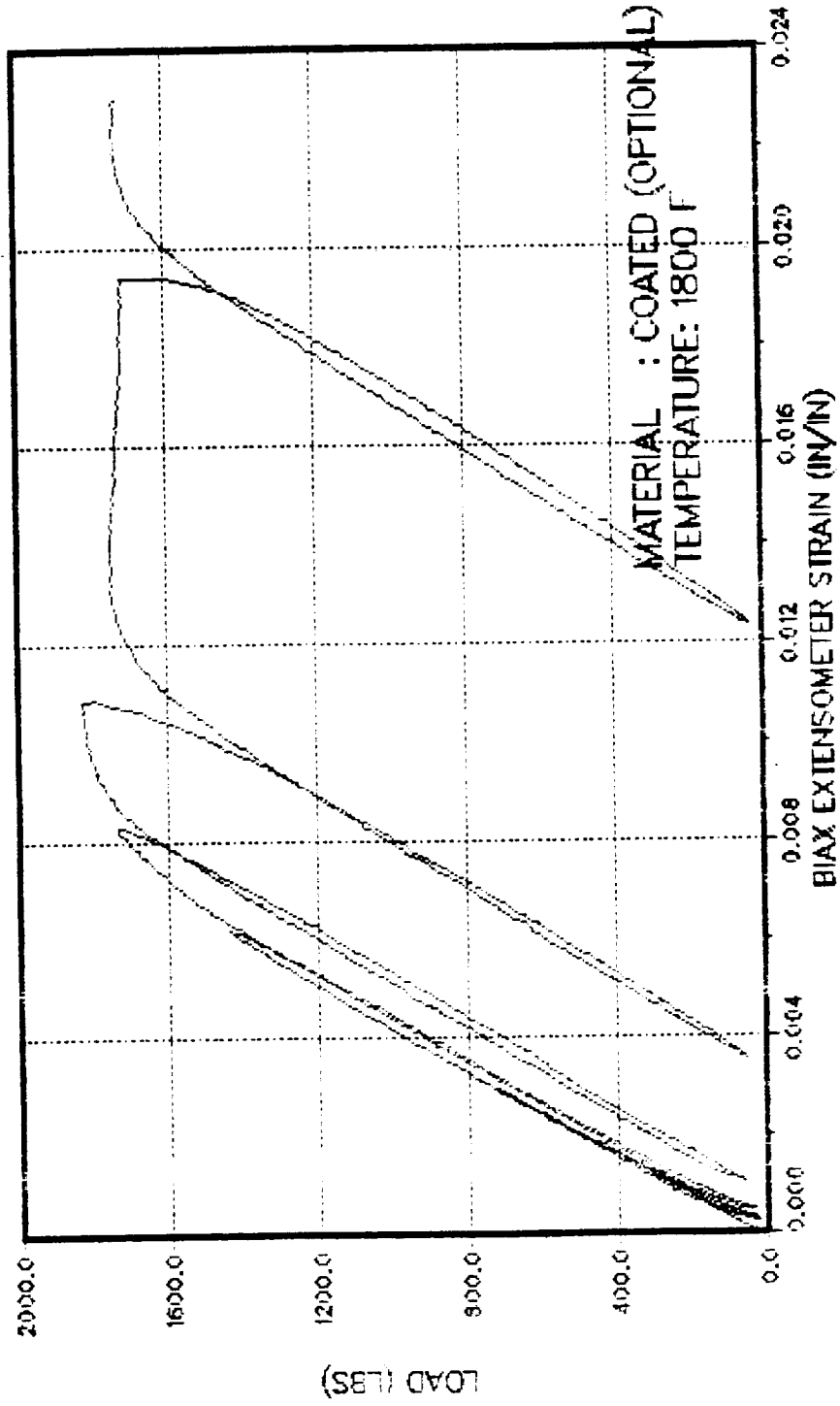




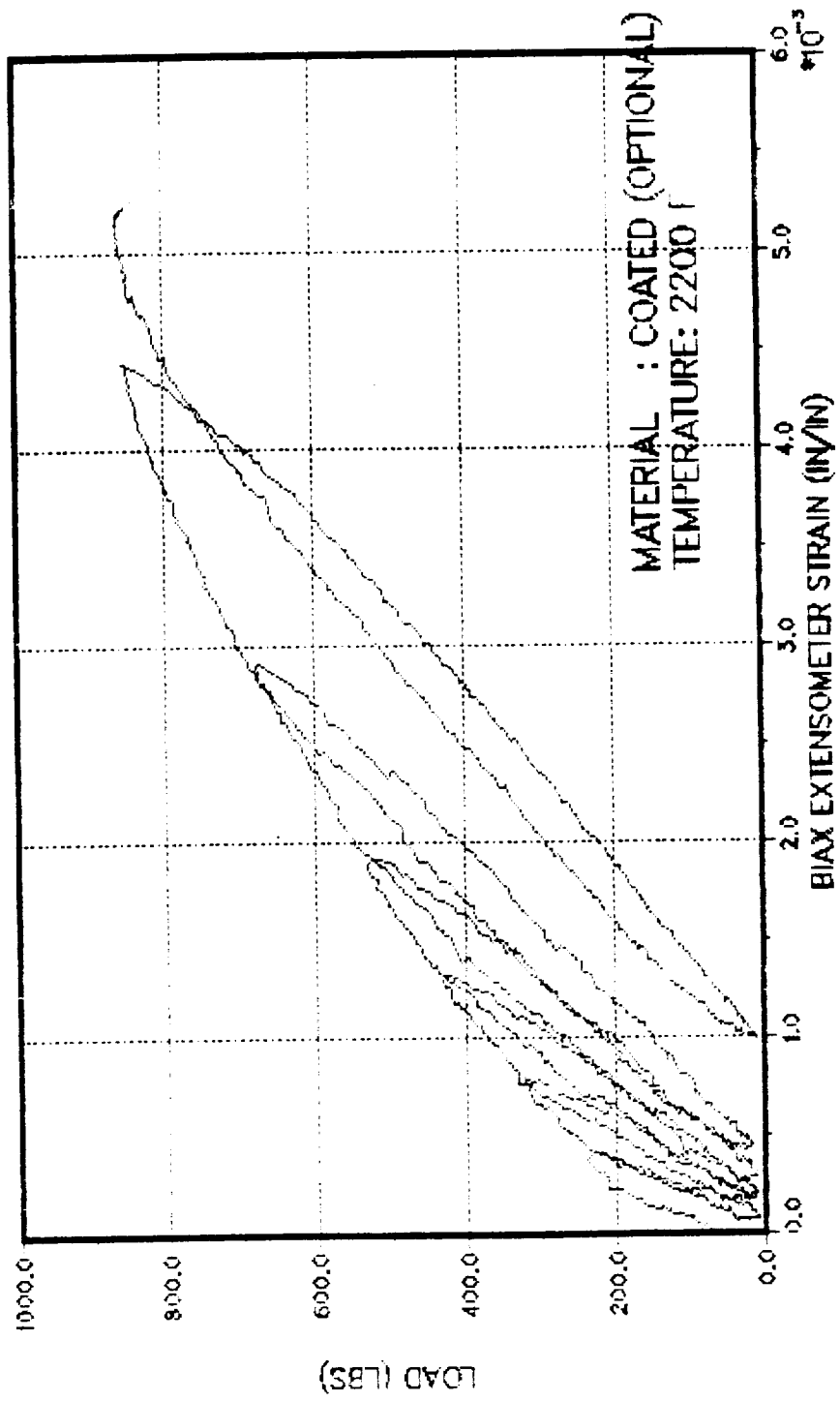
19-MAR-90 16:53 VIRPLX-1.2 Frame# 1  
PROJECT 06-1778  
SPECIMEN 653704



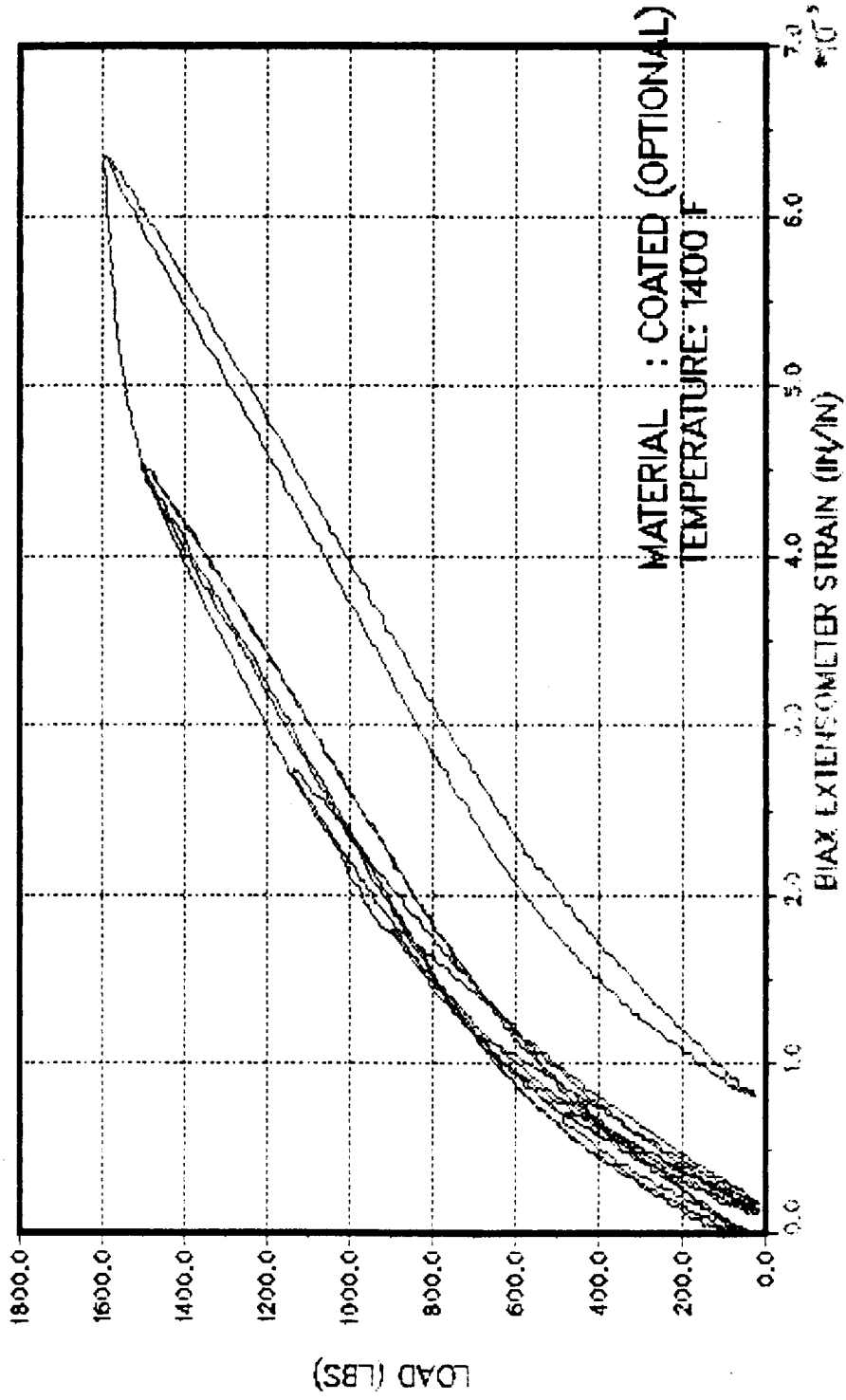
9--APR--90 22:20 VIRPLX-1.2 Frame# 1  
PROJECT 06--1778  
SPECIMEN 652802



9-APR-90 21:00 VIRPLX-12 frame# 1  
PROJECT 06-1778  
SPECIMEN 652803

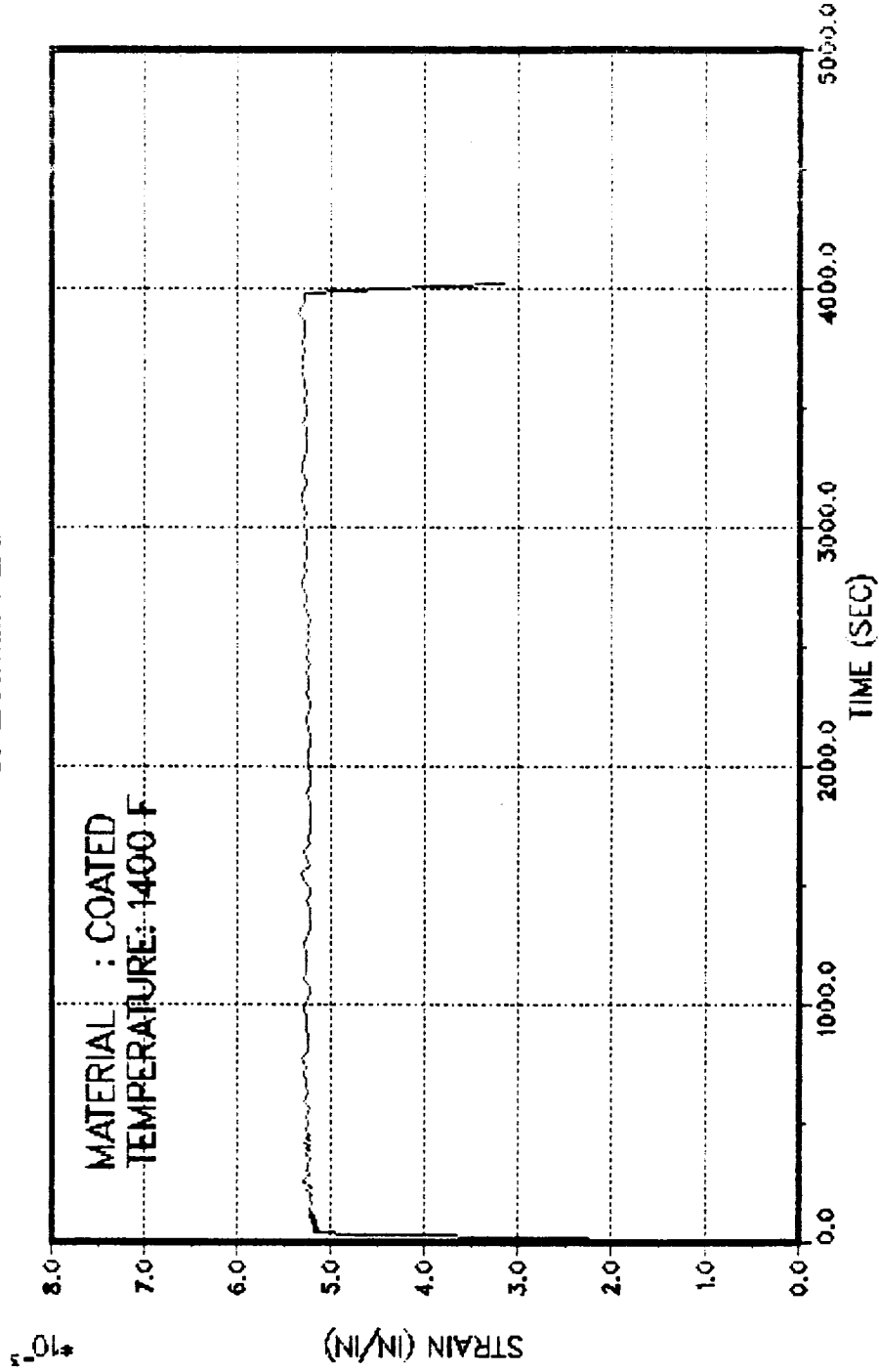


12-APR-90 07:51 VIRPLX-12 Frame# 1  
PROJECT 06-1778  
SPECIMEN 653502

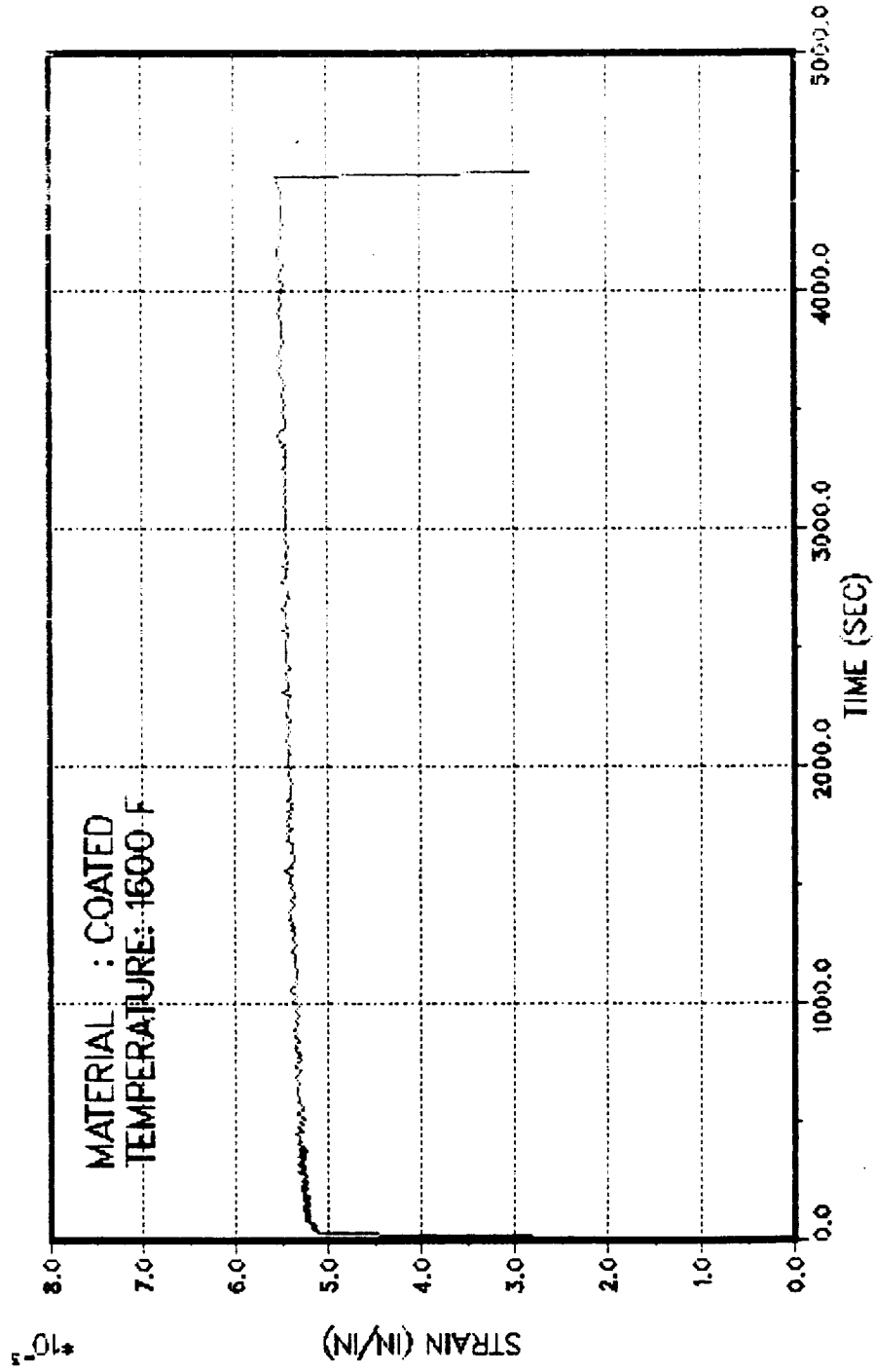


## 9 Appendix E: Computer Plots of Creep Tests

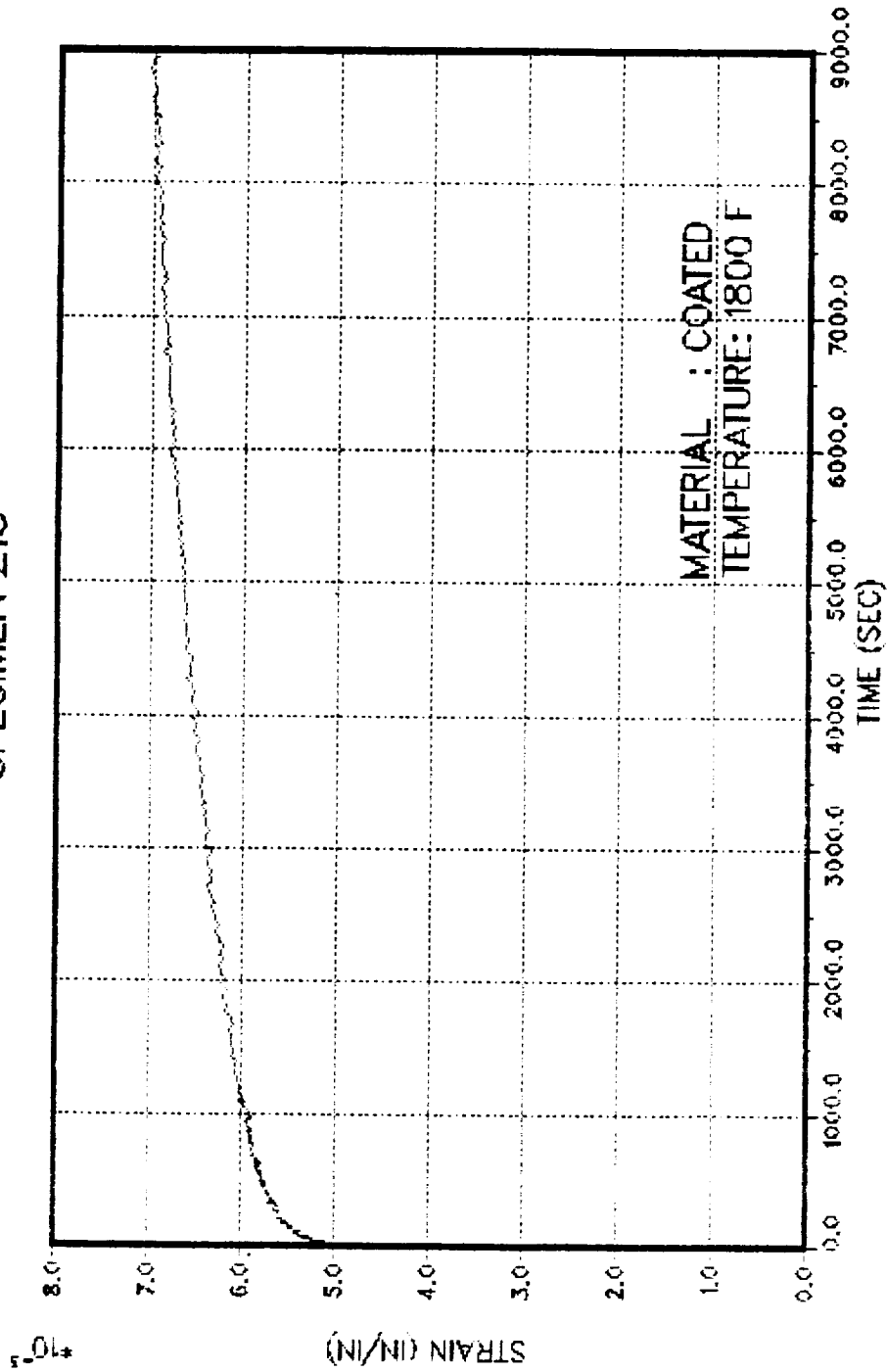
24-MAY-90 07:29 VIRPLX-1.2 frame# 1  
PROJECT 06-1778  
SPECIMEN 21A



24-MAY-90 07:39 VIRPLX-1.2 frame# 1  
PROJECT 06-1778  
SPECIMEN 21B



24-MAY-90 07:36 VIRPLX-1.2 Frame# 1  
PROJECT 06-1778  
SPECIMEN 21C





---

## 10 Appendix F: MS-DOS ASCII Data Files (Floppy Disks)